Universitetet i Stavanger

FACULTY OF SCIENCE AND TECHNOLOGY

MASTER'S THESIS

Study programme/specialisation: Petroleum Reservoir Engineering	Spring semester, 2017 Open
Author: Bendik Horvei	..... (signatur forfatter)
Programme coordinator: Anders Nermoen Supervisors: Nils Harald Giske Anders Nermoen	
Title of master's thesis: Streaming potential – qualification of method and investigating the impact of brine in sandstone core plugs	
Credits: 30	
Keywords: Streaming potential, Electrokinetic, Zeta potential, colloid science, electrical double layer, wettability, surface charge, EOR	Number of pages: 89 Stavanger, 15.05.2017

(blank page)

Streaming potential – qualification of method and investigating the impact of brine in sandstone core plugs

Master's Thesis by
Bendik Horvei
Spring 2017

University of Stavanger
The Faculty of Science and Technology
Department of Petroleum Engineering

(blank page)

Abstract

Streaming potential is an electrokinetic phenomenon caused by relative motion of ions close to a charged surface when a fluid moves past it. By measuring the streaming potential, information related to the surface properties of the rock, like charge and wettability can be gained.

To get precise measurements of the streaming potential, a good experimental setup is required. The main purpose of this thesis was to set up the experiment, get reproducible results, and investigate if there was a systematic variation in the streaming potential by varying the brine composition.

It turned out that it was important to reduce the effect of the static noise to get reproducible results. In that respect we used a method of flowing in both directions, and varied the flooding rate in a systematic way. The measurement methods implemented were paired stabilised (applying a constant rate and wait for a stable voltage and pressure) and pressure ramping with ranges between 240 seconds and 30 seconds (linearly increase the pressure and measure the streaming potential continuously).

In this work we identified a clear response on the streaming potential and the salinity of the brine. Higher salinities are trickier to measure as the coupling coefficient is smaller. The results proved to be successful for salinities of NaCl up to 2 M and $CaCl_2$ up to 0.2 M. At low salinity the measurements were reproducible, and with a variation of 2 % for the individual measurements. For medium salinities, the coupling coefficient was around 20 % higher in magnitude for rapid pressure ramping techniques (30 sec) than for slower ramping techniques (120-240 sec). For the high salinity brines, it was essential to implement rapid pressure ramping to avoid influence of static voltage.

(blank page)

Acknowledgement

First, I would like to thank Associate Professor Anders Nermoen for giving me this opportunity to work with an exciting and challenging case at the International Research Institute of Stavanger (IRIS). Anders has always believed in me and been a good motivator. His interest and eagerness regarding my work has been inspiring.

I would like to address special thanks to Senior Research Scientist Nils Harald Giske for all the work related to lab supervision. Nils has also been a good motivator and always given help or shown support whenever I needed it. I never happened once that he couldn't share time with we when I came to his office asking for help.

Professor and Chief Scientist Aksel Hiort is also thanked for good input, interesting discussions and shearing ideas regarding my thesis.

Reseach Engineer Daniel Stand deserves thanks for showing great enthusiasm and help at the laboratory.

Finally, I would like to thank all fellow students and scientists for socializing and contribute to a very nice stay here at IRIS.

Table of contents

Table of figures

List of graphs

List of tables

1 Introduction

In this thesis, the main objective was to set up the experimental equipment, run experiments, interpret, and verify the results. This means, basically, to measure the streaming potential coupling coefficient within acceptable errors by conduction reproducible measurements at the laboratory for different brines. The coupling coefficient, C, is defined as:

$$C = \frac{\Delta V}{\Delta P},$$

where ΔV is the voltage over the core and ΔP the corresponding pressure drop. The experimental setup was initially based on literature papers from Imperial College and used as a template (Jaafar, Vinogradov et al. 2009). The experiments were performed at IRIS in Stavanger. Experiments has previously been executed here by students using similar equipment, but proven unsuccessful although many sources of errors were checked and corrected for (Strand 2012; Dahle 2012; Aas 2014).

A secondary objective in the work with this thesis was to investigate what differences there was (if any) in the results obtained within each distinct brine by implementing different measuring methods. The idea was to measure the streaming potential coupling coefficient using salinities of Sodium Chloride (NaCl) and Calcium Chloride ($CaCl_2$), from 0.02 M up to 2.0 M for the NaCl and 0.0067 up to 0.2 M $CaCl_2$. One method was to implement paired stabilised experiments with different rates within each pair. The other method was to ramp the pressure up to a certain pressure (max 500 kPa) with different ramping times (240 seconds to 30 seconds). The results were compared within each other and their methodology, as well as compared with other experiments with similar characteristic.

In addition to this, a summary of some of the unsuccessful experiments that was conducted and problems that occurred during the experiments, will be presented. The idea is that this can be used as a troubleshooting user guide for later experiments.

All illustrations are self-made and inspired by the theoretical description.

2 Theory

2.1 Wettability

Wettability is a major factor regarding the reservoir characteristics due to its impact on the reservoirs fluid distribution inside the pores, and thereby the flow of fluids in a reservoir. Reservoir properties such as relative permeability, residual saturation, chemistry of the fluid, waterflood behaviour, mobility and electrical properties is directly or indirectly linked to the wettability (Anderson 1986).

Wettability is defined as *the tendency of one fluid to spread on or adhere to a solid in the presence of other immiscible fluids (Craig 1971).*From a reservoir point of view, it is a measure of the preference that the rock has on either oil or water. The fluid that spreads more on the rock is said to be the *wetting phase*. The remaining fluid is the *non-wetting phase.* The wetting fluid tends to occupy smaller pores and cover most the rock surface. The non-wetting fluid occupy the centres of the larger pores and extends over several pores (Anderson 1986).

2.1.1 Initial wetting of reservoirs

The reason why fluids have different preferences to a given solid can mainly be explained by electrical forces acting between the solid and the liquid. Carbonate has a positively charged surface due to its abundance of calcium ions (Ca^{2+}). Oils often contains a carboxyl group, -COOH, that bond between the positively charged surface and the negatively charged carboxyl group, $-COO^-$. Therefore, the oil adheres to the surface making it oil-wet (Austad 2013).

In sandstones, this is not necessary the same. Almost all clean sedimentary rocks are water-wet due to the negative surface charge between water and silicate minerals. Now clays minerals are regarded as the main wetting material in sandstones, because of the large surface area. Because clay is composed of many different minerals heterogeneously distributed in the reservoir, some areas tends to be less water wet than others (Aberdeen 1982).

2.1.2 Wettability determination by contact angle

One way of expressing wettability is by the contact angle between the wetting fluid and the surface in presence of a non-wetting fluid. If a drop of water is placed on a surface immersed in oil, a contact angle is formed. The angle ranges from 0 to 180°. The surface is regarded as water wet for angles less than 90° and oil wet for angles greater than 90°. If the angles are far away from 90°, the wetting is regarded strong. When the surface

has no strong preference for either water or oil, the wettability is regarded neutral. This is for angles around 90°.

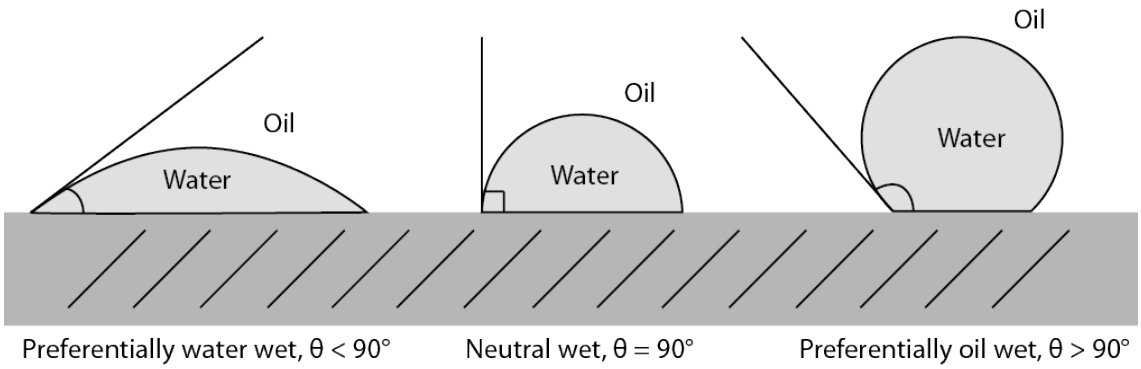

Figur 1: Wettability determination by contact angle.

As multiple minerals are found nearby each other in real reservoir system, the wettability may be highly varying. As such, the overall wettability may be determined mixet wet (or neutral wet) either because the mineral have a contact angle around 90, or the mixture of different mineral surfaces each with varying wetting angles. It is unresolved, how the two ways mixed wet situations may arise impacts the flow of immiscible fluid on pore and core scale.

2.1.3 Investigation of wettability alteration

Injection of seawater and deionized seawater has proven to change the initial wetting of the reservoir, resulting in an increase of the recovery factor, see e.g (Austad 2013). Wettability alteration can happen when the injected water is not in equilibrium with the formation water that is present in the reservoir. By chemically changing the wettability of a reservoir, residual oil can be released from small pores preferentially.

It has been claimed that the wettability of a reservoir rock saturated with brine and crude oil may cause a change in the measured streaming potential, and hence the zeta-potential (Jackson and Vinogrado 2012). This proves the connection between the wettability alteration and surface charge. Hence, streaming potential measurements be used to improve the understanding regarding the relation between wettability and surface charge.

2.2 Electrical double layer

A solid immersed in water will in general acquire a surface charge due to the disassociation of ions from the surface. To conserve electrical charge, there will be a layer of counter ions that has a net electrical charge of opposite sign than the surface. A schematic illustration of this concept is illustrated in the figure below.

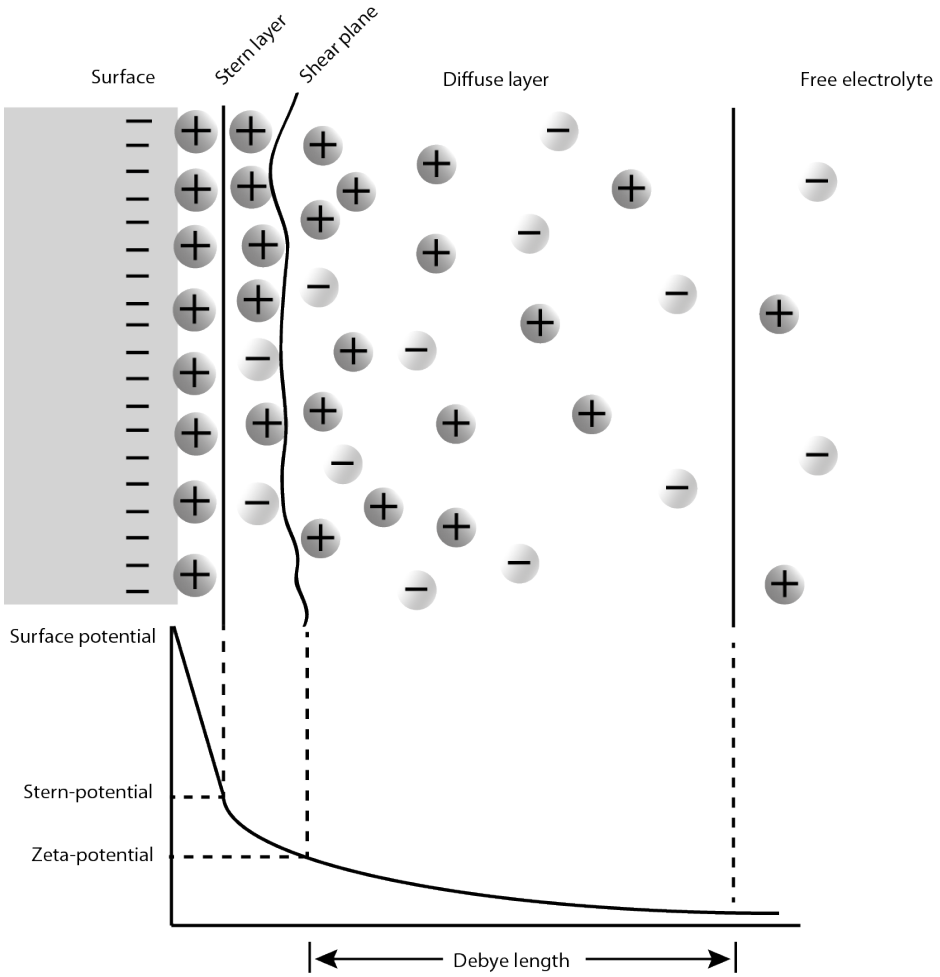

Figur 2:The electrical double layer. The surface has generated a negative charge which attracts counter-ions.

2.2.1 Surface charge

Sandstones are negatively charged for pH above 2-3, while chalk may be positively or negatively charged. Because sandstones are of relevance in this thesis, a short introduction of how surface charge is generated is presented.

Quartz is regarded as the main building block of sandstones, and most reservoir contain some clay minerals (Aberdeen 1982). The chemical compound of quartz is silica (SiO_2). The silica surface generates an ionization and adsorption process in contact with water (Shaw 1992)

Silica contains two types of neutral surface group (Revil and Pezard 1999). These are the double coordinated siloxal ($> Si_2O^0$) and singly coordinated silanol ($> SiOH^0$). The ">" symbol refers to the mineral lattice and the "0" means that there is no charge. By mineral lattice, we refer to the crystal structure of the mineral. The siloxal group can be regarded non-reactive. However, the surface silanol group can react in contact with liquid. We consider the silanol group ($> SiOH^0$) in contact with water that contains a monovalent electrolyte (like NaCl). For the process of which an ionisation (i.e. deprotonation) of the silanol groups occur, we write

$$> SiOH^0 \Leftrightarrow \quad > SiO^- + H^+. \tag{2.1}$$

Further, a cation adsorption occurs on the silica surface. The overall reaction can be written

$$> SiOH^0 + Me^+ \Leftrightarrow \quad > SiOMe^0 + H^+, \tag{2.2}$$

where Me^+ is a metal cation of the salt. If $NaCl$ was the electrolyte present in the solution, Me^+ would be Na^+. From these reactions, for non-acidic solutions there are three types of *sites* present at the silica surfaces; two neutral ($> SiOH^0$ and $SiOMe^0$) and one negative ($> SiO^-$). This negative site corresponds to the negatively charged surface.

The ionization and hence the net molecular charge is strongly affected by the pH of the solution, as the magnitude of the H^+ is directly linked to the acidity. For a very acidic solution (pH below ≈2-3) the surface may be even positively charged.

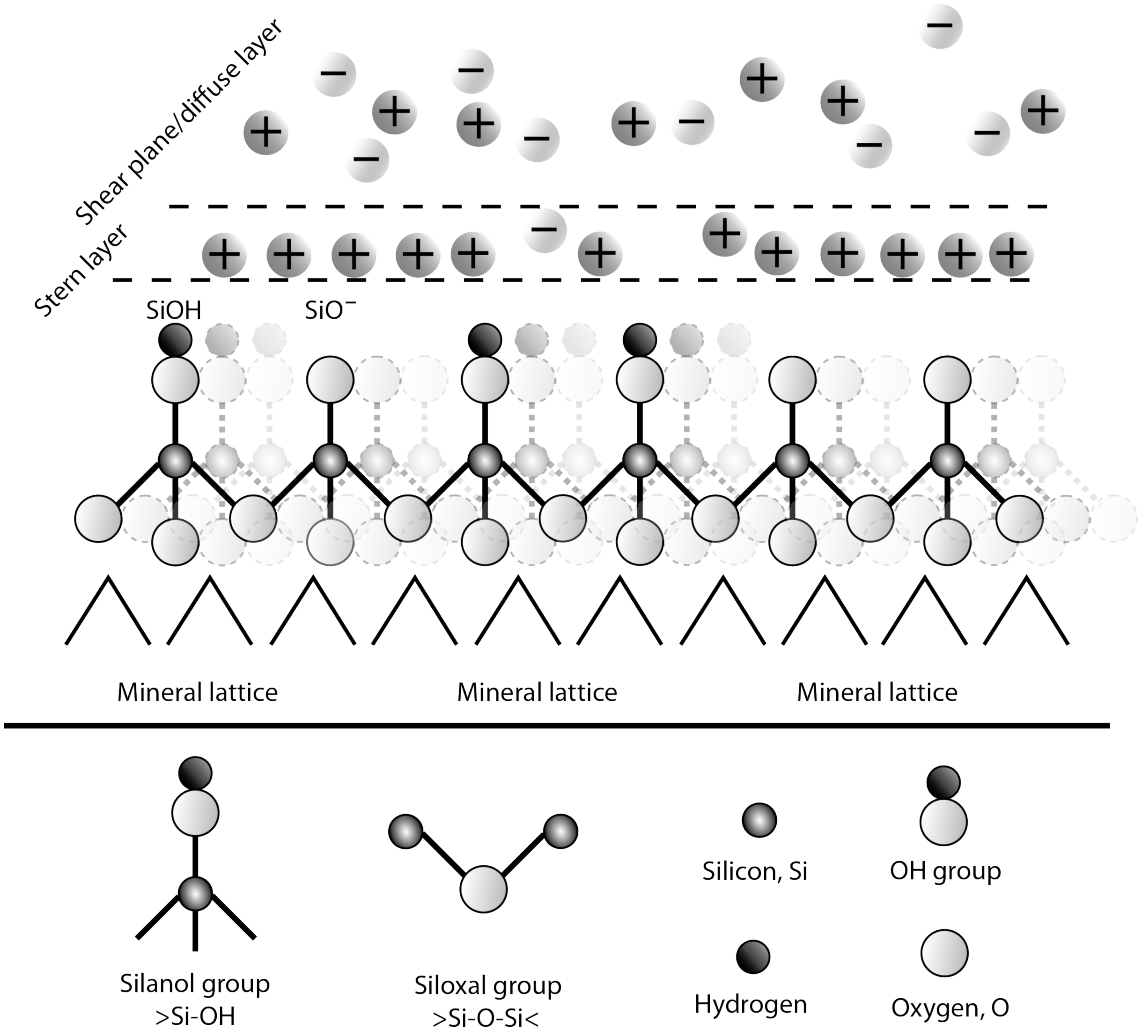

Figur 3: Concept of surface charge. The negatively charged site (> SiO^-) corresponds to the negatively charged surface which attracts cations from the electrolyte.

The idea of this concept is proposed by Revil et. al (1999). See (Revil and Pezard 1999) for more details.

The potential charge attracts ions from the electrolyte with the opposite charge. A sandstone, which are negatively charged at normal conditions (pH>2-3), will attract positively charged ions from the liquid.

2.2.2 Stern layer

The double layer is separated by two distinct layers of ions. The first layer is the one that are next to the charged surface. It is named the *Stern layer* (after Otto Stern). The ions in this region is immobile as they are strongly attached directly to the mineral surface. The Stern layer is very thin compared to the diffuse layer, with only one or two molecular diameters (Jaafar, Vinogradov et al. 2009). The electrical potential between the surface and the Stern layer decreases linearly (Donaldson and Alam 2008).

2.2.3 Diffuse layer (Gouy Chapman layer)

The amount of counter-ions in the Stern layer is usually not sufficient to balance the opposite charge of the surface. Thus, more counter-ions are attracted toward the vicinity of the surface, next to the Stern layer. This is called the *diffuse layer* (or *Gouy Chapman layer*). The theory for this layer was developed by Gouy (1910) and Chapman (1913), independently.

The counter-ions within the diffuse layer is mobile (as they are not adsorbed to the surface like in the Stern layer) and decreasing exponentially away from the Stern layer until it is electrically neutral, having the same composition as the bulk fluid (Hunter 1981). The region outside the diffuse zone, away from the rock surface, is called *the free electrolyte.* The total amount of counter-ions in the Stern- and diffuse layer is balancing the surface charge. Hence, the overall charge distribution from the surface into the pore are electrically neutral. The constant potential in the neutral electrolyte is usually regarded as *the reference* or *zero potential.*

The distance of the diffuse length is called the *Debye length* ($1/\kappa$) and range from around 3-100 nm depending on the valence and ionic concentration of the fluid (Hunter 1981).

2.2.4 Zeta potential

At the region in the diffuse layer very adjacent to the Stern layer, there is a point in which the mobility of the attracted counter-ions increases rapidly (from this point and out away from the charged surface). The zeta-potential is measured at this region, called the *surface of shear* or *shear plane.* When a force is applied perpendicular to the surface, a shear stress transfer/relocate some of the mobile counter-ions in the diffuse zone, from the shear plane. Many important properties of colloidal systems are determined directly or indirectly by the electrical charge in the shear plane (Hunter 1981).

The exact location of the shear plane is discussable, but it is said to be in a few molecular diameters from the Stern layer (Shaw 1992). Some researchers even characterise the Stern layer and the shear plane to be same (Leroy, Devau et al. 2013).

2.3 Charge distribution: a mathematical description

A simple way to present a mathematical interpretation of the charge distribution in double layer is to think of both layers of charge as fixed in parallel planes to form a molecular condenser. This interpretation is called *the flat plane model.* The theory of this chapter is mainly based on (Hunter 1981) unless otherwise is stated.

Consider the solid surface as a plane surface immersed in an electrolyte solution. The surface charge is uniformly distributed over the surface. The electrical potential at the surface is ψ_0. The counter ions, balancing the surface charge, are regarded as point charges immersed in a continuously dielectric medium. The electrostatic equation for the system can be referred to the Poisson's equation:

$$\nabla D = \rho, \tag{2.3}$$

where D is the dielectric displacement and can be written

$$D = \epsilon E. \tag{2.4}$$

E is the electric field and ϵ is the permittivity. The permittivity (ϵ) is a measure of resistance that is encountered when forming an electric field, measured in Farad per meter. ρ is the volume density of charge, having the unit C/m^3 (Columb per cubic metere) (Whelan and Hodgeson 1978). Substituting (2.3) in (2.4) and assume that the permittivity is independent of position, the equation can be written

$$E = -\frac{\rho}{\epsilon}. \tag{2.5}$$

Moreover, the electric field can be expressed as

$$\frac{d^2\psi}{dx^2} + \frac{d^2\psi}{dy^2} + \frac{d^2\psi}{dz^2} = -\frac{\rho}{\epsilon}. \tag{2.6}$$

If we consider the x-direction perpendicular to the surface wall and assume that this surface wall extends to infinity for positive and negative values of y and z, the equation can be simplified to

$$\frac{d^2\psi}{dx^2} = \nabla^2\psi = -\frac{\rho}{\epsilon} \tag{2.7}$$

When the electrochemical potential of a solute is at equilibrium, the electrical and diffusional forces on the ion must balance out:

$$\nabla \mu_i = -z_i e \nabla \psi \tag{2.8}$$

Here, μ_i is the chemical potential (or concentration) and z_i is the valence of the ion i. e is the elementary charge ($1.602 \cdot 10^{-19}$) with unit Columb. The electrical potential and the chemical concentration are, for a flat double layer, constant in planes parallel to the wall. Thus, equation (2.8) can be written

$$\frac{d\mu_i}{dx} = -z_i e \left(\frac{d\psi}{dx}\right) \tag{2.9}$$

The chemical potential per ion can be defined

$$u_i = \mu_i^0 + kT \, ln \, n_i \tag{2.10}$$

Here, n_i is the number of ions of type i per unit volume. k is the Boltzmann constant ($\approx 1.380 \cdot 10^{-23} \, J \cdot K^{-1}$), a physical constant relating the average kinetic energy of particles in a gas with the temperature of the gas (Gottlieb and Pfeiffer 1963). T is the temperature (Kelvin). Further, we have

$$\frac{d \ln n_i}{dx} = \frac{1}{n_i}\frac{dn_i}{dx} = -\frac{z_i e}{kT}\frac{d\psi}{dx} \tag{2.11}$$

Integrating (2.11) from a point in the bulk solution, where the electrical potential is neutral (ψ=0 and $n_i = n_i^0$), leads to the well-known *Boltzmann equation*:

$$n_i = n_i^0 \exp\left(-\frac{z_i e \psi}{kT}\right) \tag{2.12}$$

Boltzmann equation describes the local concentration of each type of ion in the double layer region.

The volume charge density can be related to ion concentration for the neighbourhood of the surface;

$$\rho = \sum_i n_i z_i e \tag{2.13}$$

where the summation operator defines the sum of all ions present. Substituting (2.12) into (2.13), we get

$$\rho = \sum_i n_i^0 \exp\left(-\frac{z_i e\psi}{kT}\right) z_i e \tag{2.14}$$

Now, substituting for ρ into (2.7), we obtain the well-known Poisson-Boltzmann equation;

$$\nabla^2\psi = -\frac{1}{\epsilon}\sum_i n_i^0 \exp\left(-\frac{z_i e\psi}{kT}\right) z_i e \tag{2.15}$$

We will examine an approximate solution of this equation, with some certain assumptions. First, we assume that ψ is small in the double layer. Hence, $z_i e\psi$ is much smaller than kT. Knowing this, we can assume that $e^{-x} \approx 1 - x$ for small x. This assumption is referred to as the *Debye-Hückel approximation*. The equation can be written as an exponential function;

$$\frac{\nabla^2\psi}{dx^2} = -\frac{1}{\epsilon}\left[\sum_i n_i^0 z_i e - \sum_i \frac{z_i^2 e^2 n_i^0 \psi}{kT}\right] \tag{2.16}$$

To preserve electro neutrality in the bulk, the first term in the parentheses is cancelled out. This is because the concentration of positive and negative ions in the bulk is the same. Hence, for a plane interface, the equation becomes;

$$\nabla^2\psi = \frac{\nabla^2\psi}{dx^2} = \frac{\sum z_i^2 e^2 n_i^0 \psi}{\epsilon kT} \tag{2.17}$$

We rewrite the equation;

$$\nabla^2\psi = \frac{\nabla^2\psi}{dx^2} = \kappa^2\psi \tag{2.18}$$

where

$$\kappa = \left(\frac{e^2 \sum z_i^2 n_i^0}{\epsilon kT}\right)^{1/2} \tag{2.19}$$

The parameter κ is reffered to as the Debye-Hückel parameter. Its inverse $(1/\kappa)$ is the Debye-length, which was explained previously. The valence and ion concentration of the electrolyte has a big impact on the Debye-length.

The distance of the Debye-length is typically only a few nanometres for a grain electrolyte combination (Glover and Jackson 2010).

The term $\sum z_i^2 n_i^0$ can, moreover, be rewritten as $2I$ where I is defined as the ionic strength of the bulk solution;

$$I = \frac{1}{2}\sum_{i=1}^{i=n} z_i^2 n_i^0 \qquad (2.20)$$

2.4 Balancing the surface charge

As mentioned previously, the counter-ions in the electrolyte is attracted to their opposite charge on the surface and thus balancing the charge. (Chesick 1972) explained the composition of the Stern layer and Zeta-potential behaviour this way;

If the concentrations of the ions in the Stern layer is sufficient to balance the surface charge, the electrical potential will drop linearly from the surface to the share plane where the potential of the electrolyte is neutral. Thus, a collapse of the diffuse layer. In this case, the zeta-potential is zero (there is thus no electrical potential in the shear plane). If the concentrations of ions in the Stern layer is not sufficient to balance the surface charge, the diffuse layer is present in order to balance the surface charge. Thus, there is an electric potential at the shear plane. The zeta-potential is non-zero. For sandstone, the value are usually negative.

2.4.1 Influence of salinity

The size of the double layer and the corresponding zeta-potential itself is strongly influenced by the composition of the brine, as we have now seen. The magnitude of the coupling coefficient and the zeta-potential decreases as the salinity of the brine increases due to compaction of the diffuse layer, as the Debye-Hückel parameter suggests. The compaction of the diffuse layer can be explained by the density of the ions in the brine; for low salinity brine, there is a larger distance between the ions in the solution and the diffuse layer must be larger to preserve enough counter-ions to balance the surface charge. For higher salinity brine, the distance between the ions are short and thus, a short distance of the diffuse layer is enough to balance the surface charge. This concept is illustrated in Figur 4;

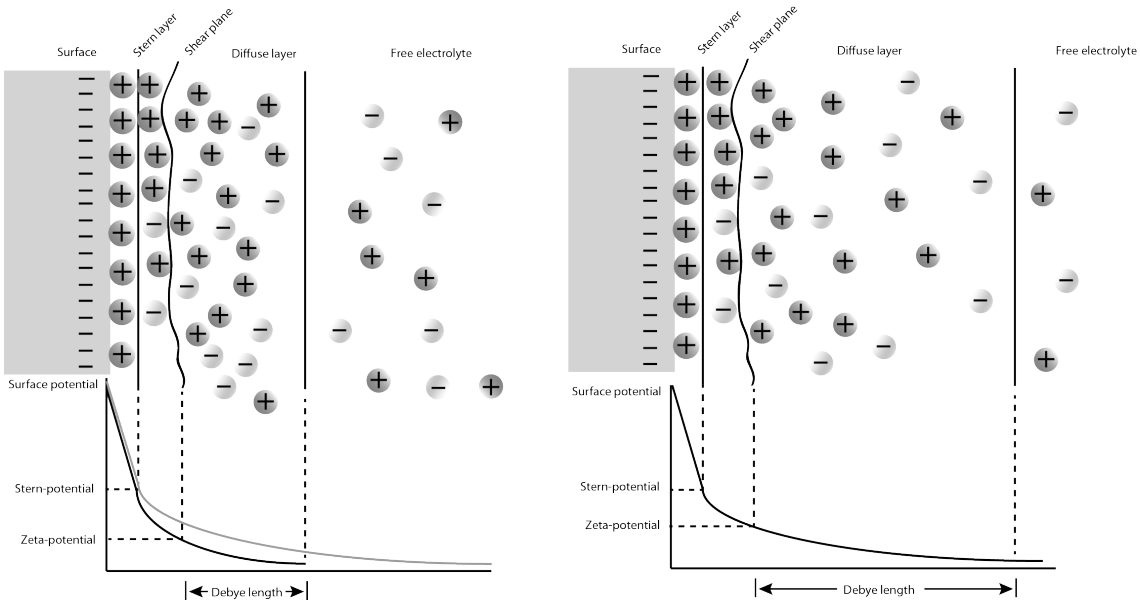

Figur 4: Compaction of the double layer. The left figure illustrates a shorter Debye-length compared to the right figure. The brine that is illustrated on the left figure contains a higher concentration of salts, thus higher density of ions. A result of this is that the magnitude of the zeta-potential is decreased.

2.4.2 Influence of pH

The pH of the brine also has a great impact on the zeta-potential. Alkaline solutions have an excess of negatively charged ions ($OH^- > H^+$) while acidic solutions have the opposite ($OH^- < H^+$). Imagine a solid generating a negatively charged surface when suspended in a solution (herby a negative zeta-potential). When acid is added to the solution there is more hydrogen ions (positive charged) present to balance the negatively charged surface. In addition to this, the surface charge itself is related the acidity of the brine (explained in the surface charge section). The diffuse layer compacts and the magnitude of the negative zeta-potential decrease. Hence, the zeta potential decreases as the pH decreases until a point where the zeta potential becomes zero. This is defined as the *zero point charge* (Donaldson and Alam 2008).

A research by (Leroy, Devau et al. 2013) showed that the pH had a big impact on the surface charge and the corresponding zeta-potential for low salinity brine (<0.1 M NaCl) on amorphous silica. The influence of pH was less significant for higher salinities.

2.5 Electrokinetic phenomena

Electrokinetic phenomena is described as relative motion of ions in the electrical double layer. Streaming potential is one type of electrokinetic phenomena which is the relevant one regarding this thesis. Among streaming potential, there are other distinct electrokinetic phenomena which are depending of what way the motion is induced. Some of them are *Electrophoresis, Electro-osmosis* and *Sedimentation potential*. It can be of interest to get a short introduction to them to get a better overview of the concept behind electrokinetics.

2.5.1 Electrophoresis

When an electric field is applied across a system of liquid with charged particles suspended, they tend to move to its desired pole. Particles with a negative charge will be attracted to a positively charged pole and opposite for positively charged particles. Measurements of the particles velocity can give information of the particles net electric charge or the surface potential if the external field is known.

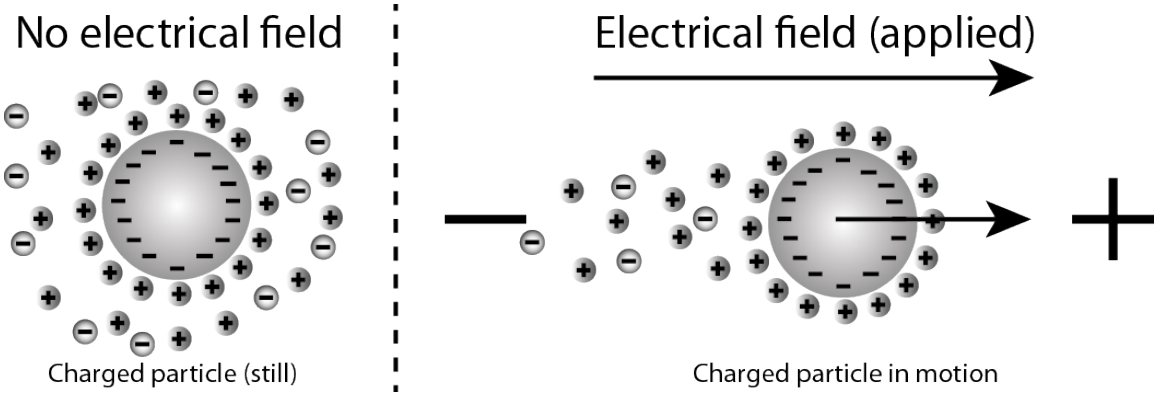

Figur 5: Electrophoresis. Motion of particles under influence of electric field. The particle in this example is negatively charge. Positive ions (cations) are attracted and adsorbed initially.

2.5.2 Sedimentation potential

The idea behind the sedimentation potential is the same as electrophoresis, just opposite. Sedimentation potential occurs from an electric field of charged particles under the influence of centrifugation or gravity. The ions in the double layer is interrupted by the charged particles, causing a displacement between surface charge and electrical charge in the diffuse layer.

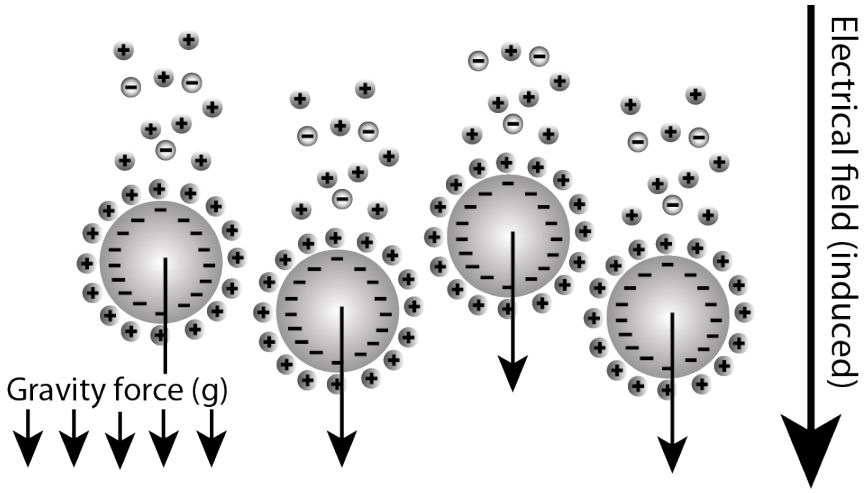

Figur 6: Sedimentation potential. Motion of particles under influence of gravity, inducing an electrical field.

2.5.3 Electro-osmosis

In electro-osmosis, movement of fluid with an excess charge occurs in a stationary solid due to an applied electric field across the system. The fluid is induced to move as its content of ions is attracted to an opposite charge of the electric field. The movement of ions brings the fluid with it. The movement of fluid toward one direction creates a differential pressure across the system. The differential pressure is proportional to the charge of the applied field; the higher voltage the higher differential pressure.

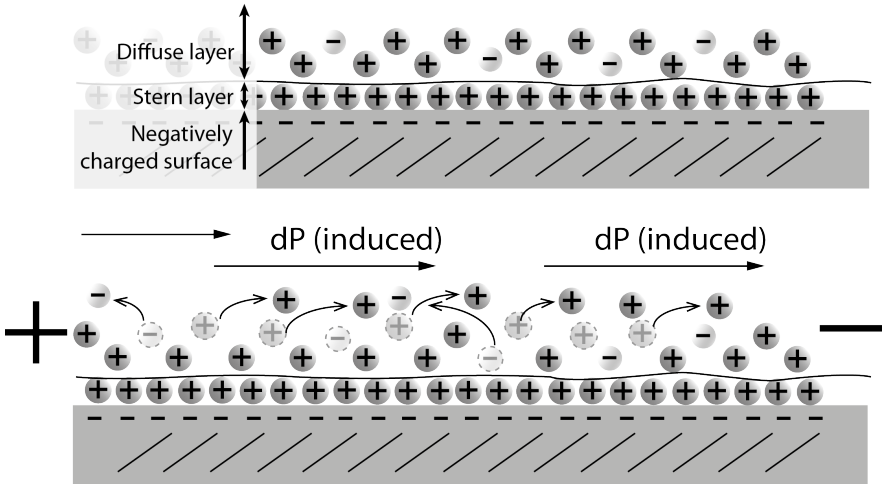

Figur 7: Electro-osmosis. Motion of liquid in porous medium under influence of electric field. The figure illustrates a negatively charged surface with an excess of cations. Due to the majority of these the cations, the flow is induced toward the right direction (to the negative pole).

2.6 Streaming potential

The last electrokinetic phenomena described is the streaming potential. It is the opposite of electro-osmosis. In streaming potential, a differential pressure is applied across the system which force the fluid to flow downstream. The fluid flow is a bearer of the mobile excess charged ions that are present in the diffuse zone of the electrical double layer (Hunter 1981). This movement of charged electrons, called the *streaming current,* accumulates downstream creating the build-up of an electric field. At the same time as the streaming current is obtained, a *conduction current* is generated as the displaced ions want to balance the excess charge. When the conduction current balances the streaming current, steady state is achieved, and the potential and the pressure should remain constant. Hence, the total current density is zero (Jouniaux and Pozzi 2000). Given that the fluid flow is laminar, the streaming potential increases linearly with respect to the differential pressure (Boleve, Crespy et al. 2007). The figure below is a proposed illustration based on the theoretical description of the streaming potential.

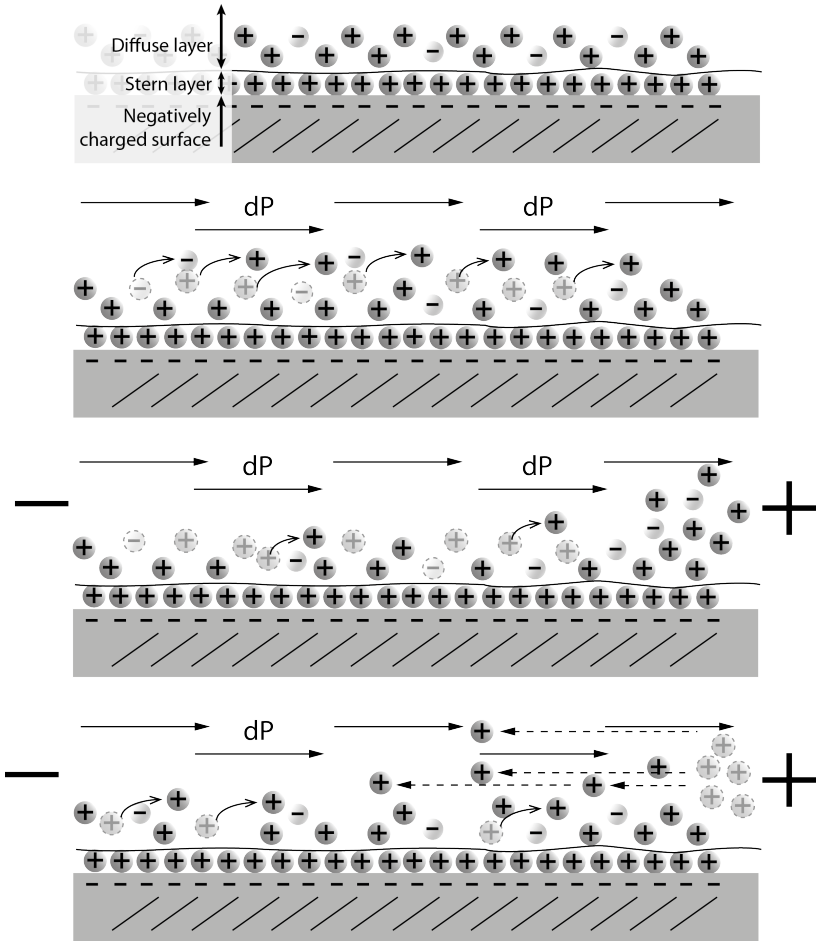

Figur 8: Streaming potential. First section, the ions are still. Second section, a hydraulic flow is applied which generates a streaming current. Section three, accumulation of ions downstream. Section four, a conduction current is generated which balances the streaming current. Steady state is achieved.

2.6.1 Coupling coefficient

When the relation between the streaming potential and the differential pressure drop is linear (i.e. laminar flow), it can be defined as the streaming potential coupling coefficient across a core or a sandpack (given that the net current is zero):

$$\frac{\Delta V}{\Delta P} = C. \tag{2.21}$$

The coupling coefficient can be solved with the slope of a linear regression of the streaming potential vs. differential pressure. The coupling coefficient can be presented as (Jouniaux and Pozzi 2000):

$$C = \frac{\epsilon_w \, \zeta}{\mu_w \, \sigma_f F}, \tag{2.22}$$

where the μ_w is the viscosity of the water. The ϵ_w is the dielectric permittivity of the water; it is a measure of resistance that is encountered when forming an electric field. σ_f is the conductivity of the brine-saturated rock and F being the formation factor; a linear relationship between the brine-saturated rock conductivity and the conductivity of the brine.

Conductivity is a measure of a materials ability to conduct an electrical current, measured in S/m (Siemens per metre). The conductivity is strongly related to the salinity of the brine, and increases with the salt concentration. The effective conductivity refers to the contribution of the brine conductivity and the formation conductivity

$$\sigma_{eff} = \sigma_w + \sigma_f. \tag{2.23}$$

The brine-saturated rock (formation) conductivity can in most cases be neglected for salinities above 0.1 M as the brine (water) conductivity will override the formation conductivity ($\sigma_w \gg \sigma_f$) (Jaafar, Vinogradov et al. 2009). Thus, the coupling coefficient can be simplified to the Helmholtz-Smoluchowski equation (Hunter 1981):

$$C = \frac{\epsilon_w \, \zeta}{\mu_w \, \sigma_w}. \tag{2.24}$$

2.6.2 Deriving the streaming potential

In this derivation, we assume that the flow and the streaming potential generates is for a capillary. This is a simplification of the pore channels in the reservoir rock. The following derivation is based on the literature of (Shaw 1992) and (Hunter 1981).

When deriving a mathematical expression for the streaming potential, one must start with expressing the Poiseuille's law. See Appendix C for more info. The linear velocity of the liquid at a distance r from the axis of the capillary is given by Poiseuille's equation (eq. A-17). We rewrite the equation as a flow in the z-direction;

$$v_z = \frac{1}{4}\frac{\Delta P}{\mu l}(R^2 - r^2). \tag{2.25}$$

The streaming current is defined as

$$I_s = \int_{vol} v_z(r)\rho(r)dV = \int_0^R 2\pi r v_z(r)dr. \tag{2.26}$$

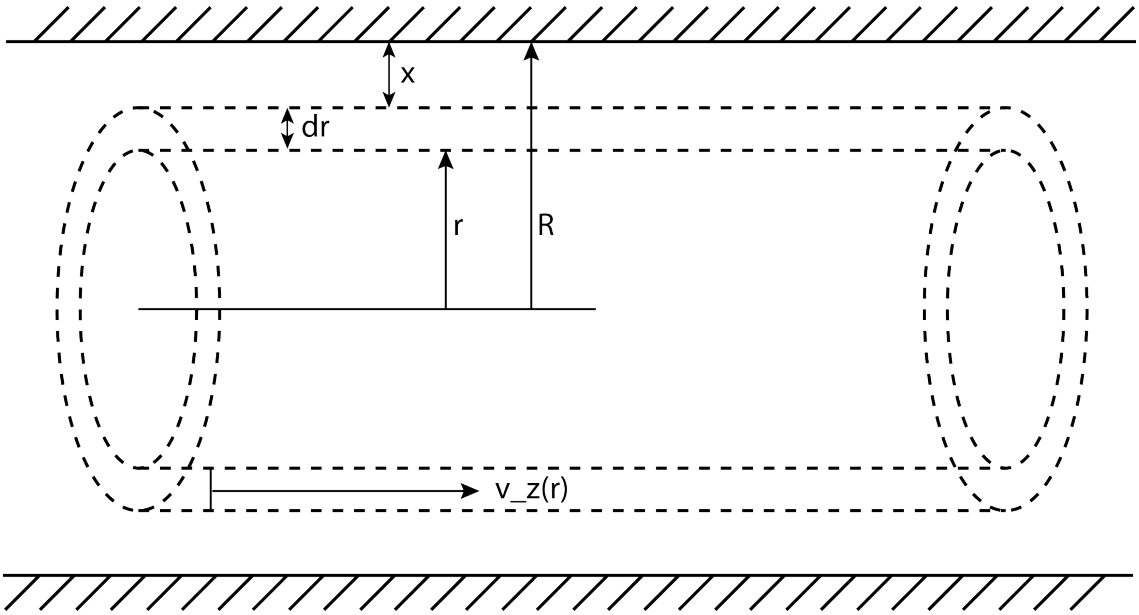

Figur 9: The concept of streaming current. The double layer is assumed to be much smaller than the bulk region and to be confined to a thin region near the wall of the capillary. Thus, only values of r near $r = R$ is of importance. The region outside this area is assumed to not bring any electric charge in the current as it is considered neutral.

The double layer is assumed to be much smaller than the bulk region and to be confined to a thin region near the wall of the capillary. Thus, only values of r near $r = R$ is of importance. The region outside this area is assumed to not bring any electric charge in the current as it is considered neutral. By this assumption, we set $r = R - x$. Hence, by substituting the Poiseuille's law;

$$v_z = \frac{1}{4}\frac{\Delta P}{\mu l}(R^2 - (R-x)^2) \\ = \frac{1}{4}\frac{\Delta P}{\mu l}(R^2 - (R^2 - 2Rx + x^2)^2). \tag{2.27}$$

The x is regarded a small number, so that x^2 can be neglected. Further:

$$v_z = \frac{1}{4}\frac{\Delta P}{\mu l}(2Rx) = \frac{1}{2}\frac{\Delta PR}{\mu l}x. \tag{2.28}$$

The formula is substituted into eq. (2.26), and using the assumption that $r = R - x$ and that x is small, we get

$$I_s = -\int_R^0 2\pi(R-x)\frac{PRx}{2\mu l}\,\rho(x)dx \approx -\frac{\pi R^2 P}{\mu l}\int_R^0 x\rho(x)dx. \tag{2.29}$$

The Poisson's equation (2.7) is substituted with respect to $\rho(x)$:

$$\rho(x) = -\frac{d^2\psi}{dx^2}\epsilon \tag{2.30}$$

$$\rightarrow I_s = \frac{\pi R^2 P}{\mu l}\int_R^0 x\frac{d^2\psi}{dx^2}\epsilon dx,$$

and integrating by parts:

$$I_s = \frac{\pi R^2 P\epsilon}{\mu l}\left\{\left(x\frac{d\psi}{dx}\right)_{x=R}^{x=0} - \int_R^0 \frac{d\psi}{dx}dx\right\}. \tag{2.31}$$

The first term in the brackets disappears because $d\psi/dx$ is zero when $x = R$, and long before that. The integration is not valid for the whole integration range. The contribution to the integral are confined entirely to the thin layer near the capillary wall (x<<R). Thus, the streaming current is, by the following assumptions

$$I_s = \frac{\pi R^2 P\epsilon}{\mu l}\int_0^\zeta d\psi = -\frac{\epsilon\zeta}{\mu}\pi R^2 P. \tag{2.32}$$

Note that ζ is the zeta-potential. There is no streaming current beyond this point (as the ions are immobile). The streaming potential (E_s) will, as discussed earlier, generate a conduction current in the reverse direction. The conduction current is, by definition, given as;

$$I_c = \pi R^2 E_s \sigma_{eff}. \tag{2.33}$$

Steady state is achieved when the streaming current equalize the conduction current ($I_s = I_c$). Thus,

$$-\frac{\epsilon\zeta}{\mu}\pi R^2 P = \pi R^2 E_s \sigma_{eff}, \tag{2.34}$$

$$-\frac{\epsilon\zeta P}{\mu} = E_s \sigma_{eff} \rightarrow E_s = -\frac{\epsilon\zeta P}{\mu\sigma_{eff}}, \tag{2.35}$$

thus we get the Helmholtz-Smoluchowski equation:

$$\frac{\Delta V}{\Delta P} = C = \frac{\epsilon_w \zeta}{\mu_w \, \sigma_w}. \tag{2.36}$$

3 Experiment arrangement

3.1 Introduction

Measuring streaming potential is not straight forward. There are difficulties obtaining a good regression as we are dealing with small variations in the electrical potential for which streaming potential are measured. Lower salinity brine or deionized water is, however, less tricky to measure due to low conductivity and thus a greater magnitude of the streaming potential coupling coefficient (C) relative to the overall conductivity of the sample. The electric signal required to read the potential across the core may be disturbed by static background noise, especially for higher salinity brines. Thus, imprecise data may be observed at high salinities. The sources of background noise can be everything from thermal disturbance to light and signals from electronic devices influencing the electric field. The electrometer itself can also disturb the current flows unless the internal impedance is set to a high value, i.e. >1 GΩ (Jaafar, Vinogradov et al. 2009).

Good results correspond to a great linear regression of the coupling coefficient when plotting the measured voltage as a function of differential pressure across the core. This is basically the case if the streaming potential is showing a stable and constant value for a constant differential pressure. If the streaming potential does not stabilise for stable values of differential pressure, the calculation of the coupling coefficient is not straight forward, because the Helmholtz-Smoluchowski is only valid at steady state. However, by running experiments with pressure ramping and at the same time continuously logging the voltage and pressure, static voltage may be less disturbing because the time spent during pressure ramping is much less than for paired stabilised experiments.

For the following sections, a detailed description of the equipment used to run experiments is presented as well as how data was processed in order to analyse the results.

3.2 Experimental setup

Researchers from Imperial College has published quite detailed papers regarding experiments of streaming potential (Measurement of streaming potential coupling coefficient in sandstones saturated with natural and artificial brines at high salinity) (Jaafar, Vinogradov et al. 2009). Therefore much of our set up is based on their methodology. The following equipment at IRIS was initially assembled, yet some adjustments was necessary to execute in order to reduce sources of error. In this chapter, the "final" setup template is presented, which was the fundamental to run experiments presented in chapter 4.

3.2.1 Core

Berea Sandstone cores were used in these experiments. Berea sandstones has been widely used as a model rock for porous media flow and within oil industry research. Berea is a sedimentary rock mainly composed of quartz held together by silica. The permeability of these sandstones ranges widely from a few millidarcy toward several Darcy (www.bereasandstones.com). Two sandstone cores with low permeability was chosen to this experiment so that sufficient pressure difference could be obtained. They were both drilled from the same block.

Figur 10: Berea sandstone cores. Both are from the same mother core.

The table below shows some properties of the core and herby the permeability calculated. The mathematical calculation of the permeability estimation is presented in the Appendix.

Table 1: Core properties.

	Core number	
Property	**Core I**	**Core II**
Length (cm)	6.98	6.81
Diameter (cm)	3.73	3.70
Weight dry (g)	163.36	159.9
Weight wet (g)	177.2	172.3
Brine viscosity (cP)	1	1
Brine density (mu)	1000	1000
Porosity (%)	18.15	16.98
Permeability	39.11 ± 1.36	40.05 ± 1.13

3.2.2 Core holder

The core was assembled with in a core holder (in-house IRIS design) made of stainless steel. The core itself was held in place with an inlet end-piece and an outlet end-piece that was non-metallic (plastic). When measuring the streaming potential, it is very important that the core and brine is separated from all conductive materials so that no electrical current is going other ways than through the core and brine itself, hence the plastic end-pieces.

The core was placed in a rubber sleeve and tightly confined with Marcol oil as confining fluid. To make sure that the confining pressure was maintained, a cylinder of compressed nitrogen was connected to the confining chamber. The confining pressure was kept around 30 kPa, which is significantly more than the maximum differential pressure applied across the core (5 kPa).

The core was saturated with brine by connecting a vacuum pump to the core holder, close the valves and then open with brine connected to the valves.

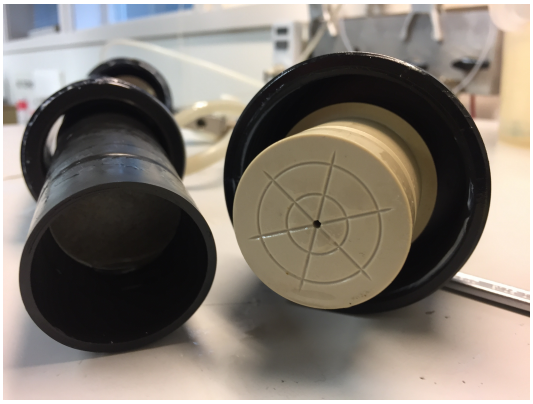

Figur 11: Rubber sleeve and core holder peak. The core is fully isolated by plastic to avoid conductance beyond desired area. End piece of peak (plastic) shown.

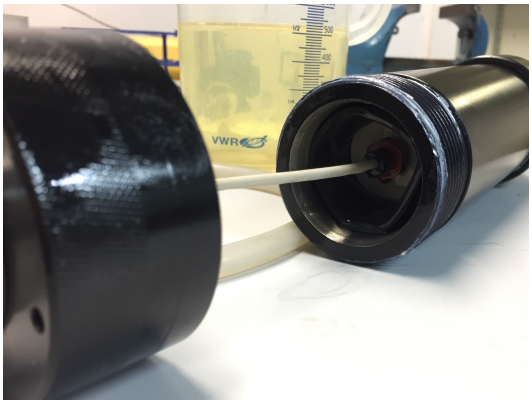

Figur 12: Peak and tube. The peak is connected to a plastic tube to avoid that the core and brine conduct toward to the core holder, which are made of steel.

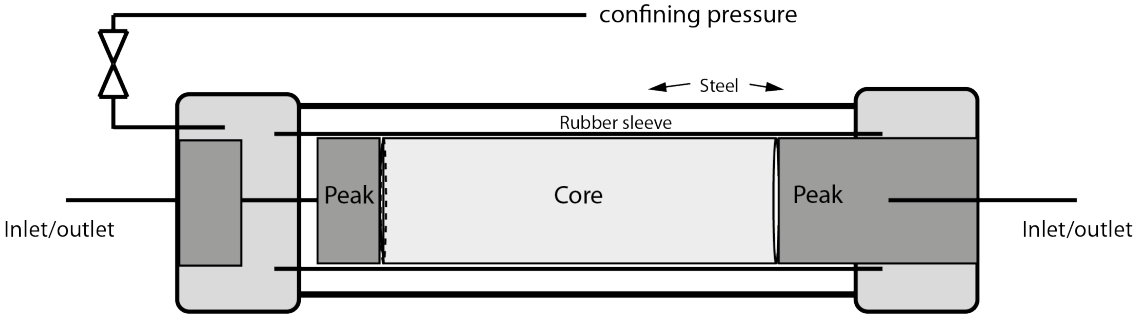

Figur 13: Core holder. The core is radial surrounded by a rubber sleeve and two plastic peaks on each side. The confining fluid is present in the entire core holder and maintained by compressed nitrogen trough a purge in case of pressure leakage.

Figur 14: Assemble the core holder. The core was placed in the rubber sleeve and connected to the peak valves, it was tightly confined with synthetic oil.

Figur 15: Manual hydraulic pump to generate a confining pressure around the core in the core holder.

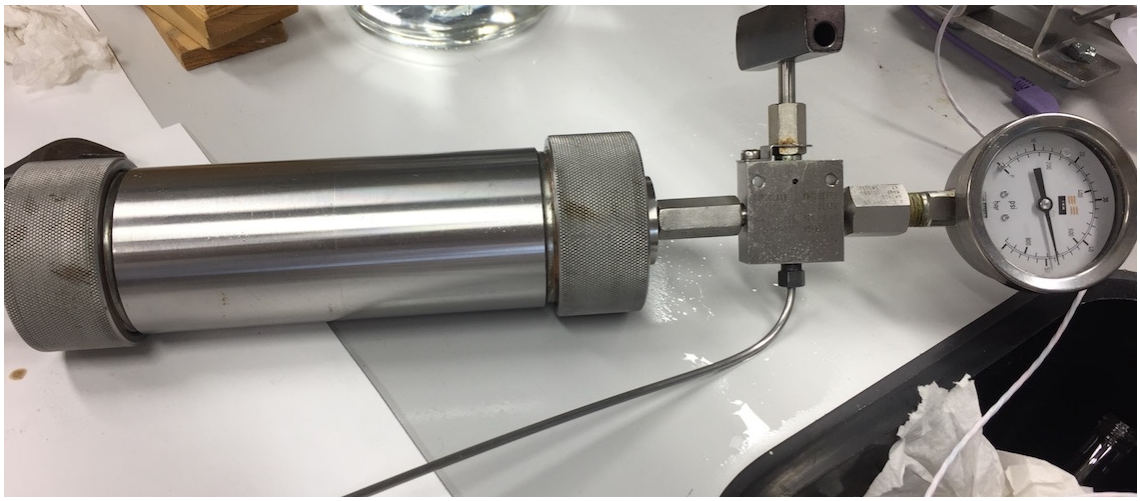

Figur 16: Confining pressure. Cylinder filled with compressed nitrogen in order to maintain confining pressure.

3.2.3 Pressure vessel, brine reservoir, pump and flowlines

The core holder was connected to two cylinders by plastic tubes, one for each side of the core holder. The cylinders were further connected to a pump with oil (isopar-H) as the driving force. Thus, the cylinder contained oil as the upper phase to translate the pressure into the brine as the lower phase. The reason oil was used as pump fluid instead of the brine is to;

- prevent flow of an electrical current through the pump parallel to the core sample. Oil is a non-conductive fluid and will prevent that any electrical signal from the pump may disturb the potential measurements across the core.

- allow air bubbles to migrate from the brine and up to the top of the oil column.
- prevent exposure of the brine to the air, which could cause a change in the pH.
- reduce corrosion of the pump.

All parts of the cylinders that was directly in contact with the brine was made of plastic. All the flowlines were plastic, except for the valves that was metallic. The metallic parts that was touching the table was separated with clipped rubber sleeves to prevent conduction of unwanted electrical noise that could travel through the table in to the equipment through the metallic valves.

Theoretically, nothing else than the electrical potential across the core should be measured from the electrodes as the brine was separated from everything except the core itself.

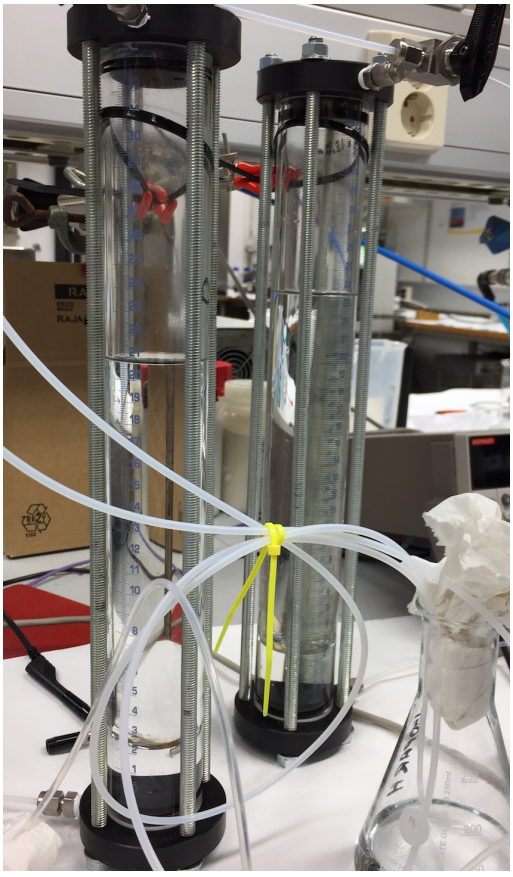

Figur 17: Cylinders. The pressure from the oil column in the upper zone is translated down to the brine zone (Jaafar, Vinogradov et al. 2009).

Figur 18: Isolation of metallic valves. All valves and other metallic parts that has any connection to the brine must be prescind from any sources that may disturb the measurements. This metallic valve was separated from the table with a clipped rubber sleeve.

A Waters pump [515 HPLC] was used during the first month of experiments. It was later replaced with a Quizix pump [QX model]. This is a sophisticated pump which is known to deliver fluid with a very high precision. With such a pump, all errors regarding non-

stability rate could be eliminated. In addition, the Quizix pump could ramp up the pressure, and thus, pressure ramp experiments could be performed.

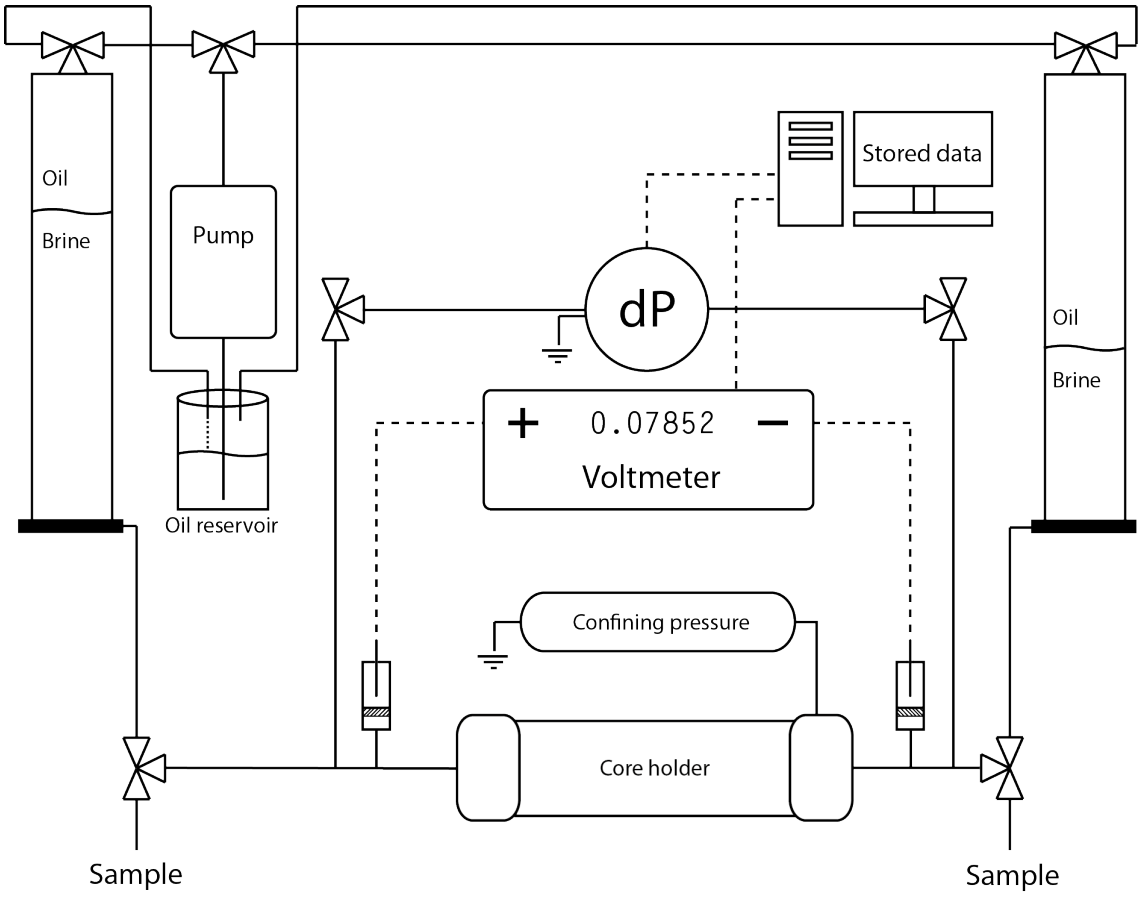

Figur 19: Experimental overview.

3.2.4 Differential pressure gauge

The differential pressure across the core was measured by connecting tubes from the inlet and the outlet of the core toward a pressure gauge. This pressure gauge measured the pressure hydraulically on both sides of the core and thus calculated the differential pressure. The fluid that was connected to the pressure gauge was replaced with Isopar in order to prevent any electrical circuit that would occur via the gauge itself. If brine was used as differential pressure fluid, a parallel electrical current would travel via the pressure gauge as well as through the core.

The isopar was prior mixed with colorant (Sudan blue) as a safety to detect any intrusions to the brine tubes.

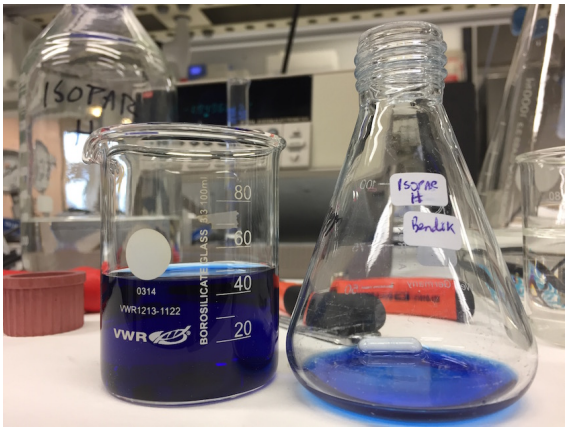

Figur 20: Isopar with colorant.

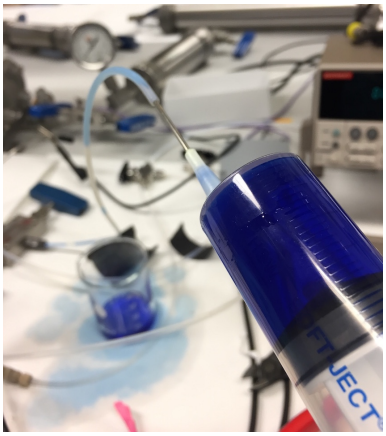

Figur 21: Injection of coloured isopar to the pressure gauge tubes using a needle.

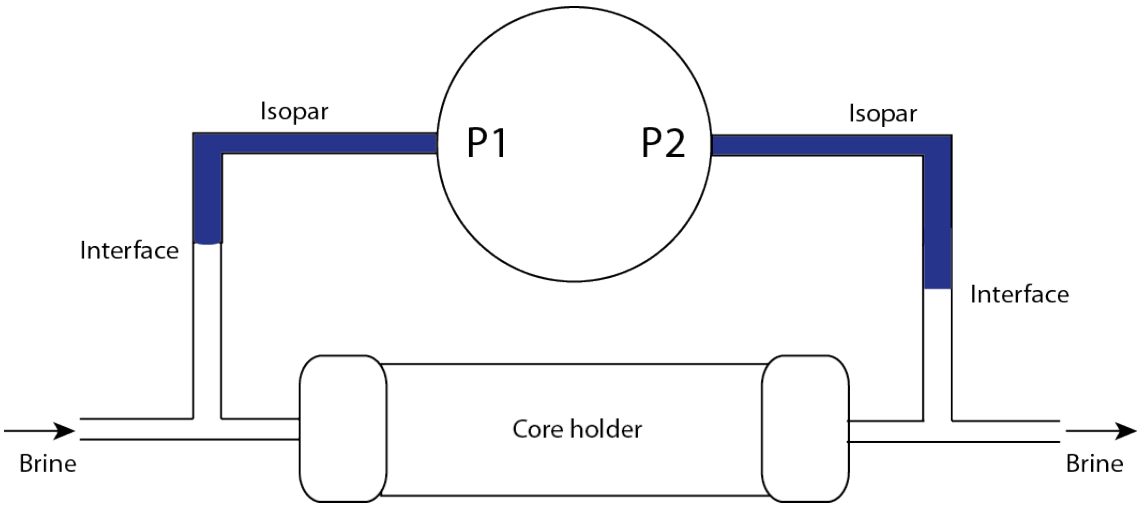

Figur 22: Differential pressure gauge. Brine is injected from one side. Pressure from the brine is translated equally to the core and to the gauge via the coloured isopar. The isopar might come too close to the brine-tube. This would be detected and prevented by changing some of the isopar fluid.

3.2.5 Electrodes

The streaming potential was measured using a pair of non-polarized silver chloride (Ag/AgCl) electrodes. A silver chloride electrode is a type of *reference electrode,* which means it has a stable and well-known electrode potential. It functions as a redox electrode. The equilibrium is between the silver metal (Ag) and its salt, silver chloride (AgCl) (Karplus 2014). The chemical equation for this process can be written as

$$Ag^+ + e^- \rightarrow Ag(s), \tag{3.1}$$

$$AgCl(s) \rightarrow Ag^+ + Cl^-, \tag{3.2}$$

and the overall process can be presented as

$$AgCl(s) + e^{-} \rightarrow Ag(s) + Cl^{-}. \quad (3.3)$$

Non-polarized electrodes are used in surveys requiring precise and sensitive measurements. Polarization effects is noise that occur using metal electrodes, distorting the measurements one are looking for (Geoscience 2017).

Each electrode was located in a small brine reservoir that was in contact with the flowing brine, allowing the measurement of ions from the current. A low-permeable porous disc (glass filter) separated the electrode and its reservoir from the flow path to prevent streaming current that potentially could disturb the stability of the electrical measurements. The electrodes and its reservoir chamber was positioned a slight distance away from the core holder and out of the flow path to eliminate electrode flow effects.

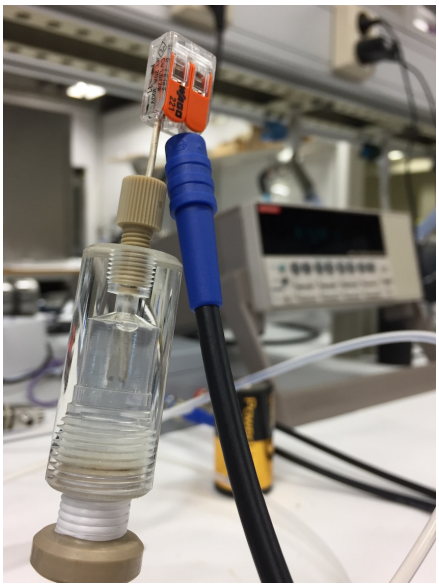

Figur 23: Electrode.

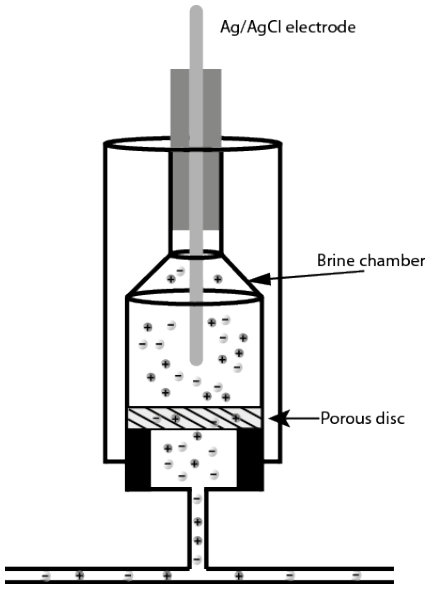

Figur 24: Concept of the electrode. Silver chloride electrode detects streaming currents by reactions.

3.2.6 Electrometer

The electrical potential across the core was measured using a Keithley model 6514. The electrometer is able to measure with a high digit resolution (10 μV) and has an input impedance of >200TΩ on voltage measurements (Model 6514 User Manual). It periodically measures internal voltages corresponding to offsets to maintain stability and accuracy over time and changes in temperatures. This process is known as autozeroing.

In the process of installing the electrometer and enable it for measurements, the *Zero correct* function was enabled to algebraically subtract the voltage offset term from the measurement. The display should show VCZ, which indicates that the displayed reading is zero corrected.

3.2.7 Brine

Synthetic brine was prepared by mixing a specific amount of Sodium Chloride (NaCl) or Calcium Chloride ($CaCl_2$) with deionized water. The brine was stirred for at least one hour using magnet stirrer and filtrated trough 0.45 micrometer filter using a vacuum pump.

The composition of the brines used in the experiments was 0.02 M, 0.1 M, 0.3 M, 0.6 M, 1.2 M and 2.0 M for NaCl and 0.0067 M, 0.033 M, 0.1 M and 0.2 M for $CaCl_2$.

3.2.8 Equilibrium between the core and the brine

The electrical double layer (and hereby the zeta-potential) are sensitive to the interaction between the brine composition and the surface of the sample. Thus, it is important that prepared brine to be equilibrium with the core sample.

Equilibrium was obtained by circulating the brine through the core via the pump. The volume was minimized (unnecessary quantity that would prolong the time needed to obtain equilibrium between the core and the brine). Effluent samples were analysed to verify equilibrium. Two samples taken between *some hours* showing the same value of pH and conductivity would indicate equilibrium (a fluctuation of 0.10-0.15 pH was acceptable). The brine was, during circulation, stirred with a magnet to mix the brine properly during circulation. The brine reservoir was sealed with parafilm to prevent exposure of air that could cause a change in pH.

By experience; circulation 1 litre of brine trough the core during one night with a rate of 3-4 ml/min proved to be satisfying.

After equilibrium was observed, the brine was injected to the cylinder reservoirs and the pumps driving fluid was changed back to isopar. Experiments could now be performed.

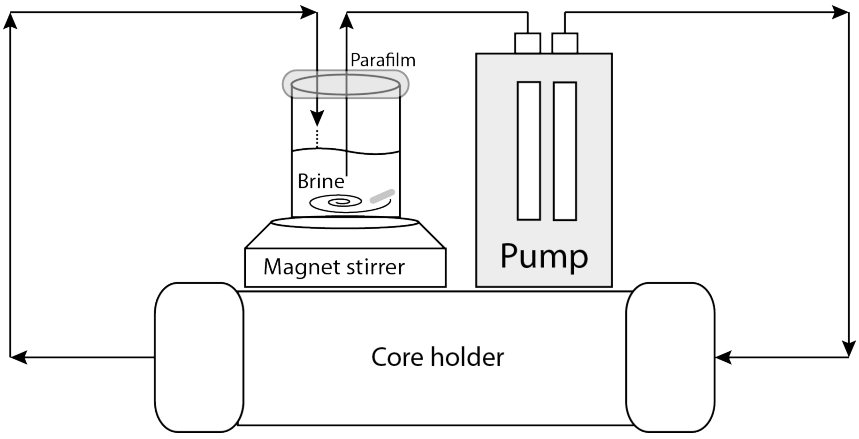

Figur 25: The process of circulating the brine.

3.2.9 Surface conductance

It was necessary to find the resistance of the saturated formation as well as calculating the formation factor. If these factors are known, one can use eq. (2.22). Hence, the estimation of the zeta potential for low salinities of the brine should work out. The estimation of surface conductance and formation factor is explained in detail in section 3.3.

The Berea core 1 was assembled into another core holder with steel tubes that could conduct electricity from the core and trough the tubes. Since the two Berea cores was taken from the same long mother core, the same formation factor was used for both. The resistivity of the fluid saturated core was measured using a FLUKE PM6304 impedance measurement device. Two electrodes were connected from the devise: one on the steel tube next to the core holder (which was directly in contact with the core) and the other on the confining pressure tube (to work as grounding).

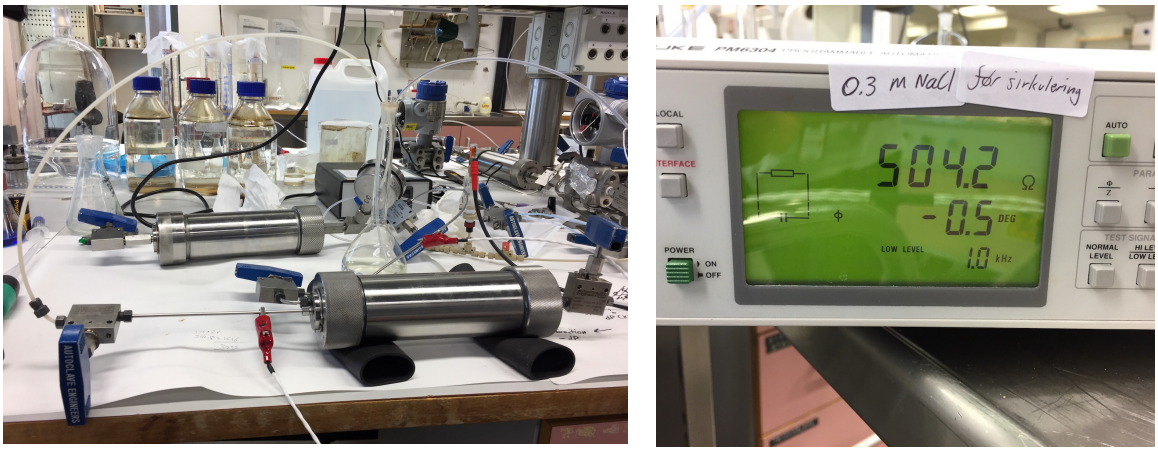

Figur 26: Resistance measurement. Brine is injected trough the core and wasted until the resistance remains constant. Thus, the core is fully saturated with one distinct brine.

3.3 Experimental implementation and data processing

The streaming potential coupling coefficient can be obtained from the slope of a linear regression when plotting the electrical potential as a function of differential pressure. This is done by applying a constant rate from the pump, then wait until the differential pressure across the core has stabilised as well as the streaming potential is constant with a low variation in the static voltage. When stabilised pressure and streaming potential is noted, a new constant rate is applied in the opposite direction. The same procedure is repeated for different rates. The more rates applied, the better is the accuracy of the linear regression. In this thesis, at least four paired rates (eight distinct data points) has been the standard procedure. The reason that the direction of flooding is changed every time is to avoid polarization effects.

3.3.1 Paired experiments

The method just described above works well in samples saturated with brine of low salinities (<0.1 M). For brines saturated with higher salinities, the magnitude of the streaming potential is much smaller, and temporal variations in background noise must be accounted for. These variations can be eliminated by executing *paired experiments.* The procedure of the experimental implementation itself is exactly the same as described in the previous paragraph, but the way the data in processed is different;

Vinogradov (Jaafar, Vinogradov et al. 2009) presented a mathematical method in which variations in background noise could be eliminated by conducting paired experiment for a short time interval (ca. 1 hour each pair). We did this by flooding in one direction with a constant rate, then stop the pump and switch the flooding direction of the core. Start the pump and flood with the same rate. The stabilised voltage in each experiment within a pair is given by;

$$V_{m1} = V_s + V_{static1}, \tag{3.4}$$

$$V_{m2} = -V_s + V_{static2}. \tag{3.5}$$

V_m is the measured voltage and the two numbers refer to each direction within the pair. For each direction V_m is separated into two terms; V_s is the actual streaming potential and V_{static} is the static potential/background noise. The static voltage is assumed constant within a pair ($V_{static1} = V_{static2}$). Now, the pressure difference and the stabilised voltage for the first direction (number 1) is subtracted from the one for the second other direction (number 2). This yields

$$V_{m1} - V_{m2} = 2V_s, \tag{3.6}$$

$$\Delta P_{m1} - \Delta P_{m2} = 2\Delta P. \quad (3.7)$$

A plot of $(V_{m1} - V_{m2})$ as function of $(\Delta P_{m1} - \Delta P_{m2})/2$ should give an approximately strait line. A linear regression of this plot gives the streaming potential coupling coefficient.

The table below illustrates an example of how the output data for a paired experiment is presented in the result section. Flooding in A-direction yields negative differential pressures and increased voltages, while B-directions is vice versa. The STD DEV is the standard deviation of the voltage logged. Vmax-Vmix is the difference in the voltages measured for which the pressure was stable. A high number implies a more unstable experiment. If the number is low or not even mentioned, the experiment can be regarded satisfactorily stable. If the linear regression is based on the *mathematical paired experiment* the data comes from the two last columns ((Vm1-Vm2)/2 (mV) and dP/2).

A-direction				**B-direction**				**Paired stabilised**	
Volt (mV)	dP (kPa)	STD DEV	Vmax-Vmin	Volt (mV)	dP (kPa)	STD DEV	Vmax-Vmin	(Vm1-Vm2)/2 (mV)	dP/2
56.900	-13.5	0.043	0.04	55.66	12.2	0.07	0.07	-0.619	-12.8
57.599	-26.2	0.061	0.06	54.94	24.2	0.06	0.06	-1.328	-25.2
58.719	-49.8	0.032	0.03	53.81	47.3	0.04	0.04	-2.453	-48.5
61.042	-97.6	0.043	0.04	51.40	93.6	0.17	0.17	-4.820	-95.6
63.337	-144.4	0.026	0.03	49.28	139.8	0.17	0.17	-7.031	-142.1
65.795	-196.8	0.065	0.14	47.70	189.3	0.38	1.29	-9.046	-193.1

Figur 27: Example of data output from paired stabilised experiment.

The figure below (Figur 28) illustrates a screenshot of a testing procedure from the laboratory. 0.3 M NaCl was used. The pressure (blue line) is increased stepwise up to a certain top. The streaming potential (green line) follows continuously. When the pressure is decreased stepwise, the streaming potential follows continuously, but its static value has changed. The voltage is not the same within the same pressure anymore. Such problems are dealt with using equation (3.6) and (3.7), assuming that the static voltage is the same within each pair.

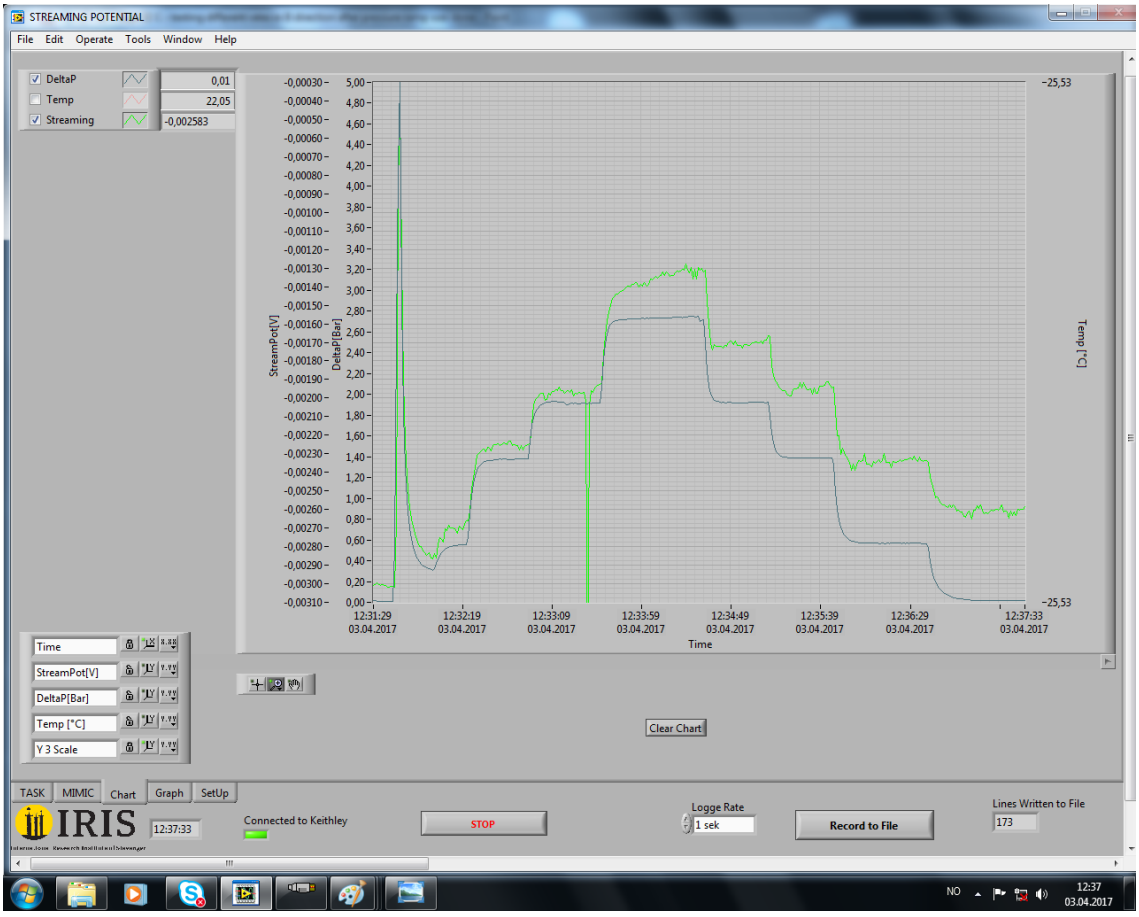

Figur 28: Screenshot from the laboratory computer. Pressure is increased and decreased stepwise. The streaming potential does not have the same value within the two distinct pressures due to variation in static voltage.

3.3.2 Pressure ramping

Another method conducted was the *pressure ramping method*. The differential pressure across the core was increased linearly from zero and up to approximately 400-500 kPa over a period of 30, 60, 120 and 240 seconds. The data was logged every second in the pressure ramping period.

This method is very simple and effective to implement. In cases where the magnitude of the streaming potential is very small and the variations of the background noise is making a serious impact of the stability, the ramping method can be a powerful tool dealing with the stability problems. The short experiment period cause a very limited change in the static voltage compared to the stabilised method which may take several hours to implement. This is important to have in mind, especially for experiments where data interpretation is difficult using the paired stabilised method. However, the disadvantage using the pressure ramping method is that uncertain results can be obtained as an equilibrium state may not be achieved if the pressure is ramped too quickly.

For each time interval, the ramping was first implemented in one direction (negative differential pressure). Then, the injection was implemented the opposite direction (positive differential pressure). Ideally the slope of both directions should be the same.

For the Excel data processing, the static background noise was reset to zero immediately when the pressure ramping started.

The screenshot below illustrates a successful pressure ramping with a time range of 240 second using 0.02 M NaCl + CaCl2 residuals. The streaming potential glides smoothly along with the pressure that is ramped linearly.

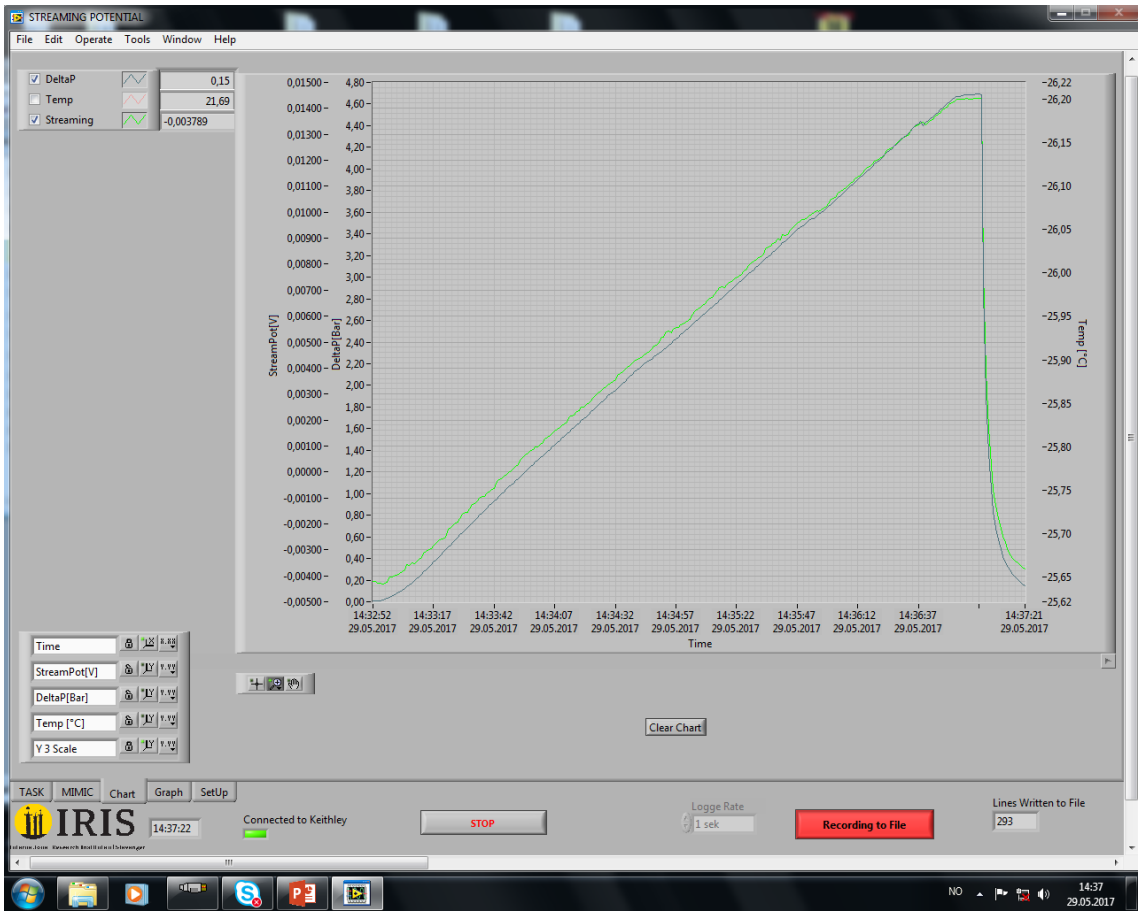

Figur 29: Pressure ramping LabView.

3.3.3 Saturated brine conductivity

The conductivity of the saturated brine was measured using two electrodes on an external core holder over the frequency range of 0.1, 1, 10 and 100 kHz. The measured parameters were impedance (Z), frequency (f) and resistance (R). The reactance (X) was calculated as

$$X = \sqrt{Z^2 - R^2}. \tag{3.8}$$

The value of the resistance (R) that corresponded to the minimum reactance (X) based on different frequencies was taken to be the resistance of the sample. That is, small inequalities within impedance and reactance. Frequencies corresponding to minimum reactance was for almost all measurements 10 kHz. The following rock conductivity is calculated using the following formula:

$$\sigma_f = \frac{L}{R\pi r^2}. \tag{3.9}$$

L and r^2 is the length and radius of the core.

3.3.4 Interpretation of the formation factor (F)

The formation factor is measured by plotting the measured values of the saturated rock conductivity as a function of the brine conductivity. A slope of a linear regression though the linear region is made. An inverse of this slope yields the formation factor. See figures below. The formation factor yield 21.10 based on NaCl measurements and 22.12 from $CaCl_2$ measurements. Hence, they differ with 4.8 %.

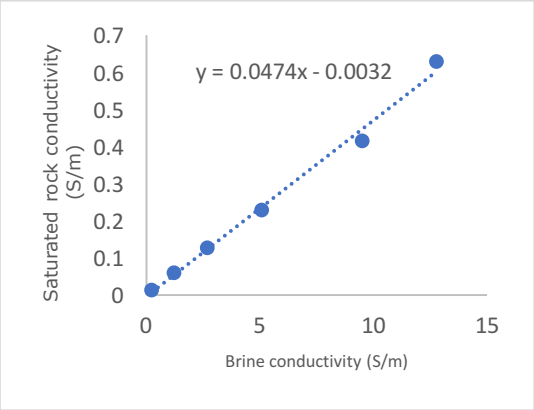

Graph 1: Formation factor NaCl. F=21.10. Saturated rock conductivity vs. brine conductivity from 0.02 M to 2.0 M. The inverse of the slope of a linear regression yields the formation factor.

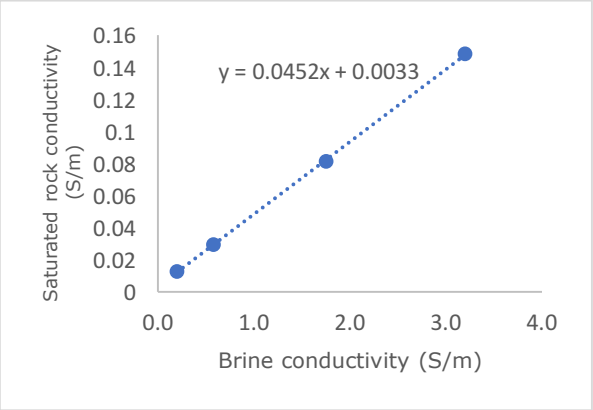

Graph 2: Formation factor CaCl2. F=22.12. Saturated rock conductivity vs. brine conductivity from 0.0067 to 0.2 M. The inverse of the slope of a linear regression yields the formation factor.

3.3.5 Zeta-potential

The zeta-potential is calculated by substituting equation (2.22):

$$\zeta = \frac{C\mu F\sigma_f}{\epsilon_w}. \tag{3.10}$$

The permittivity is expressed as relative permittivity of water times the permittivity of free space (vacuum);

$$\epsilon_w = \epsilon_{rw}\epsilon_0\,, \tag{3.11}$$

where the relative permittivity, ϵ_{rw}, is dependent on the salinity of the brine. It is calculated based on an empirical formula (Appendix B.1). For deionized water, the value is around 78.3 (unit less) for temperatures around 25 °C. Permittivity of free space is $8.85 \cdot 10^{-12}\ F/m$. The SI units for F (Farad) is $[s^4\ A^2\ m^{-2}\ kg^{-1}]$. Conductivity is expressed in Siemens/metre, which the SI units for Siemens is $[s^3\ A^2\ m^{-2}\ kg^{-1}]$. SI units for viscosity (μ) is Pas (Pascal second), and its magnitude is assumed to be 10^{-3}. The units for the coupling coefficient are mV/MPa. We verify the units:

$$\zeta[mV] = \frac{C[mV\ M^{-1}Pa^{-1}]\mu[Pas]\sigma[Sm^{-1}]F_{(formation)}}{\epsilon_w[8.85 \cdot 10^{-12}Fm^{-1}]} = \frac{[VsS] \cdot 10^{-6}}{[8.85 \cdot 10^{-12}F]} \tag{3.12}$$

The 10^{-6} occurred because pressure was expressed in $(MPa)^{-1}$. Substitute for S and F;

$$\zeta[mV] = \frac{Vs\ s^3\ A^2\ m^{-2}\ kg^{-1}10^{-6}}{8.85 \cdot 10^{-12}\ s^4\ A^2\ m^{-2}\ kg^{-1}} \tag{3.13}$$

$$\zeta[mV] = [mV]\frac{10^{-6}}{8.85 \cdot 10^{-12}} \tag{3.14}$$

Hence, for the numerator, insert the coupling coefficient $[mV(MPa)^{-1}]$, viscosity $[Pas]$ and conductivity $[S/m]$ at the numerator. For the denominator one insert the relative permittivity.

3.4 Observations to qualify the setup

This section describes some important observations that was made to make the experimental setup work. In addition, some pitfalls are presented.

3.4.1 The importance of pressure gauge filled with isopar

The paper that was used as template for the setup (Imperial College) did not comment anything about how the differential pressure gauge worked. As an attempt to qualify the setup, there were great instability in the beginning. It was observed that the static voltage changed rapidly when valves on the pressure gauge was turned. The problem was not there if the differential pressure gauge was disconnected (and pressure was based on calculations from the pump rate). The overall problem was fixed when the gauge fluid was changed to non-conductive isopar oil. The figure below illustrates the significance of the problem, even with a low salinity brine (0.02 M NaCl).

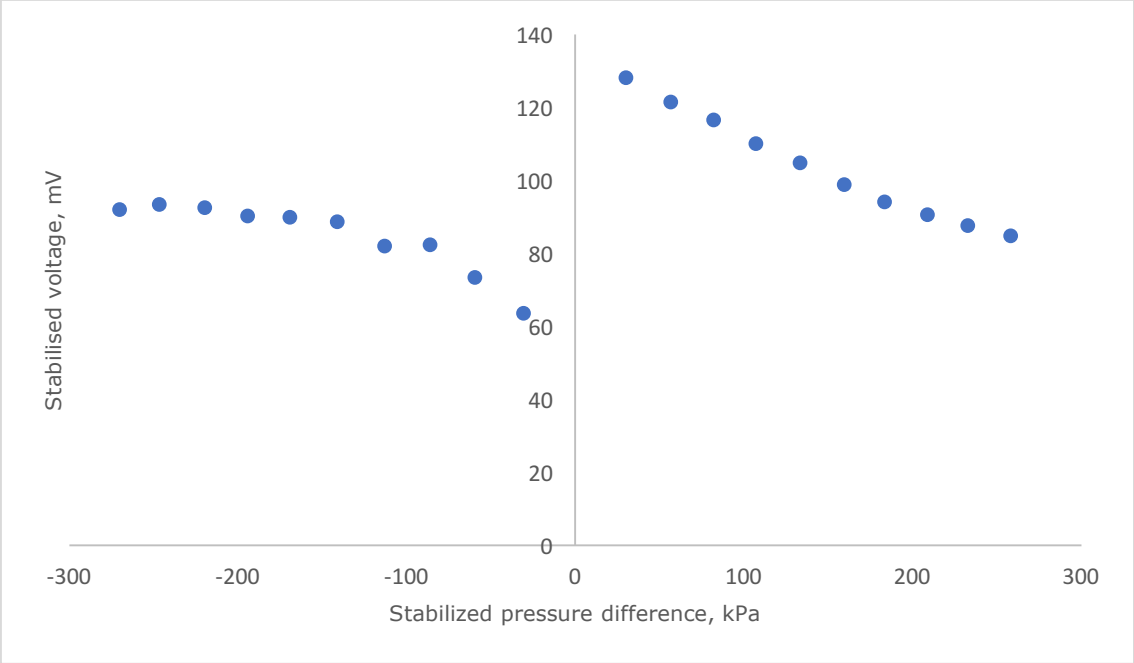

Figur 30: Differential pressure gauge filled with conductive fluid (brine). A parallel circuit trough the core and the gauge cause a nonlinear trend and a rapid change in background noise.

3.4.2 Mind the hidden bubble

A situation that could cause severe problems regarding the logging of the streaming potential could be linked to a hidden air bubble in the tube connected to the electrode. It was observed that the signal could suddenly appear when flicking the electrode. A suspected air bubble was detected as it migrated upward when the electrode chamber was turned upside down. To solve such a problem, the tube was properly filled to be sure that no air was left behind. See figure below.

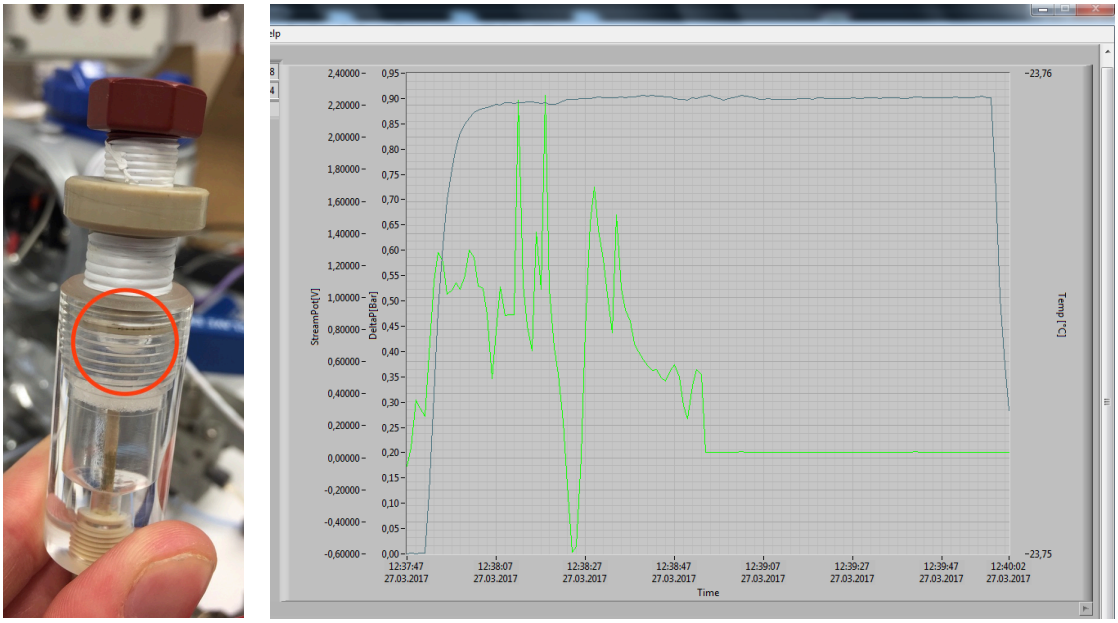

Figur 31: Hidden air bubble. The scapegoat was detected because it was believed that the problem had to do with the electrode somehow. The graph illustrates how stability suddenly appeared (green line) when the electrode chamber was flicked vigorously several times. In the first section the streaming potential is rapidly changing with several volts in magnitude, even the pressure is stabilised. It is credible that this bubble was blocking coherent brine between the electrode chamber and the brine from the rest of the system.

3.4.3 Degassing the brine

Degassing the brine using nitrogen prior to circulation was attempted as a method to speed up the equilibrium. This process did not prove to be useless as the pH increased ca. 0.5 during one hour of degassing. However, it was concluded to not be efficient enough. It was simpler to just run a circulation during one night with a sufficient rate.

3.4.4 Faraday cage

The struggle with fluctuating static voltage was never solved completely. It was tried to move and assemble the entire equipment (except pump and computer) into a heating chamber. The idea was that this could work as a faraday cage to protect the measurements from background noise from other devises. Unfortunately, this did not work at all. It could even look like the variation of static voltage increased after the equipment was moved into the chamber.

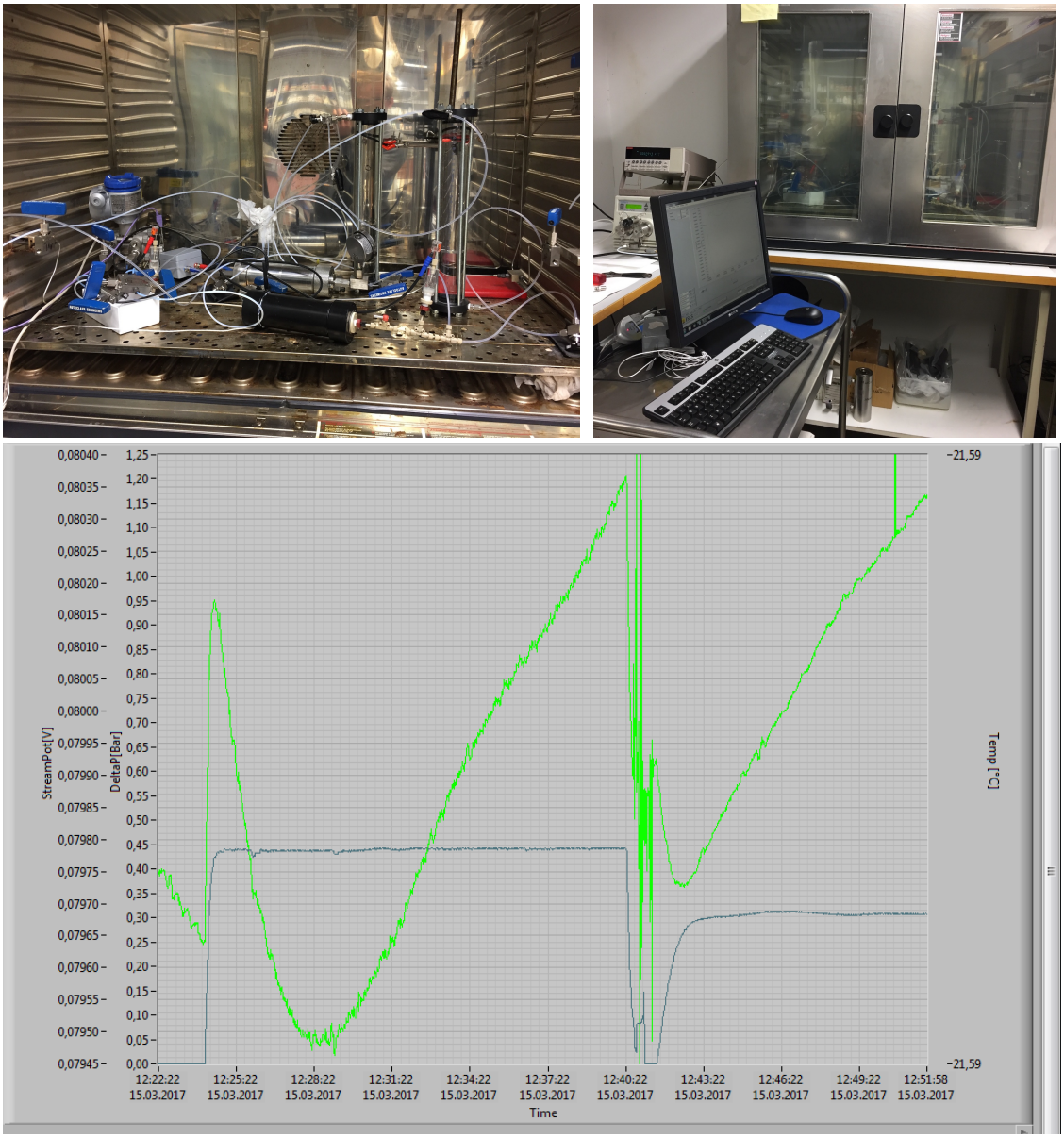

Figur 32: Faraday cage. Attempt to reduce the fluctuation by seal the entire system in a heating chamber. Unfortunately, this even increased the problem of instability.

3.4.5 Disturbance from pump

The figure below illustrates the disturbance of the pump if no isopar is put in between as did in the experimental setup. In the current situation, the brine is in equilibrium with the core under a circulation process of constant rate.

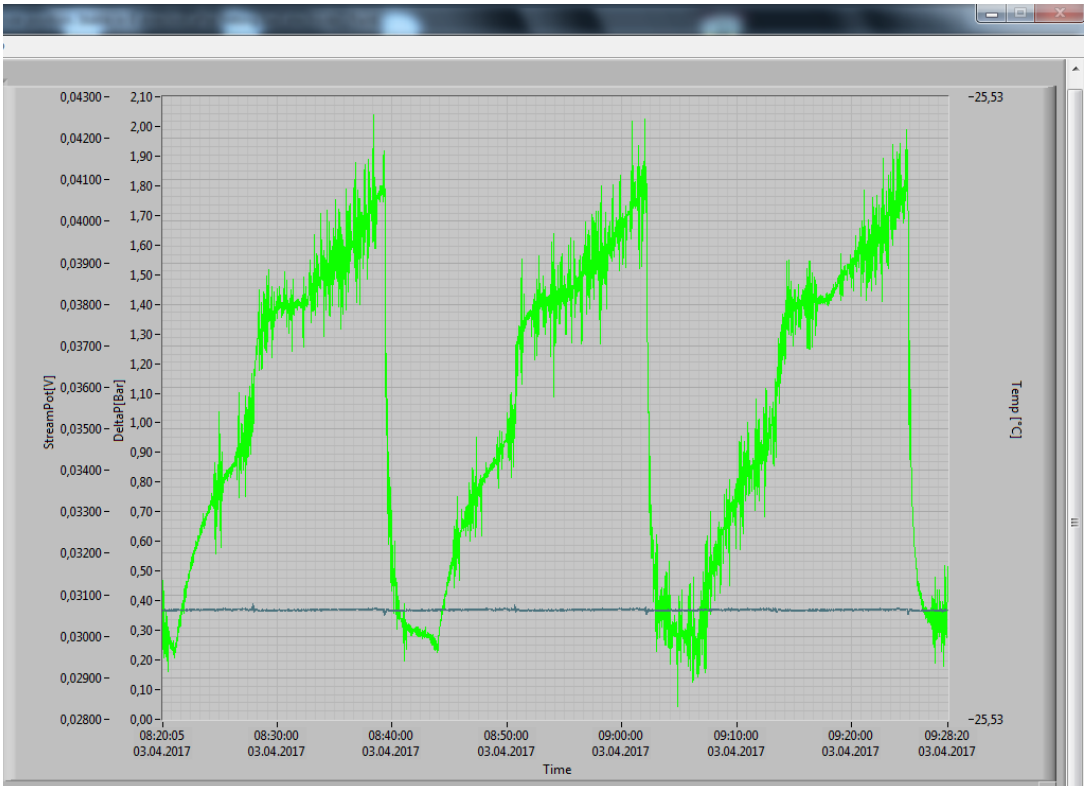

Figur 33: Pump disturbance. If the brine is flooded directly from the pump into the core, a parallel circuit is present.

4 Results

The results of the experiments will be presented in the order of the brines salinity, from low salinity to high salinity. The NaCl-brine is presented first. Then, the $CaCl_2$-results are presented. The experiments with low salinity brines was usually first conducted as they were easier to implement.

4.1 NaCl experiments with different salinity

A summary of all the results obtained from all the salinities are given in (Table 2). Samples of pH and conductivity was taken to verify stabilisation prior to the experiments. The original and final values are shown. For the *coupling coefficient* section; *paired* refer to the paired stabilised experiments while the numbers refer to the time range of each distinct pressure ramping experiments. Note that some of the experiments do have a higher uncertainty than the other. Information and uncertainty regarding each experiment are presented in more details in the coming sections.

Table 2: Summary of results for NaCl brine.

	pH		**σ (S/m)**		**Coupling coefficient (mV/MPa)**					**Expt**
Sal	Orig.	Equi.	Orig.	Equi.	Paired	240	120	60	30	
0.02	7.75	7.56		0.2081	48.0					9
					44.7					8
					55.3					10
					48.3					13
	7.75	8.08			51.1		53.1			28
0.1	5.73	8.08	0.472	0.829	13.3					21
					11.7					22
0.3	5.59	8.12		2.54		4.10	4.70	4.80	5.10	33
					5.20			4.80	4.80	34,35
0.6	5.60	9.02		5.52	2.57		2.49	2.45	2.46	37,38
					5.20			4.80	4.80	39
1.2	6.03	8.49	9.10	9.03				0.62	0.74	40,41
2.0	5.68	8.78	14.64	14.09			0.40	0.35	0.34	44
										45

4.1.1 0.02 M NaCl experiments (no LabView for data acquisition)

The first brine with its lowest salinity was the 0.02 M NaCl brine. In these experiments, we performed manual reading of dP and dV as LabView for data acquisition was not installed. Several initial tests were performed to verify that the voltage and pressure signal and the other results made sense. It was said that the experimental setup and results proved to give reliable results when three nearly identical experiments were conducted at different times.

or the three first experiments presented, no computer was installed to register and log the data. Hence, the streaming potential was determined by reading from the electrometer when the voltage was stable, i.e. when the temporal variation in background noise was less than 1 mV it was determined a stable reading. The results of the experiment gave a coupling coefficient of 44.7 mV/MPa with R^2=0.9941, 48.0 mV/MPa with R^2=0.9955 and 55.3 mV/MPa with R^2=0.9965, where the slope was obtained by a linear regression when plotting stabilised voltage as a function of stabilised pressure (see Graph 3). The linearity of the regression was regarded accurate as they are all above 0.99. The difference in the magnitude of the coupling coefficient was, however, 10.6 mV/MPa, which corresponds to a difference of 23.7 %. Because no computer was used to do the logging, one must have in mind that there are uncertainties related to time-dependence in the voltage signal (as will be shown later). The results are presented in the graph below.

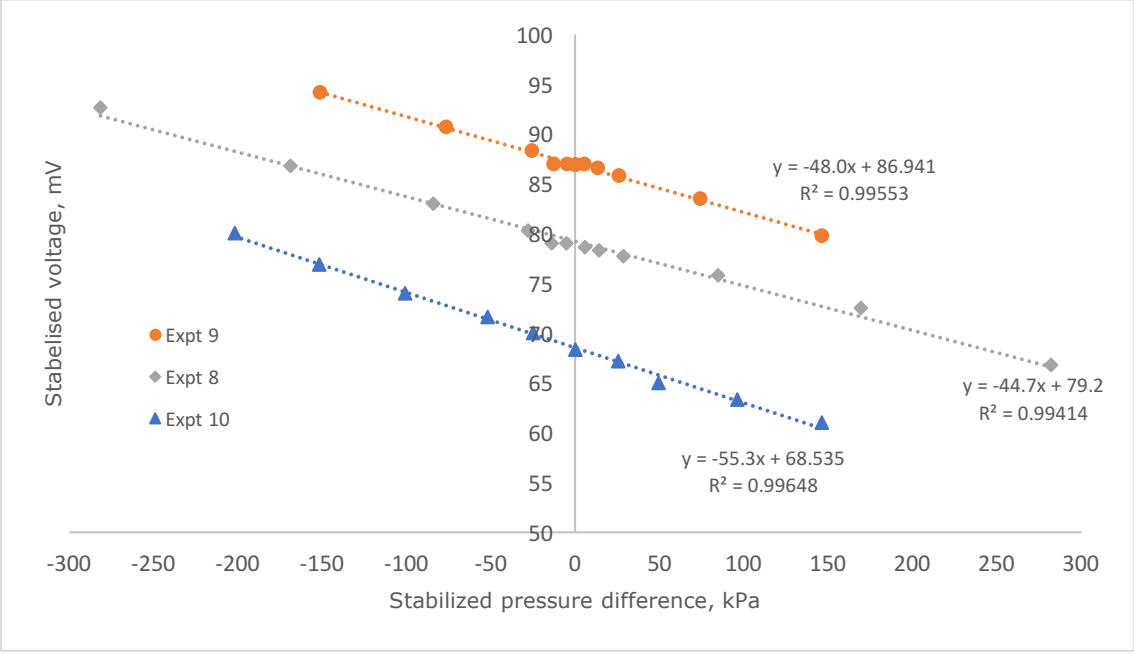

Graph 3: Stabilised voltage against pressure difference for Berea sandstone core 1 using 0.02 M NaCl. Three nearly identical experiment was conducted where the coupling coefficient yield 44.7 mV/MPa with R^2=0.9941, 48.0 mV/MPa with R^2=0.9955 and 55.3 mV/MPa with R^2=0.9965.

As seen, the static voltage is not constant, but rather different with a magnitude of ca. 17 mV within the lowest and highest static voltage from the experiments conducted. Note that these experiments were executed on different days. An offset of 17 mV in between experiments are not of any significant importance as long as a linearity between dP and dV are seen within each experiment (at least less than 1 mV for low salinity brines).

In the rest of the experiments a computer was installed to logged and store data from the differential pressure gauge and voltage difference across the core. This reduced the statistical errors and it provided an improved visualization of the results that were obtained.

4.1.2 0.02 M NaCl experiment

A new experiment was conducted using the 0.02 M NaCl brine with the computer logging. The logging results can be seen in Graph 4 below. Here, Core 1 was used. The green line shows how the streaming voltage potential changes with respect to the pressure applied across the core (blue line). The measured voltage (green line) can be regarded stable and accurate as it remains constant within each distinct stabilised differential pressure. The only exception was the last pair conducted (from approx. 3000 sec and onwards) as the streaming potential did not stabilise and its initial static voltage seem to have been adjusted positively 1 mV from the beginning of the experiment (from 56 to 57 mV), which for some reason happened for the last rate conducted.

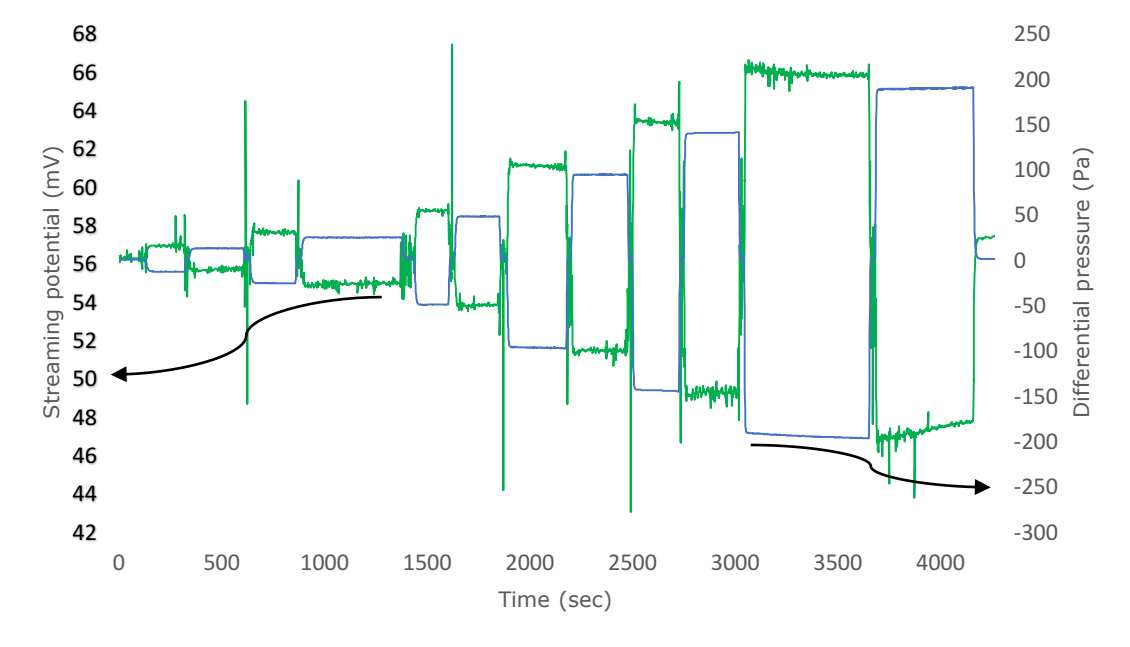

Graph 4: Streaming potential and differential pressure conducted on Core 1 using 0.02 M NaCl. The green line illustrates the streaming potential on the left axis. The stabilisation is satisfying for both pressure and voltage for almost all pairs conducted.

The average voltage and pressure difference from the last minute within each rate was taken as the basis for the coupling coefficient illustrated below in Graph 5. The slope of a linear regression yield the steaming potential coupling coefficient of 48.3 mV/MPa with R^2=0.9982. The uncertainty of the last stabilised pressure conducted is previewed with an error scatter. The magnitude of this error is smaller than the size of the dots except the last reading, however removal of this pair (highest differential pressure) would yield the same coupling coefficient.

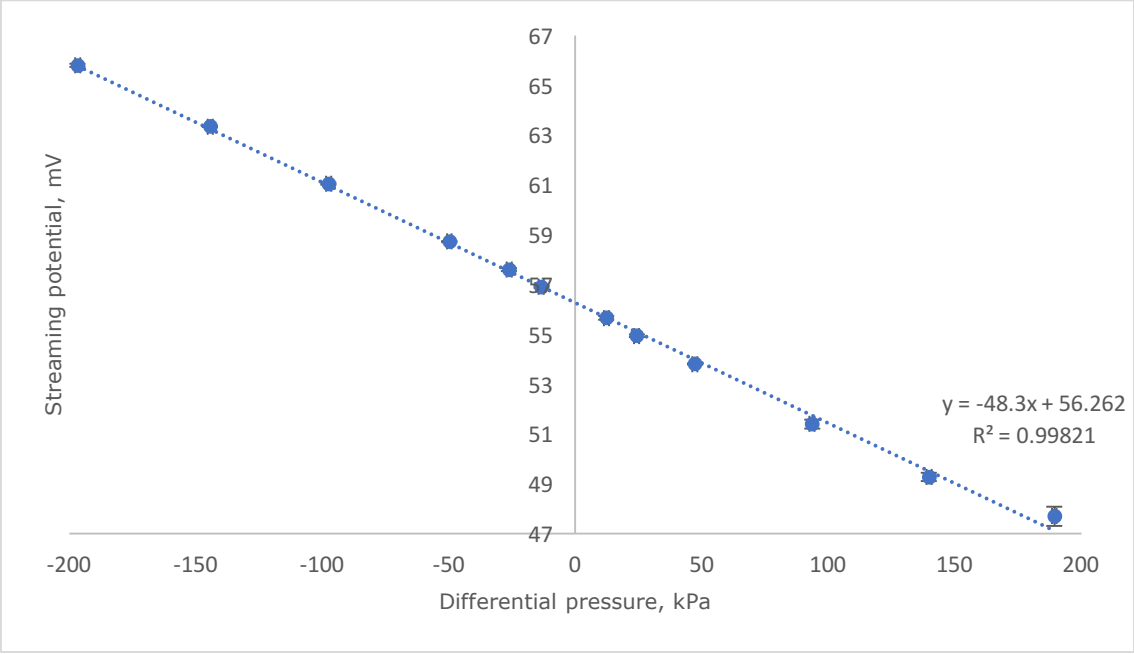

Graph 5: Streaming potential coupling coefficient for Core 1 with 0.02 M NaCl. The average voltage and pressure difference from the last minutes within each rate taken as the basis for the coupling coefficient. The slope of a linear regression yield 48.3 mV/MPa with R^2=0.9982.

Table 3: 0.02 M NaCl paired stabilised.

A-direction				B-direction				Paired stabilised	
Volt (mV)	dP (kPa)	STD DEV (V)	Vmax-Vmin	Volt (mV)	dP (kPa)	STD DEV (V)	Vmax-Vmin	(Vm1-Vm2)/2 (mV)	dP/2
56.900	-13.5	0.043	0.04	55.66	12.2	0.07	0.07	-0.619	-12.8
57.599	-26.2	0.061	0.06	54.94	24.2	0.06	0.06	-1.328	-25.2
58.719	-49.8	0.032	0.03	53.81	47.3	0.04	0.04	-2.453	-48.5
61.042	-97.6	0.043	0.04	51.40	93.6	0.17	0.17	-4.820	-95.6
63.337	-144.4	0.026	0.03	49.28	139.8	0.17	0.17	-7.031	-142.1
65.795	-196.8	0.065	0.14	47.70	189.3	0.38	1.29	-9.046	-193.1

4.1.3 0.1 M NaCl experiment

For the two next experiments presented, a brine with 5 times higher salinity were used as a 0.1 M NaCl was injected into the same core (Core 1). The logging results for the first of the two 0.1 M NaCl experiments are presented in the graph below (Graph 6 and 7).

Clearly, the difference in the streaming potential within each pair is now less than for the previous low-salinity brine due to higher conductivity of the brine, and thus, a smaller magnitude of the streaming potential coupling coefficient is observed. In the primary y-axis of Graph 6 (0.1 M) the streaming potential varies from 77 to 84 mV (7 mV) while in Graph 4 (0.02 M) it varied from 44 to 68 mV (24 mV) such that transient effects leading to variations are getting more important compared to the signal itself. The streaming potential did stabilise after one minute within most of the rates conducted for this current experiment. Once again, the streaming potential had more difficulties stabilising for higher rates (pressures above 150 kPa). After this experiment was completed, the static voltage went back to its initial value (ca 80.1 mV).

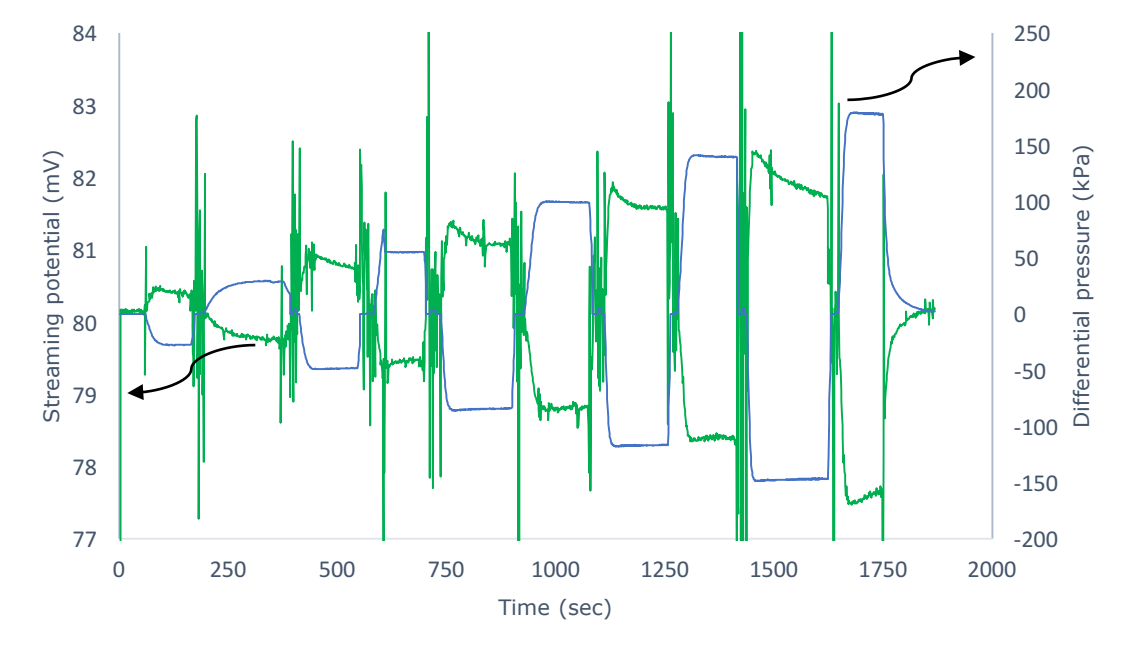

Graph 6: Streaming potential for core 1 using 0.1 M NaCl. The streaming potential did stabilise for most of the rates conducted, but had more difficulties for higher rates.

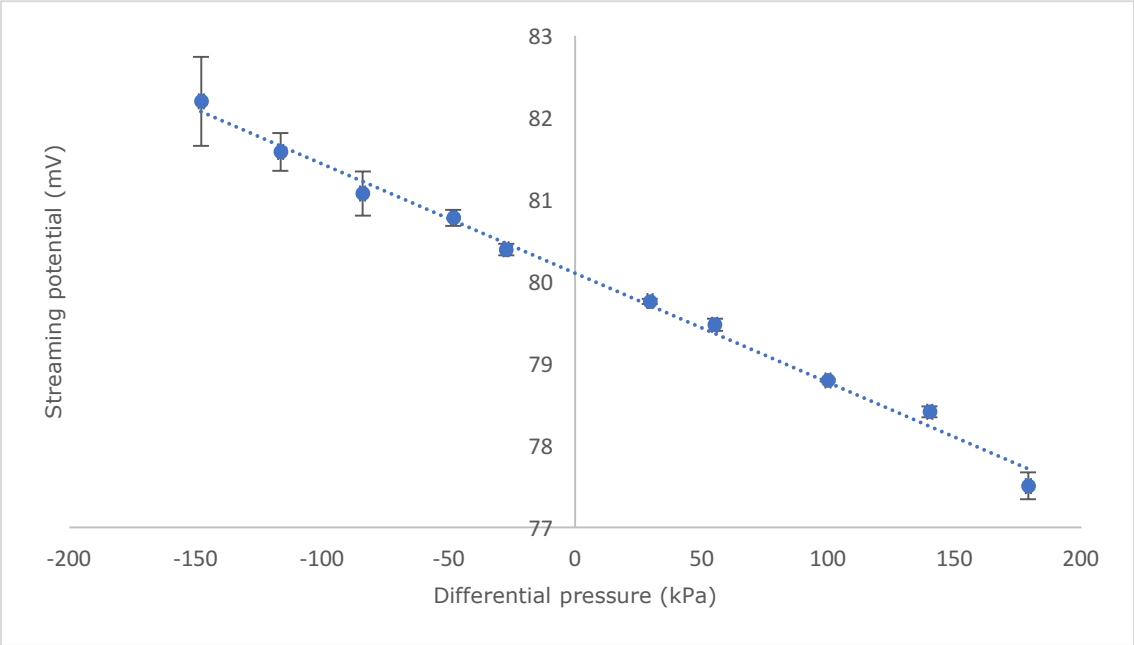

Graph 7: Streaming potential coupling coefficient on Core 1 with 0.1 M NaCl. The average voltage and pressure difference from the last minute within each rate was taken as the basis for the coupling coefficient. The slope of a linear regression yield 13.3 mV/MPa with R^2=0.9940.

Table 4: 0.1 M NaCl.

A-direction				B-direction				Paired stabilized	
Volt (mV)	dP (kPa)	STD. DEV	Vmax-Vmin	Volt (mV)	dP (kPa)	STD. DEV	Vmax-Vmin	(Vm1-Vm2)/2 [mV]	dP/2
80.392	-27.4	0.213	0.069	79.757	29.4	0.171	0.032	-0.317	28.4
80.778	-48.3	0.111	0.096	79.472	55.1	0.078	0.073	-0.653	51.7
81.075	-84.1	0.104	0.271	78.794	99.8	0.158	0.015	-1.140	92.0
81.583	-116.6	0.282	0.228	78.409	140.0	0.027	0.068	-1.587	128.3
82.201	-148.0	0.214	0.542	77.505	179.0	0.202	0.163	-2.348	163.5

Another identical experiment using 0.1 M NaCl brine is presented in Graph 8. What can be seen here is that the static potential decreased during the experiment. This can be seen by studying the values of the streaming potential for positive pressures applied. These potentials remained almost constant with increasing pressure compared to the potential measured for negative pressures applied.

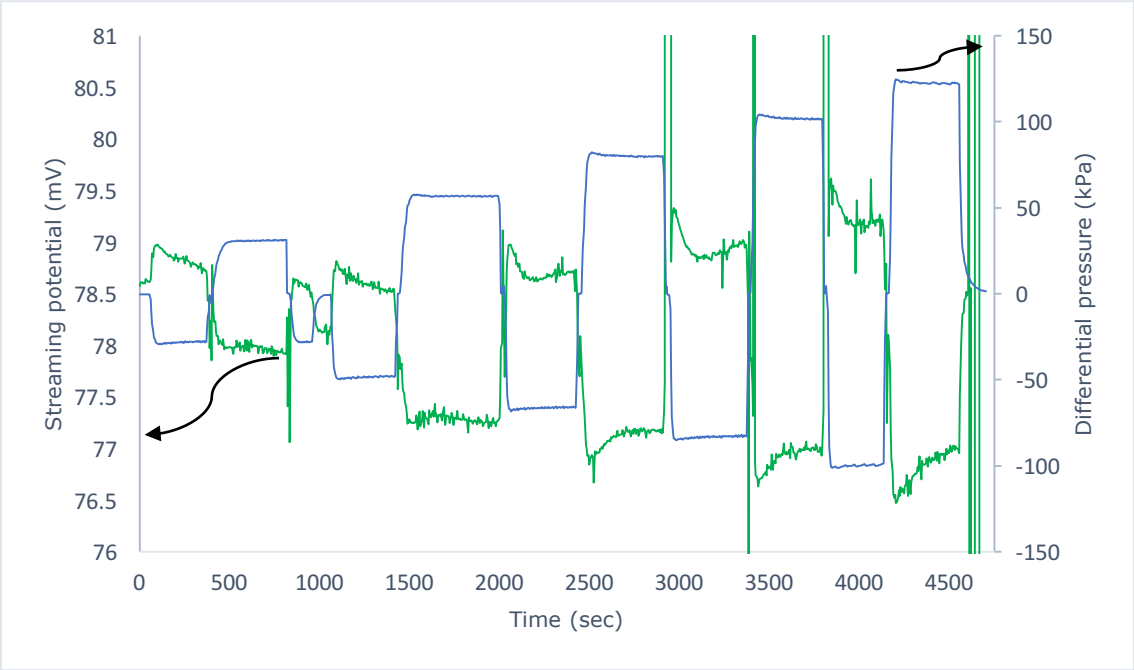

Graph 8: Streaming potential for core 1 using 0.1 M NaCl. The static potential decreased during the experiment.

The streaming potential coupling coefficient is obtained by a slope of a linear regression, and illustrated below.

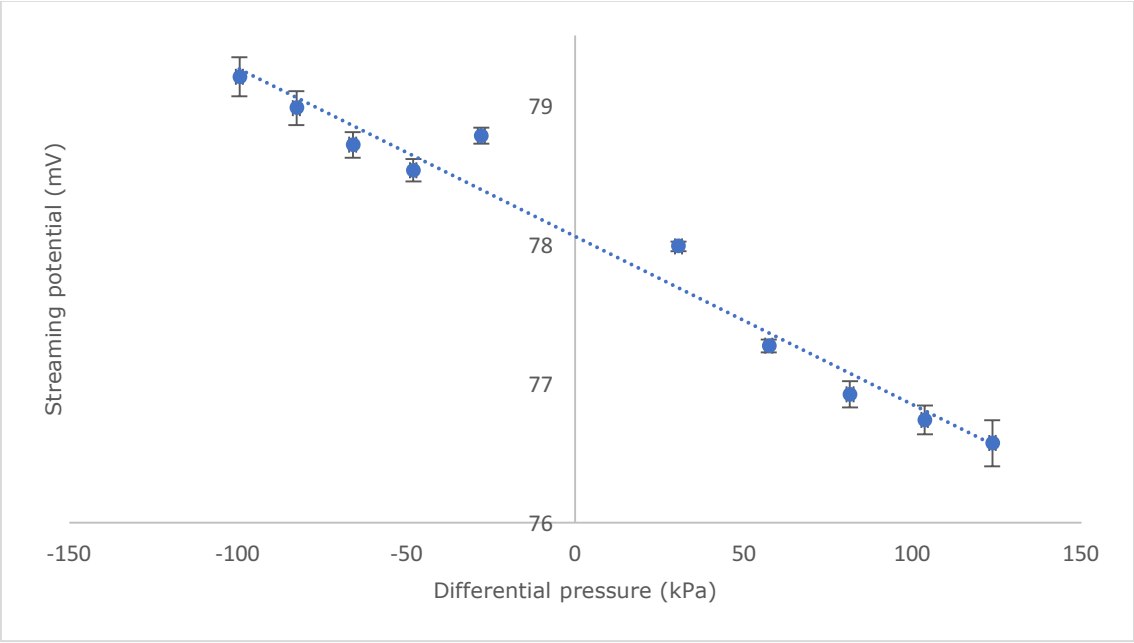

Graph 9: Streaming potential coupling coefficient for Core 1 using 0.1 M NaCl yield 12.1 mV/MPa with R^2=0.9657. The accuracy of the linear regression is not as good as for the previous experiments due to temporal variation of static voltage.

The accuracy of the linear regression in Graph 9 is impaired due to that variation of the static potential. However, the technique of implementing paired experiments eliminates the variation of static potential within each pair by using formula (3.6) and (3.7) For the graph illustrated below (Graph 10), this technique has been used. The linear regression has improved from R^2=0.9657 to R^2= 0.9929 and the coupling coefficient changed from

12.1 mV/MPa to 8.5 mV/MPa. The last results can be regarded more trustworthy as variation of static potential should not affect any results regarding the calculation of the streaming potential coupling coefficient.

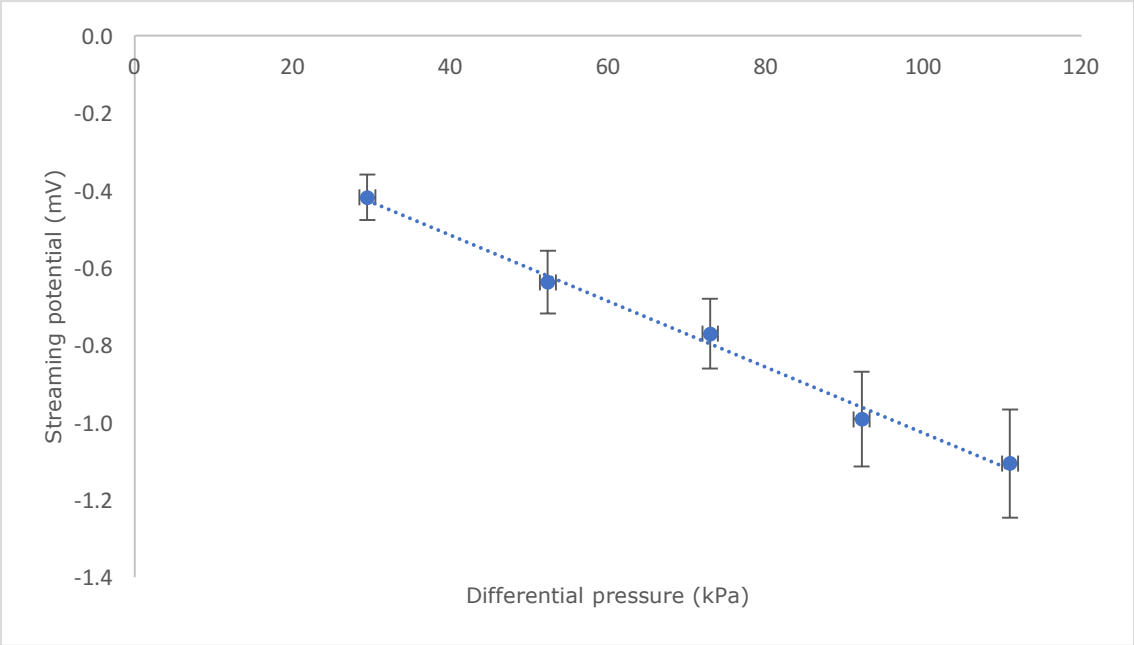

Graph 10: Streaming potential coupling coefficient for 0.1 M NaCl using the technique of eliminating the variation of static potential within each pair. The linear regression is more accurate. The coupling coefficient yield 8.5 mV/MPa with R^2=0.9929.

Table 5: 0.1 M NaCl.

A-direction				B-direction				Paired stabilized	
Volt (mV)	dP (kPa)	Vmax-Vmin	STD. DEV	Volt (mV)	dP (kPa)	Vmax-Vmin	STD. DEV	(Vm1-Vm2)/2)	dP/2
78.780	-27.887	0.235	0.058	77.943	31.088	0.0650	0.0361	-0.418	29.488
78.532	-48.074	0.255	0.081	77.257	56.681	0.0280	0.0459	-0.638	52.377
78.715	-66.012	0.276	0.090	77.173	79.890	0.2380	0.0945	-0.771	72.951
78.979	-82.721	0.303	0.122	76.996	101.608	0.2430	0.1031	-0.992	92.165
79.204	-99.607	0.309	0.140	76.991	122.322	0.4520	0.1638	-1.106	110.964

4.1.4 0.3 M NaCl experiment

All the next experiment was conducted on another nearly identical Berea sandstone. The core was replaced because it was suspected that some particles had entered the core and caused a dramatic change in permeability.

For the next experiments, the salinity of the NaCl brine was tripled to a concentration of 0.3 M, here variations in the voltage are plotted between 3 and 8 mV. In addition to the paired stabilisation method used, the differential pressure ramping method (by linearly increasing the flow rate with time) was also implemented.

The standard stabilised pressure method is presented first in Graph 11. As observed, the transient fluctuations and trends in the 'static' voltage for each dP is getting serious as it never seem to stabilise for positively values of pressure difference applied, but rather decreases continuously. The change of the static voltage within this experiment had a magnitude of 1.85 mV.

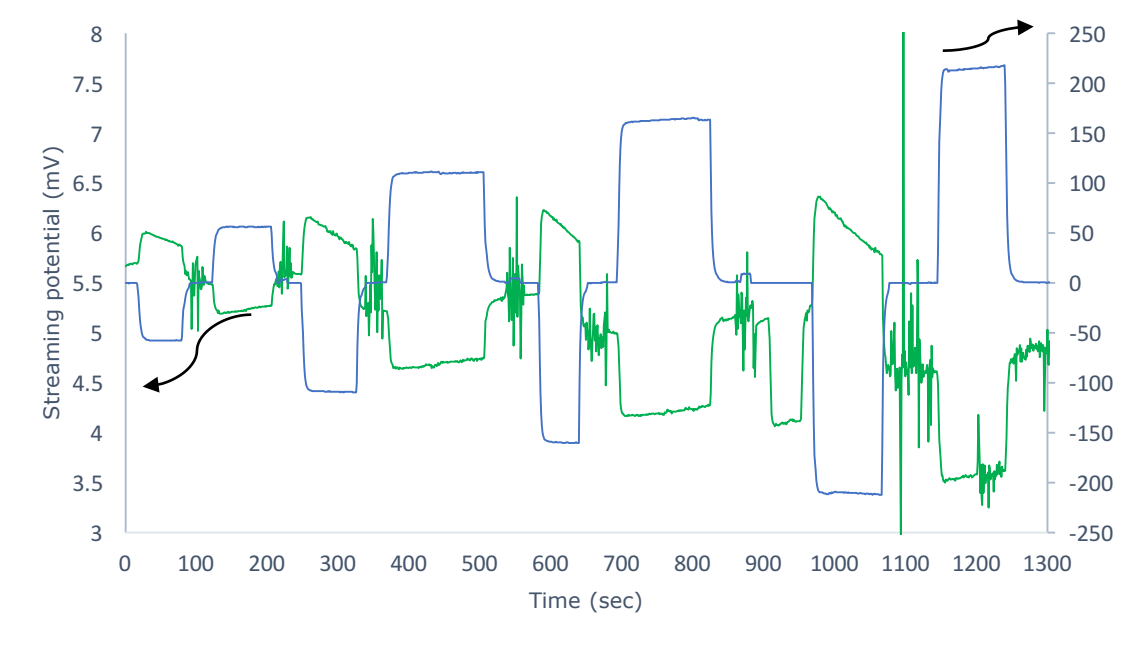

Graph 11: Paired stabilised method for 0.3 M NaCl. The impact of the variation in static voltage is more significant than for the low salinity brines.

In an ideal situation, one should wait until the voltage stabilised before register the value of the streaming within each pair. This was not possible because the stabilisation did not seem to occur over 200-300 seconds, and by waiting for very long times would give non-logical results as the fluctuation of static voltage would deviate significantly away from its initial value.

Thus, in order to reduce the impact of the transient variation of the static voltage *within* each pair, the value of the streaming potential was picked just before changing the flooding direction and then, after the flooding direction was changed within the same pair. As such, the new streaming potential voltage value was picked immediately after the flow direction was changed. The time difference between these two registered values are thus only one minute; the time required to turn valves and prepare for change in flow direction.

The coupling coefficient of the paired stabilised method is presented below, and the variation of static voltage between every pairs is removed. The slope of a linear regression yield 5.2 mV/MPa with R^2=0.9988.

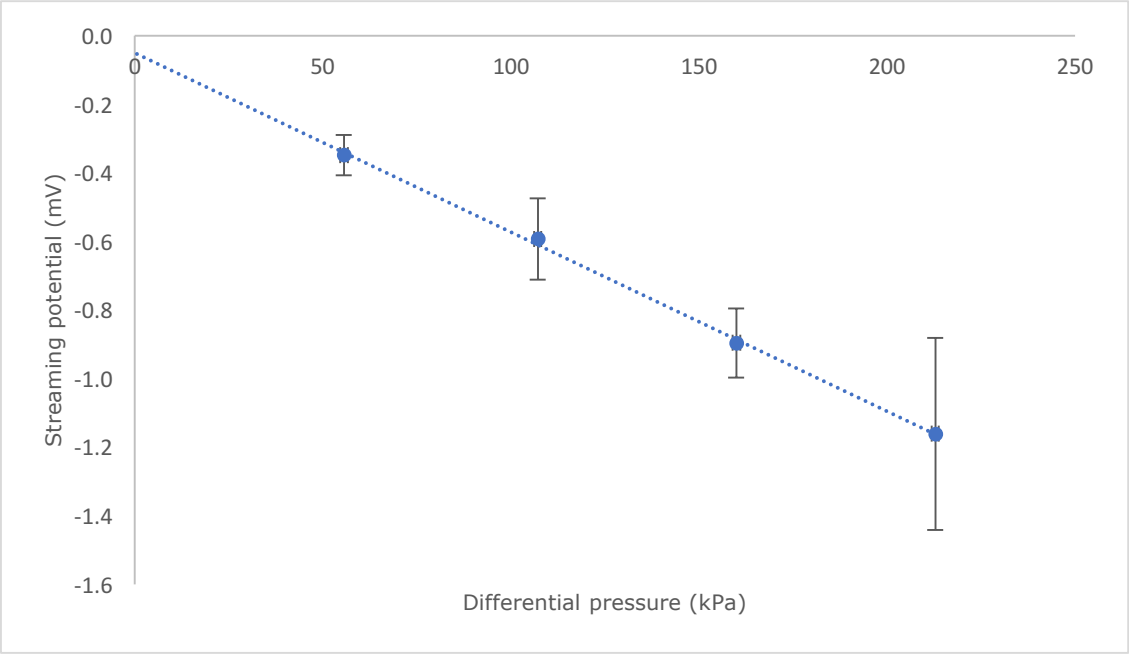

Graph 12: Paired stabilised method for 0.3 M NaCl. The slope of a linear regression yield 5.2 mV/MPa with R2=0.9988.

Table 6: 0.3 M NaCl. Paired stabilised.

A-direction				B-direction				Paired stabilised	
Volt (mV)	dP [kPa]	Std.dev (V)	Vmax-Vmin	Volt (mV)	dP (kPa)	Std.dev (V)	Vmax-Vmin	(Vm1-Vm2)/2	dP/2
5.891	-57.5	0.035	0.113	5.195	53.8	0.0234	0.044	-0.348	55.6
5.864	-109.4	0.086	0.294	4.679	104.9	0.0329	0.073	-0.593	107.1
5.958	-160.7	0.072	0.290	4.166	159.3	0.0287	0.089	-0.896	160.0
5.853	-211.7	0.175	0.522	3.530	214.0	0.1046	0.093	-1.162	212.8

Because dealing with variations in static voltage was challenging, a pressure ramping method was conducted in which the flow rate was increased linearly with time. This experiment proved to give a lot better linearity between the voltage and pressure difference across the core. Four different ramping times was implemented for the 0.3 M NaCl brine. The result of this experiment gave a coupling coefficient of 4.11 mV/MPa with R^2=0.994 for ramping time for the 240 second ramping, 4.69 mV/MPa with R^2=0.998 for a ramping time of 120 seconds, 4.95 mV/MPa with R^2=0.999 for a ramping time of 60 seconds and 5.12 mV/MPa with R^2=0.999 for a ramping time of 30 seconds. The coupling coefficients obtained from the different pressure ramping times deviated with about 25 % for the longest and shortest time range as can be seen in Table 7. This shortest pressure ramping time range yield the greatest value of the coupling coefficient, 5.12 mV/MPa, while the longest ramping time range yield the 4.10 mV/MPa.

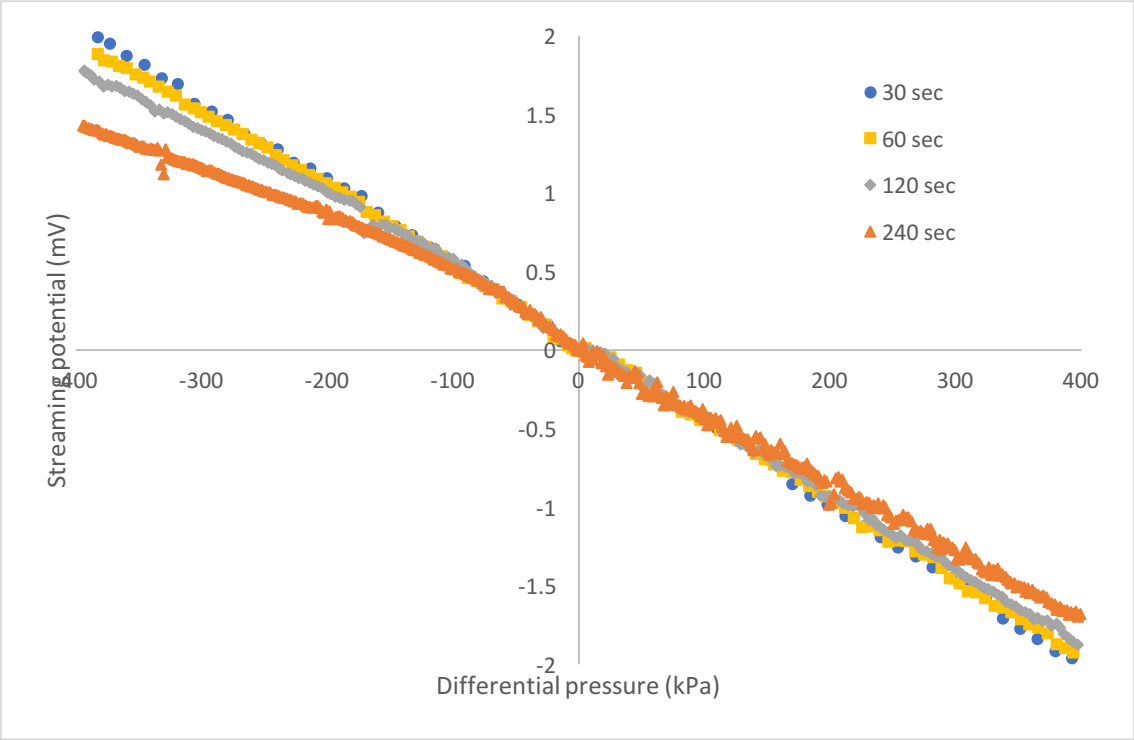

Graph 13: 0.3 M NaCl pressure ramping. Four different ramping times was implemented. The result of this experiment gave a coupling coefficient of 4.11 mV/Mpa with R^2=0.994 for ramping time of 240 seconds, 4.69 mV/Mpa with R^2=0.998 for ramping time of 120 seconds, 4.95 mV/Mpa with R^2=0.999 for ramping time of 60 seconds and 5.12 mV/Mpa with R^2=0.999 for ramping time of 30 seconds.

Table 7: Pressure ramping 0.3 M NaCl.

Pressure ramping 0.3 M NaCl		
Time range	C (mV/MPa)	Regression
240 sec	4.11	0.994
120 sec	4.69	0.998
60 sec	4.95	0.999
30 sec	5.12	0.999

It was also tried to implement pressure ramping with even greater time interval than 240 seconds. This proved to be more difficult because the streaming potential signal tended to deviate away from the initial value as the differential pressure was increased. Several experiments had to be performed in the 240 second case, before a successful experiment was obtained, while for the shorter ramping times the experiment was successful with only one try. The graph (Graph 14) below illustrates an example of a pressure ramping that was unsuccessful, using a time range of 480 seconds.

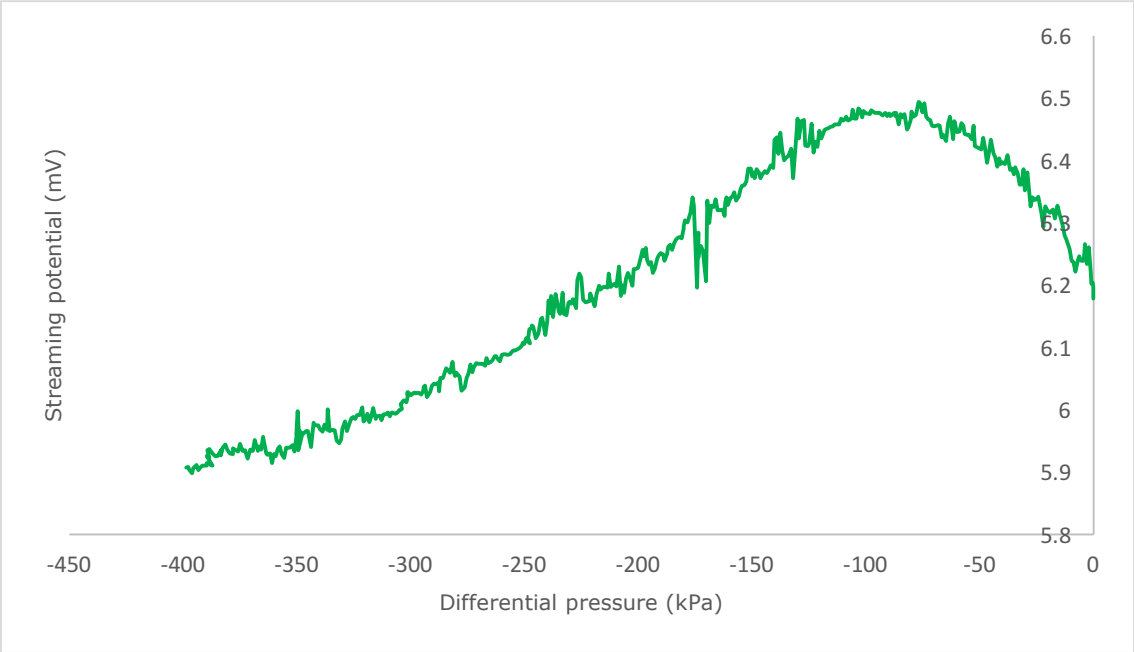

Graph 14: Unsuccessful negative pressure ramping with a range of 480 seconds for 0.3 M NaCl. The pressure is ramped from 0 toward -400 kPa. The streaming potential has clearly deviated before the pressure reached -100 kPa, and the experiment is useless.

4.1.5 0.6 M NaCl experiment

For the next experiments, the concentration of the NaCl is doubled to 0.6 M. The paired stabilised method is presented below. The trend is similar as for the previous brine as the static voltage decreased simultaneously for almost all negative stabilised pressures while it remained stable for positive stable pressures. The first pair remained stable for both flooding directions. The change of the static voltage had a magnitude of 0.33 mV, which is 5 times less than for the previous 0.3 M NaCl experiment using the paired stabilised method.

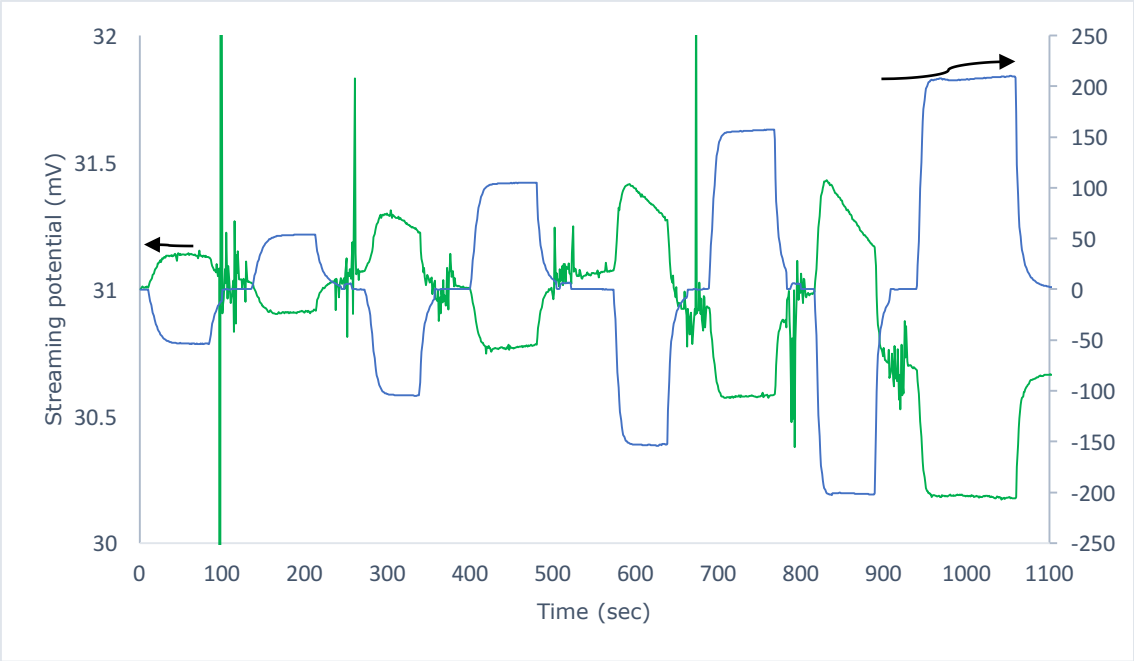

Graph 15: 0.6 M NaCl, paired stabilised.

The coupling coefficient from this experiment is presented below, which gained a magnitude of 2.57 mV/MPa with R^2=0.998.

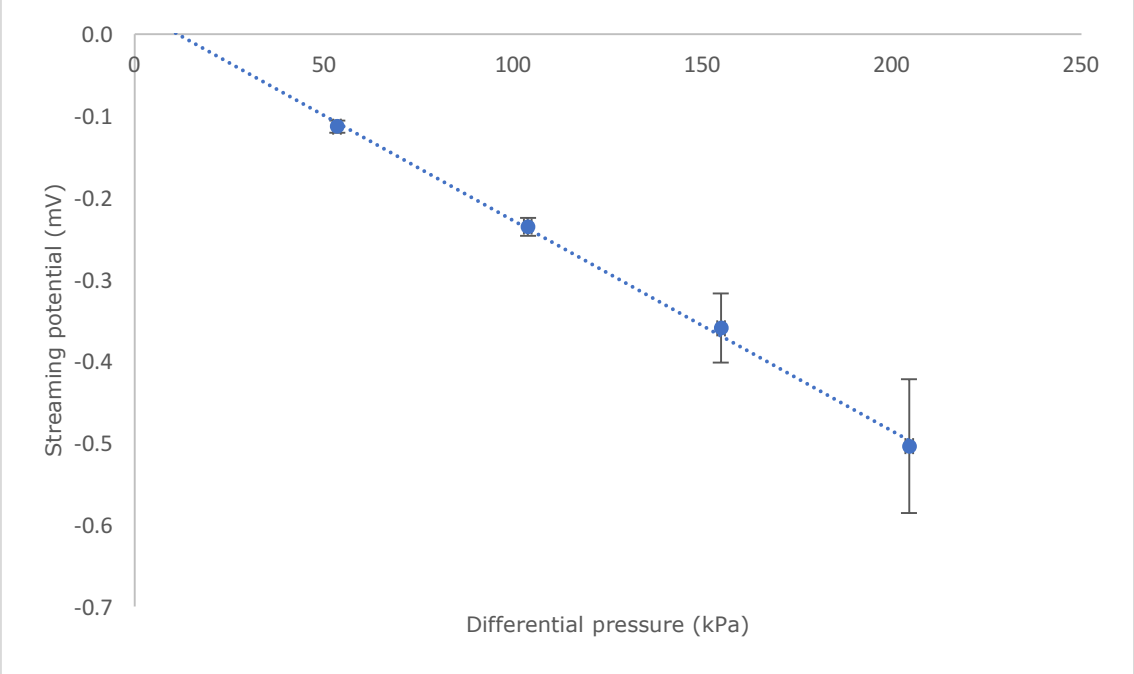

Graph 16: Streaming potential coupling coefficient of 0.6 M NaCl obtained using the paired stabilised method yield 2.57 mV/MPa with R^2=0.998. Both flooding directions of the first pair remained very stable.

Table 8: Paired stabilised 0.6 M NaCl.

A-direction				B-direction				Paired stabilised	
Volt (mV)	dP (kPa)	STD. DEV (mV)	Vmax-Vmin	Volt (mV)	dP (kPa)	STD. DEV (V)	Vmax-Vmin	(Vm1-Vm2)/2 (mV)	dP/2
31.135	-53.4	0.005		30.909	53.5	0.0024		-0.113	53.4
31.241	-104.9	0.005	0.057	30.769	102.8	0.0064	0.008	-0.236	103.8
31.298	-153.4	0.039	0.111	30.578	156.3	0.0039	0.005	-0.360	154.8
31.193	-201.9	0.077	0.258	30.185	207.1	0.0042	0.005	-0.504	204.5

The pressure ramping method was also attempted for the 0.6 M brine. The result can be regarded accurate for the pressure ramping range of 30 and 60 seconds, while the linearity of 120 seconds had a small deviation for the higher negative pressure area as can be seen in Graph 17. Due to this, one the positive pressure region was taken as basis for the linear regression for all three experiments. The results of these three ramping methods yield a coupling coefficient of 2.49 mV/MPa with R^2=0.999 for the 120 second range, 2.45 mV/MPa with R^2=0.999 for the 60 second range and 2.46 mV/MPa with R^2=0.999 for the 30 second range (Table 9). The coupling coefficients between the greatest and shortest ramping time differ by only 1.6 %. However, the regression was

only based for positive pressure which clearly has an impact on the precise linearity. The results are illustrated below:

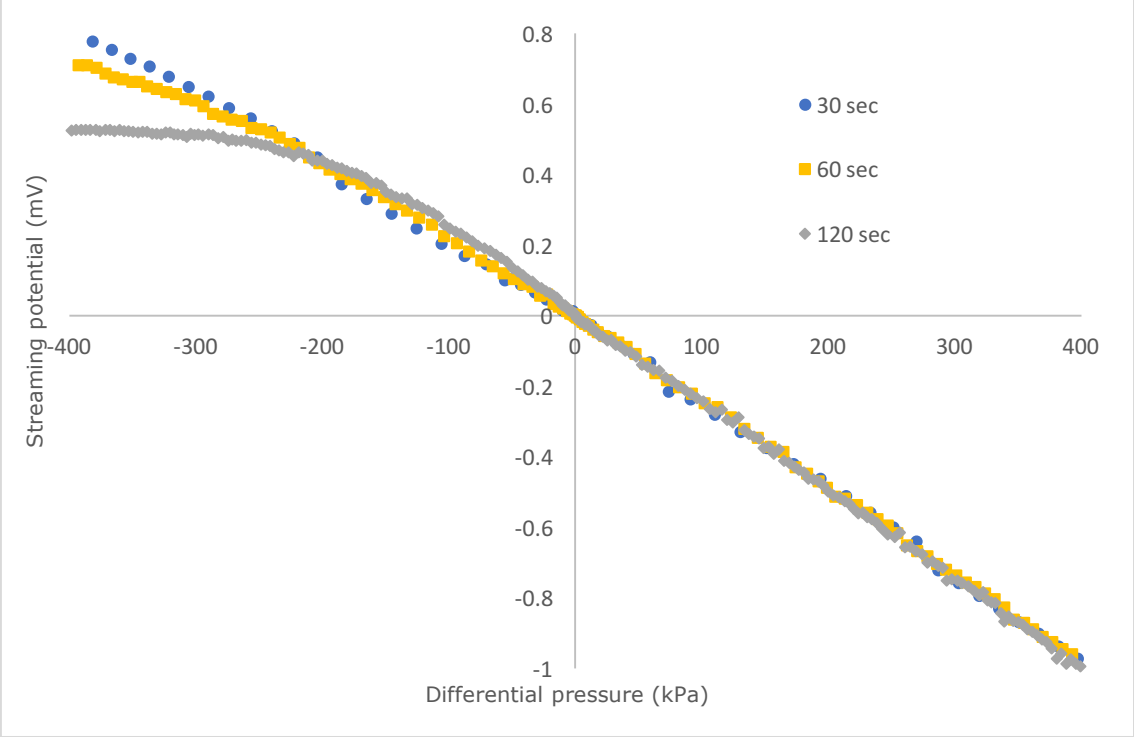

Graph 17: 0.6 M NaCl pressure ramping. Results: coupling coefficient of 2.49 mV/MPa with R^2=0.999 for the 120 second range, 2.45 mV/MPa with R^2=0.999 for the 60 second range and 2.46 mV/MPa with R^2=0.999 for the 30 second range. The regression was only based on the results from the positive pressure ramping due to uncertainty in the negative pressure area.

Table 9: Pressure ramping 0.6 M NaCl.

Pressure ramping 0.6 M NaCl		
Time range	C (mV/MPa)	Regression
240 sec		
120 sec	2.49	0.999
60 sec	2.45	0.999
30 sec	2.46	0.999

4.1.6 1.2 M NaCl experiment

It was not possible to get reasonable results by conducting paired stabilised experiment for the brine of 1.2 M NaCl due to too much variation of static voltage during which the experiment was conducted. However, the pressure ramping method gave reasonable results for time range of 60 seconds and less while the 120 second experiment gave unsuccessful results. The slope of a linear regression for the pressure ramping yield a coupling coefficient of 0.62 mV/MPa with R^2=0.9946 for the 60 second range and 0.74 mV/MPa with R^2=0.9989 for the 30 second range, which is a difference of 19 % for the slopes (see Graph 18 and Table 10).

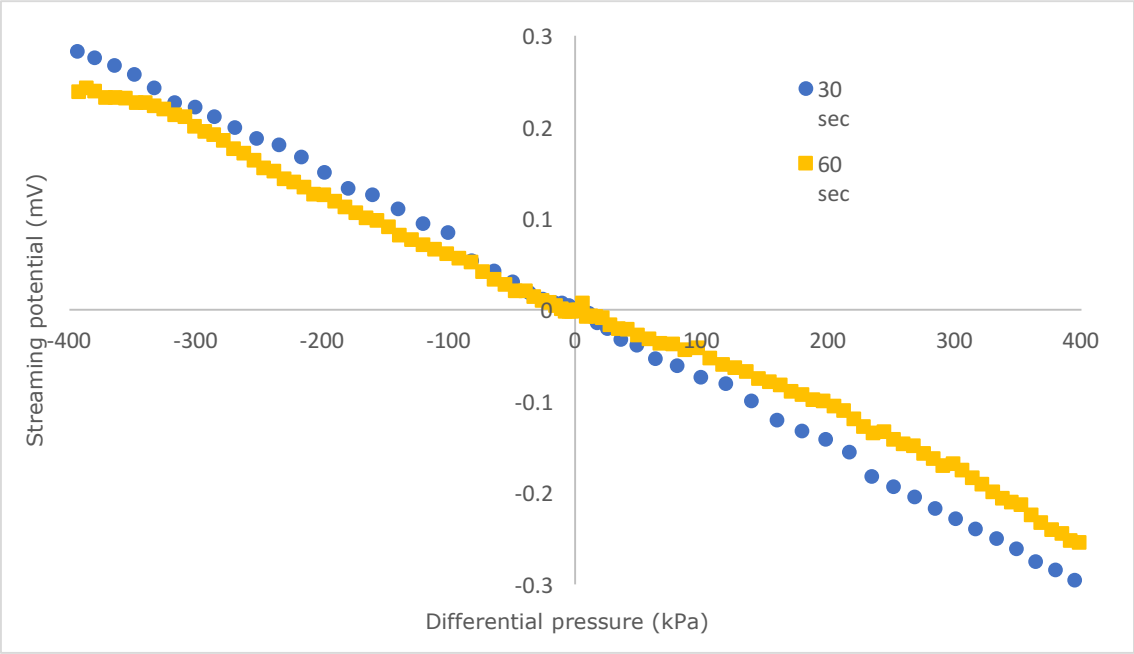

Graph 18: 1.2 M NaCl pressure ramping. The slope of a linear regression for the pressure ramping yield a coupling coefficient of 0.62 mV/MPa with R^2=0.9946 for the 60 second range and 0.74 mV/MPa with R^2=0.9989 for the 30 second range.

Table 10: pressure ramping 1.2 M NaCl

Pressure ramping 1.2 M NaCl		
Time range	C (mV/MPa)	Regression
240 sec		
120 sec		
60 sec	0.62	0.9946
30 sec	0.74	0.9989

4.1.7 2.0 M NaCl experiment

The last experiment of NaCl with the highest concentration of 2.0 M is presented. The 120 second ramping time is also included here, even it was more unstable than for the shorter ramping times (see Graph 19). The coupling coefficient from on the slope of a linear regression yield 0.40 mV/MPa with R^2=0.8712 for the 120 second range, 0.35 mV/MPa with R^2=0.9676 for the 60 second range and 0.34 mV/MPa with R^2=0.9707 for the 30 second range. The coupling coefficient of the 120 second range was 17.6 % greater than the 30 second time range (see Table 11 and Graph 19).

Table 11: Pressure ramping 2.0 M NaCl

Pressure ramping 2.0 M NaCl		
Time range	C (mV/MPa)	Regression
240 sec		
120 sec	0.40	0.8712
60 sec	0.35	0.9676
30 sec	0.34	0.9707

What is important to look after with this experiment it that the coupling coefficient of the longest ramping time is the one with largest magnitude. To compare with the 0.3 and 1.2 M experiments, the trend was opposite; shorter ramping time gave higher values of the coupling coefficients (while the 0.6 M had almost the same magnitude in the linear region regardless of ramping time).

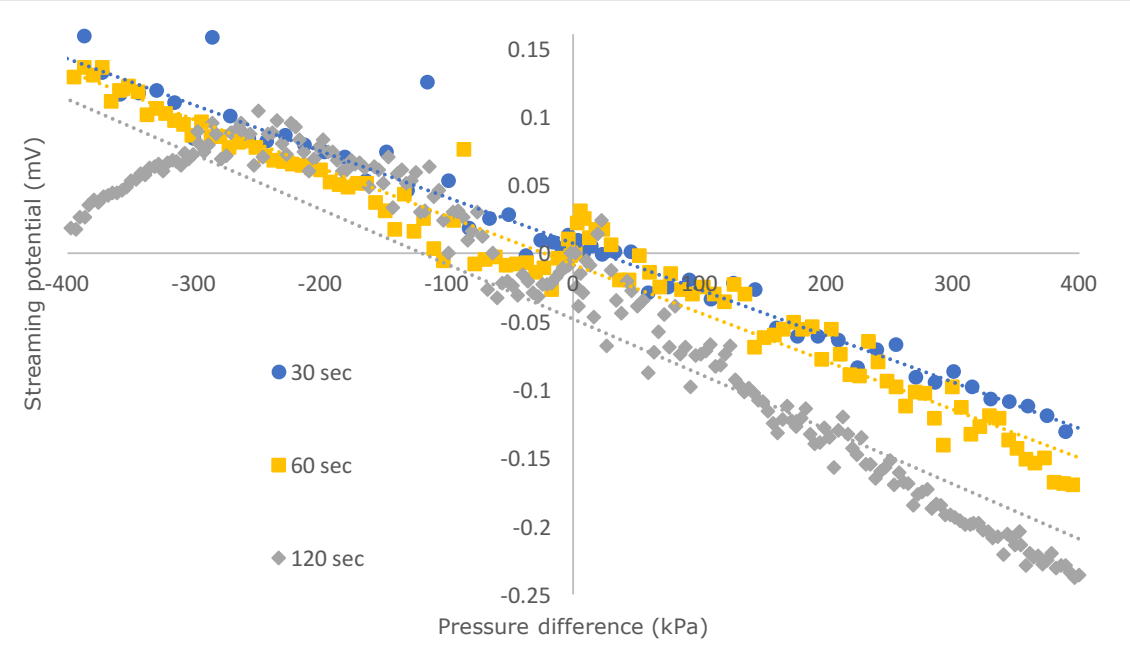

Graph 19: 2.0 M NaCl with pressure ramping. The coupling coefficient from on the slope of a linear regression yield 0.40 mV/MPa with R2=0.8712 for the 120 second range, 0.35 mV/MPa with R2=0.9676 for the 60 second range and 0.34 mV/MPa with R2=0.9707 for the 30 second range.

4.1.8 Overview coupling coefficient

Certain experiments have been implemented using different concentrations of the monovalent salt Sodium Chloride (NaCl) on Berea sandstone cores. The values of the streaming potential coupling coefficient vs. brine salinity for all the previously presented experiments using the paired stabilised technique is shown logarithmically in Graph 20

below. An empirical relation between the coupling coefficients and salinities for these experiments yield

$$C = -1.775M^{-0.852} \quad (3.15)$$

where C is the coupling coefficient and M is the concentration of the salinity, as molarity. This regression matches the data with R^2 = 0.995. All the coupling coefficients are of negative value. It's only the magnitude of the coupling coefficient that are present in the graphs. Hence, the sign of the empirical formula is negative.

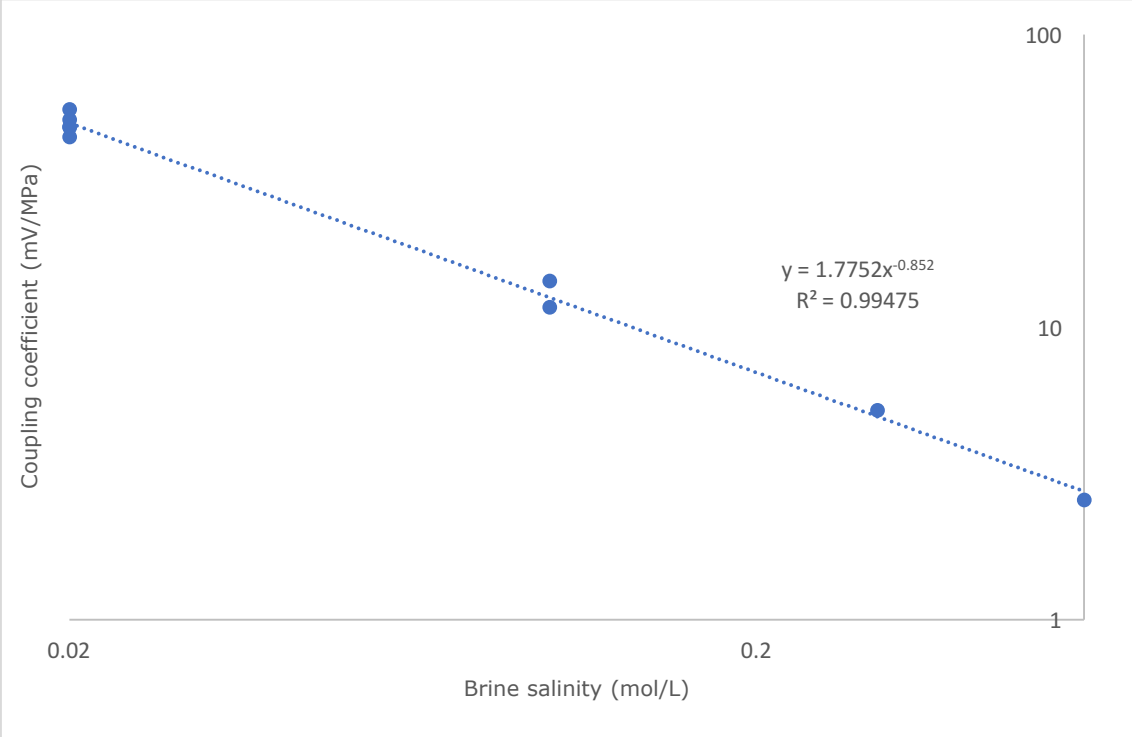

Graph 20: Coupling coefficient vs. brine salinity NaCl, region [0.02 M, 2.0 M].

Furthermore, we'll have a look at the coupling coefficients for the experiments conducted based on all the pressure ramping techniques, Graph 21. An empirical relation for the coupling coefficient within each specific ramping time is present;

Pressure ramping 120 sec $C = -1.121M^{-1.025}, R^2 = 0.995$ (3.16)

Pressure ramping 60 sec $C = -1.004M^{-1.084}, R^2 = 0.969$ (3.17)

Pressure ramping 30 sec $C = -1.052M^{-1.072}, R^2 = 0.969$ (3.18)

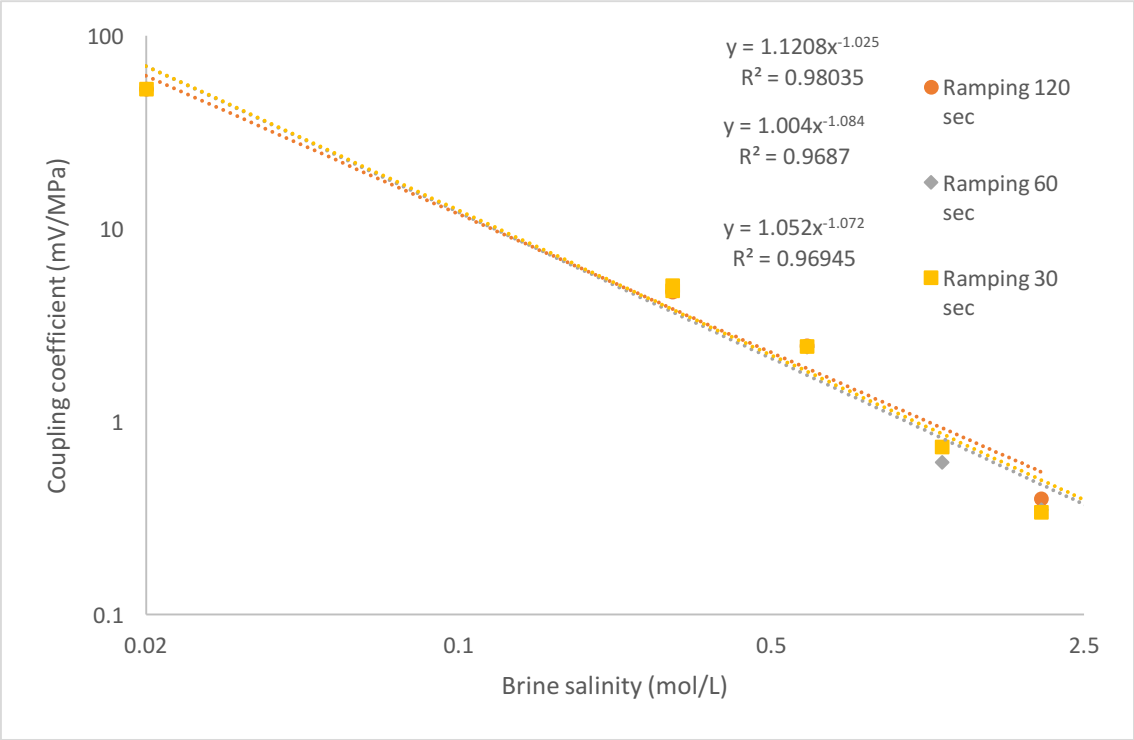

Graph 21: Coupling coefficients vs. brine salinity NaCl, region [0.02 M, 2.0 M] with pressure ramping, range [120, 60, 30] sec.

Experiments implemented in the region of 0.02 M to 0.6 M concentration shows no serious difference of the coupling coefficient with respect to the different ramping times, as the graph suggests. However, it was observed from experiment 0.3 M NaCl (Graph 13) that the magnitude of the coupling coefficient was greater (24.4 % difference) for the shortest ramping time implemented, but again infinitely small differences for experiment 0.6 M NaCl where the longest ramping time shows greatest coupling coefficient (by only 1.2 % (Graph 17)).

Graph 22 shows all entire experimental overview. For the empirical formula of the paired stabilised experiments, the constant is higher (eq. (3.15)). However, no paired experiments were conducted for the higher salinity region.

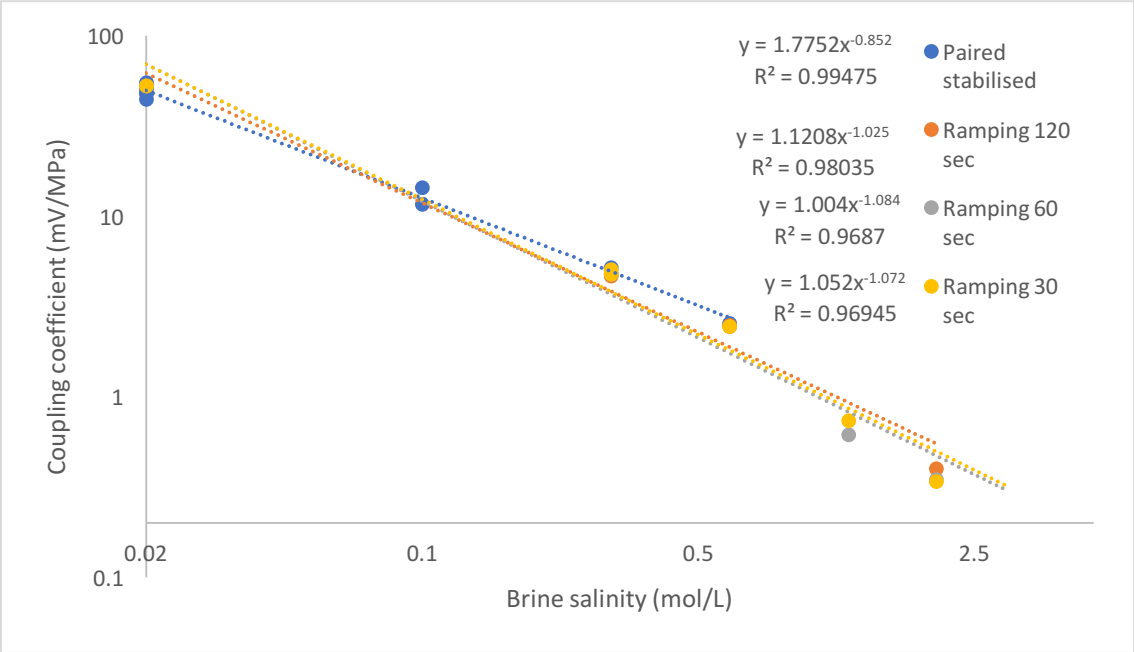

Graph 22: Coupling coefficients vs. brine salinity NaCl, all results.

4.1.9 Overview zeta-potential

Graph 23 shows all the calculated zeta-potentials for the experiments conducted on NaCl based on equation (3.10). Simply, increasing brine salinity yields decreasing zeta-potential. However, the zeta-potential for 0.02 M NaCl deviates from the trend of the remaining zeta-potentials.

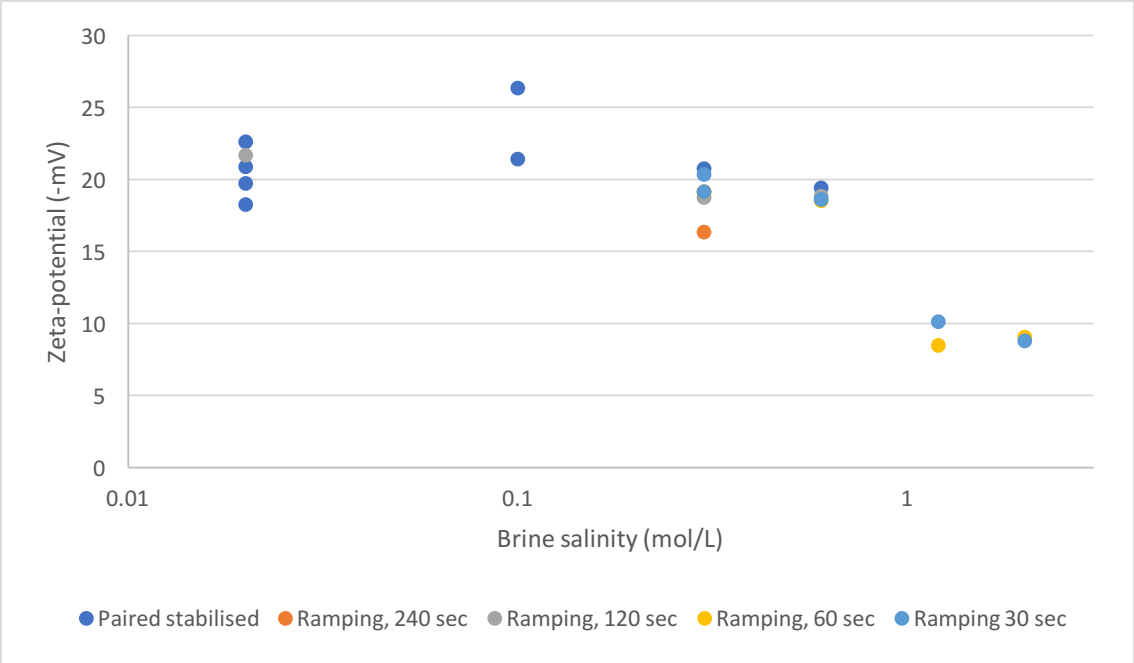

Graph 23: Zeta-potential NaCl. Underestimated values are corrected for.

The next graph is showing the zeta-potentials using Smoluchowski's equation. Values of low salinity brines are underestimated as the rock conductivity is not accounted for. For the salinities above 0.1 M, the underestimation doesn't seem to occur.

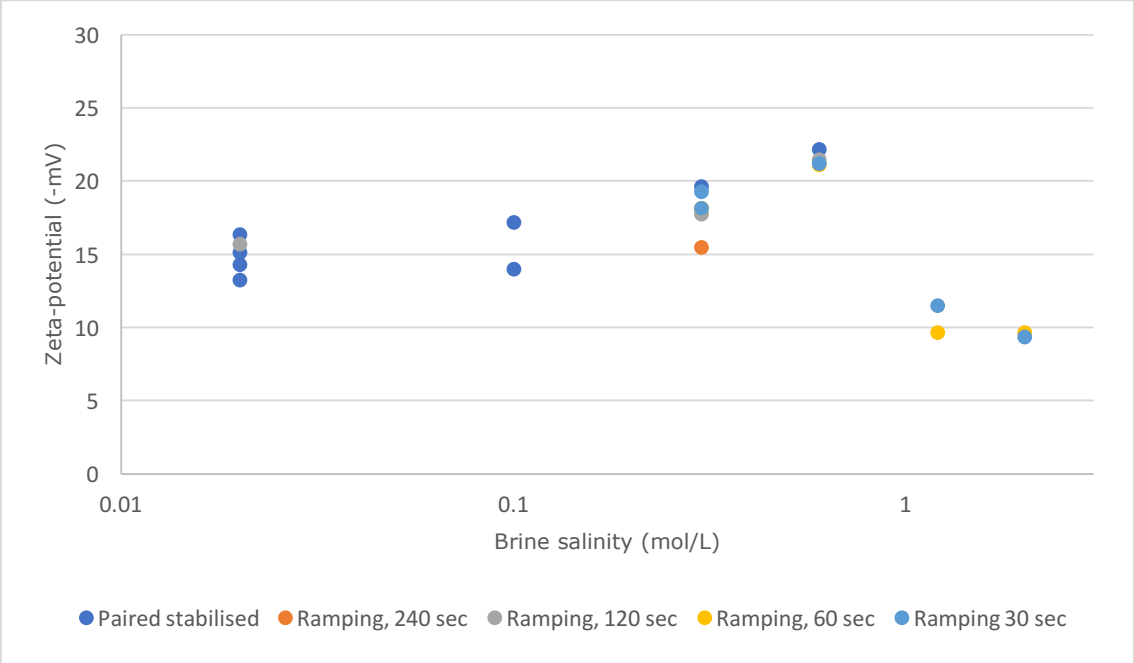

Graph 24: Zeta-potential NaCl using Smoluchowski's equation. Underestimated values are not corrected for.

4.2 $CaCl_2$ experiments with different salinity

The results of the experiments conducted using Calcium Chloride will be presented in order of salinity. The overall concentrations for these experiments are of less concentration than for NaCl. The reason is that the ionic strength of $CaCl_2$ is three times greater than for NaCl due to the divalence of the Ca^+ cation of the Calcium Chloride, (eq. (2.20).

A summary of the results are presented in the table below.

Table 12: Summary CaCl2.

	pH		**σ (S/m)**		**Coupling coefficient (mV/MPa)**					**Expt**
Salinity	Orig.	Equi.	Orig.	Equi.	Paired	240	120	60	30	
0.0067	6.20	7.34	0.116	0.113	19.03	19.29	19.2	19.0	18.91	45,48
0.033	5.68	7.20	0.573	0.572			5.59	5.78	5.95	49
0.1	5.75	7.21	1.79	1.792				0.883	1.050	50
								1.111	1.134	51
0.2	5.46	6.66	3.26	3.42			0.414	0.54	0.379	52
							0.352	0.349	0.395	53

4.2.1 0.0067 M $CaCl_2$ experiments

The brine of lowest salinity is presented in Graph 25. Stability seems to have been achieved relatively immediately, like within a few seconds. The two last positively pressures conducted, small fluctuations occurred. However, the overall experiment can be regarded successful.

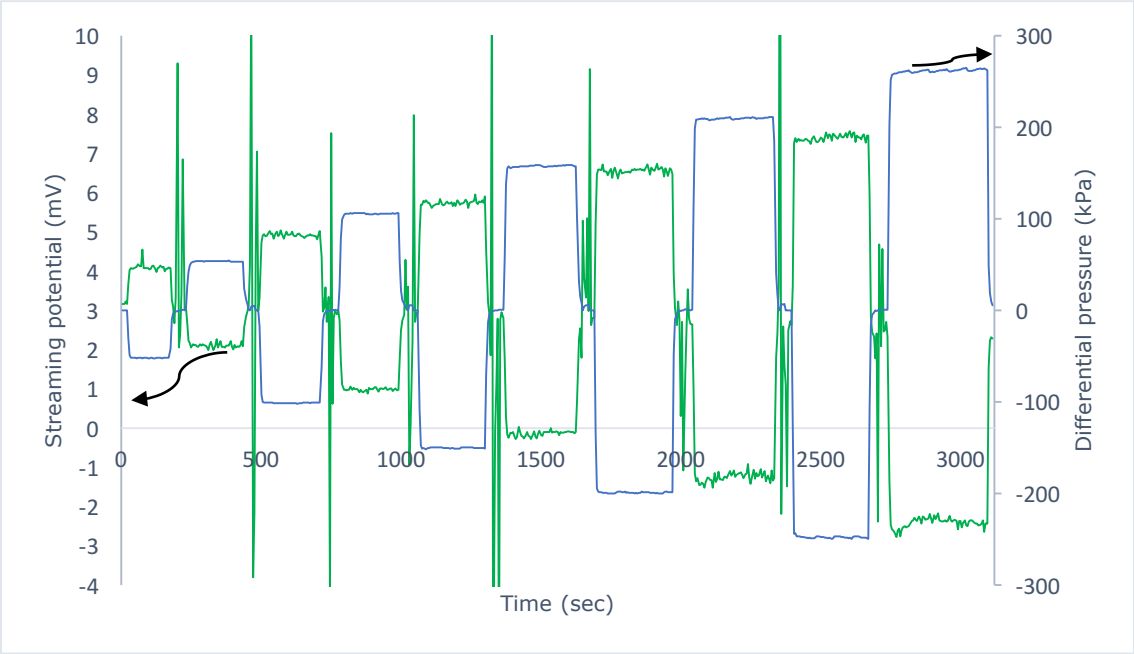

Graph 25: Streaming potential with 0.0067 M $CaCl_2$. Low salinity corresponds to very stable results.

Streaming potential as a function of pressure is presented in Graph 26 below. The slope of a linear regression yield a streaming potential coupling coefficient of 19.0 mV/MPa with R^2=0.998.

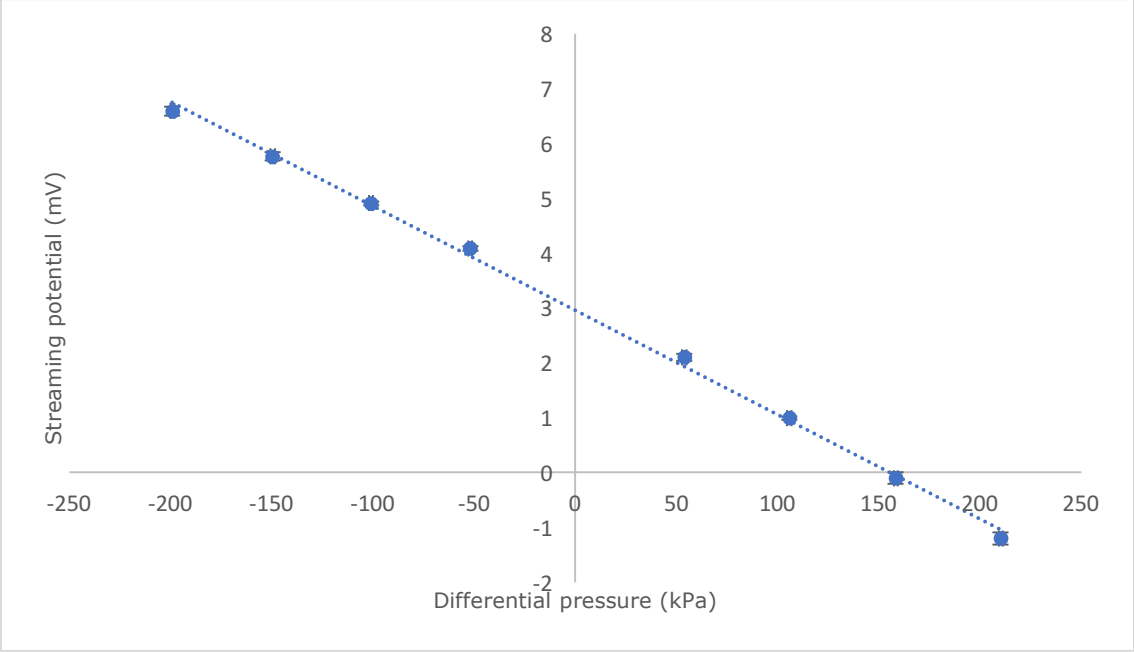

Graph 26: Streaming potential coupling coefficient for 0.0067 M $CaCl_2$. The slope of a linear regression yield 19.0 mV/MPa with R^2=0.998.

Table 13: 0.0076 M $CaCl_2$.

A-direction				B-direction				Paired stabilised	
Volt, mV	dP (kPa)	STD. DEV (mV)	Vmax-Vmin	Volt, mV	dP (kPa)	STD. DEV (V)	Vmax-Vmin	(Vm1-Vm2)/2 [mV]	dP/2
4.085	-51.9	0.043		2.102	53.9	0.0614		-0.991	52.9
4.909	-101.0	0.031		0.992	105.7	0.0316		-1.959	103.4

5.765	-149.6	0.078		-0.101	158.3	0.1012		-2.933	154.0
6.593	-199.1	0.082		-1.202	210.2	0.1095		-3.898	204.7

Pressure ramping was conducted with four different ranges, all of them with very species accuracy. The slope of a linear regression yield a coupling coefficient of 19.29 mV/MPa with R^2=0.9996 for the 240 second range, 19.2 mV/MPa with R^2=0.9998 for the 120 second range, 19.03 mV/MPa with R^2=0.9996 for the 60 second range and 18.91 mV/MPa with R^2=0.9992 for the 30 second range. The greatest and the smallest coupling coefficient differed with a magnitude of 0.38 mV/MPa which corresponds to a percentage of only 2 %.

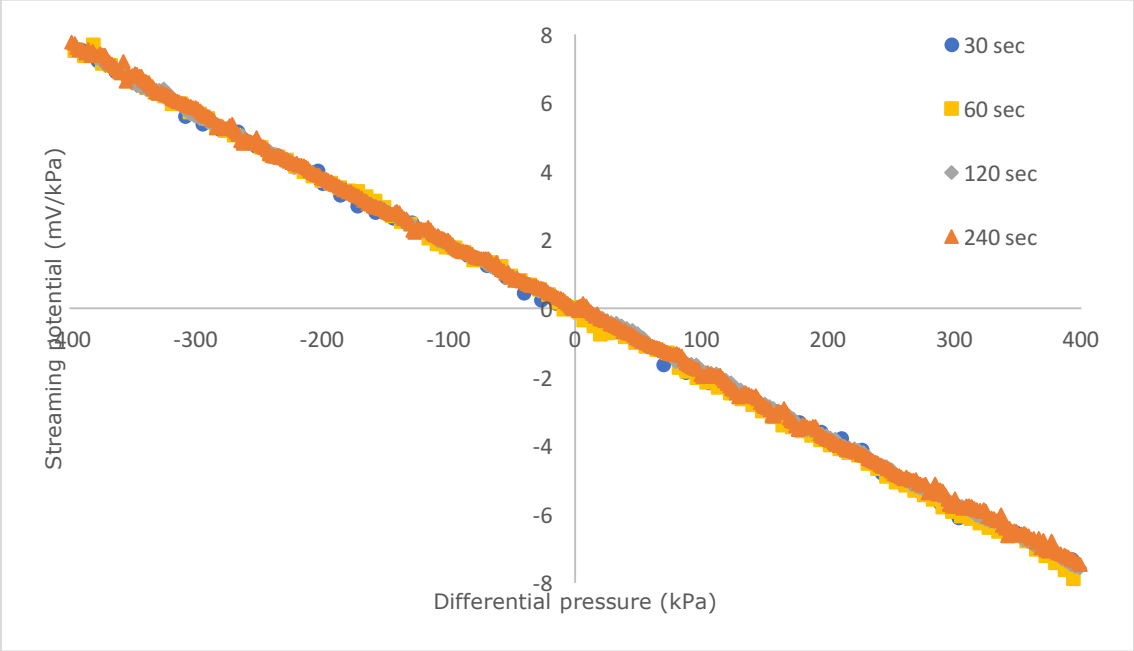

Graph 27: Pressure ramping 0.0067 M $CaCl_2$. The slope of a linear regression yield a coupling coefficient of 19.29 mV/MPa with R^2=0.9996 for the 240 second range, 19.2 mV/MPa with R^2=0.9998 for the 120 second range, 19.03 mV/MPa with R^2=0.9996 for the 60 second range and 18.91 mV/MPa with R^2=0.9992 for the 30 second range.

Table 14: Pressure ramping 0.0067 M CaCl2

Pressure ramping 0.0067 M CaCl2		
	C (mV/MPa)	Regression
240 sec	19.29	0.9996
120 sec	19.20	0.9998
60 sec	19.03	0.9996
30 sec	18.91	0.9992

4.2.2 0.033 M $CaCl_2$ experiment

The next concentration of $CaCl_2$ has five times concentration than the previous. Stability problems occurred when trying to run paired stabilised experiments due to the

significance regarding variation of static voltage. Thus, results with paired stabilised experiments are not included here.

The pressure ramping results are shown in Graph 28. No problems occurred for any of the three ramping times that was implemented. The coupling coefficients calculated gave 5.59 mV/MPa with R^2=0.9936 for 120 second ramping time, 5.78 mV/MPa with R^2=0.9966 for 60 second ramping time and 5.95 mV/MPa with R^2=0.9937 for 30 second ramping time. The 30 second ramping had the greatest coupling coefficient with 6.4 % higher magnitude that for the 120 second ramping time.

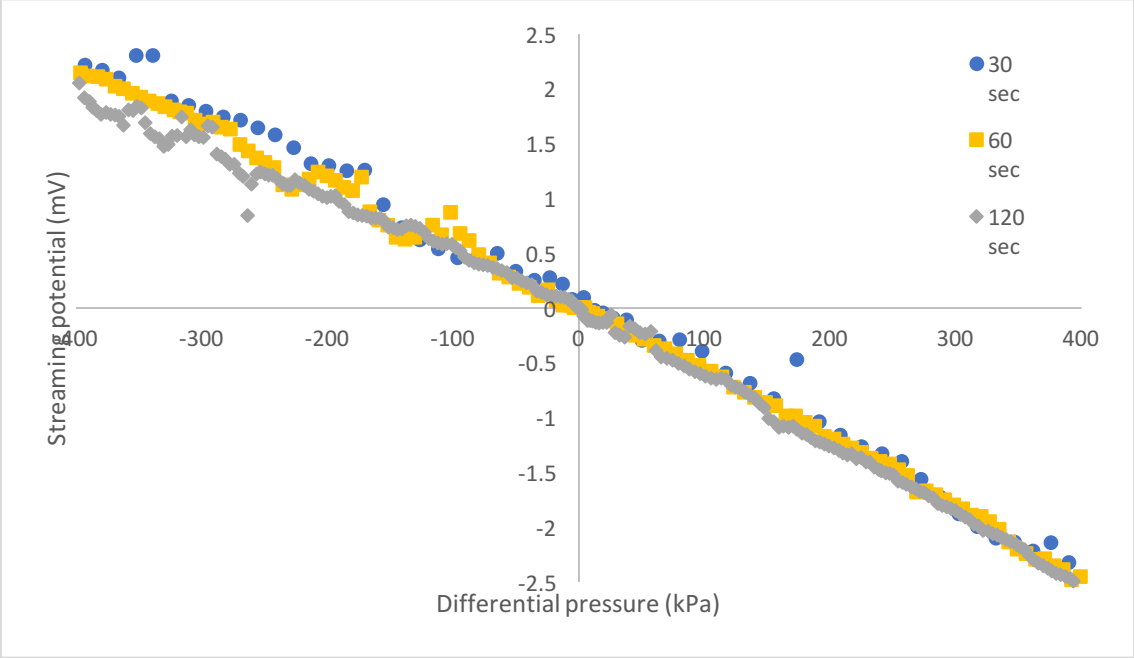

Graph 28: 0.033 M $CaCl_2$ with pressure ramping. The slope of a linear regression gave 5.59 mV/MPa with R^2=0.9936 for 120 second ramping time, 5.78 mV/MPa with R^2=0.9966 for 60 second ramping time and 5.95 mV/MPa with R^2=0.9937 for 30 second ramping time.

Table 15: Pressure ramping 0.033 M CaCl2.

Pressure ramping 0.033 M CaCl2		
Time range	C (mV/MPa)	Regression
240 sec		
120 sec	5.59	0.9936
60 sec	5.78	0.9966
30 sec	5.95	0.9937

4.2.3 0.1 M $CaCl_2$ experiment

The next brine had a salinity three times higher than the previous experiment. Only ramping times of 60 seconds or less managed to provide linear results. Thus, results of 120 second ramping time is not included.

Two identical experiments are presented. The first experiment yield a coupling coefficient of 0.88 mV/MPa for the 60 second ramping time with R^2=0.958 and 1.05 mV/MPa with R^2=0.985 for the 30 second ramping time (Graph 29). The slopes are steeper in the positive pressure area compared to the negative pressure area. The 60 second ramping shows this clearly as the electrical potential difference are 0.58 mV in the region from 0 to 450 kPa while the magnitude is only 0.27 mV in the region from 0 to -450 kPa. This explains the less accuracy of the regression that was of R^2=0.958.

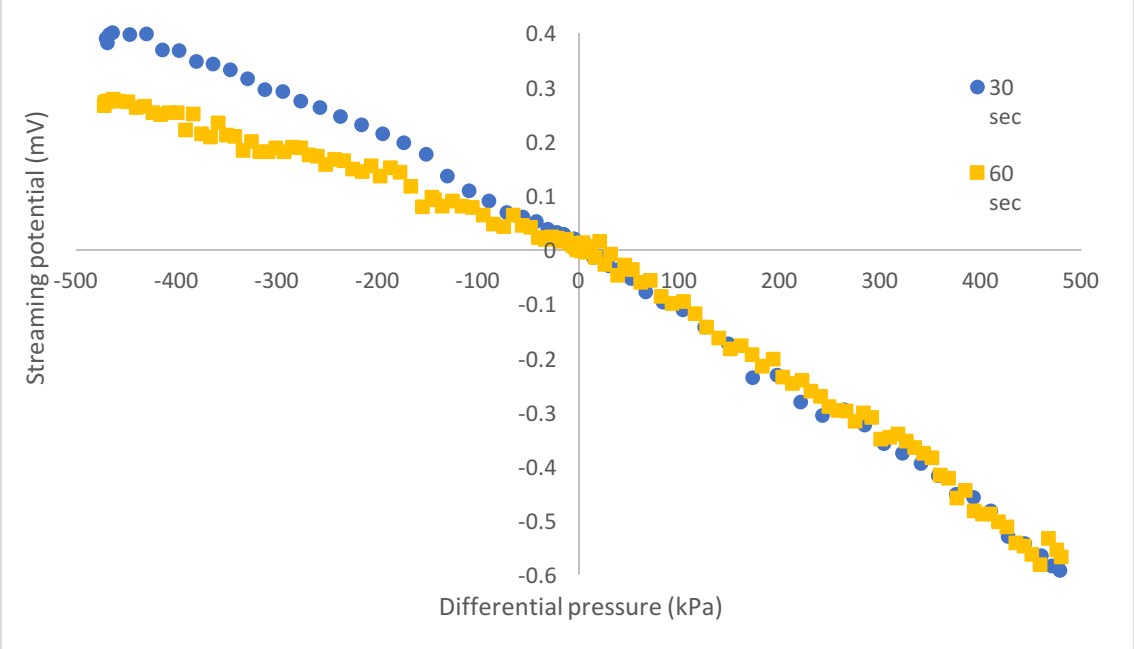

Graph 29: Pressure ramping of 0.1 M $CaCl_2$. The coupling coefficient yield 0.88 mV/MPa for the 60 second ramping time with R^2=0.958 and 1.05 mV/MPa with R^2=0.985 for the 30 second ramping time. The potential deviates in the negative pressure area for the 60 second ramping time.

Table 16: Pressure ramping 0.1 M CaCl2.

Pressure ramping 0.1 M CaCl2		
Time range	C (mV/MPa)	Regression
240 sec		
120 sec		
60 sec	0.88	0.958
30 sec	1.05	0.987

An identical experiment was conducted to check for similarities. The new results show a very similar trend (Graph 30); the streaming potential deviates very quick for negative pressures of 60 seconds. The coupling coefficient by the slope of a linear regression yield

0.94 mV/MPa with R^2=0.9702 for the 60 second ramping time and 1.11 mV/MPa with R^2=0.9922 for the 30 second ramping time.

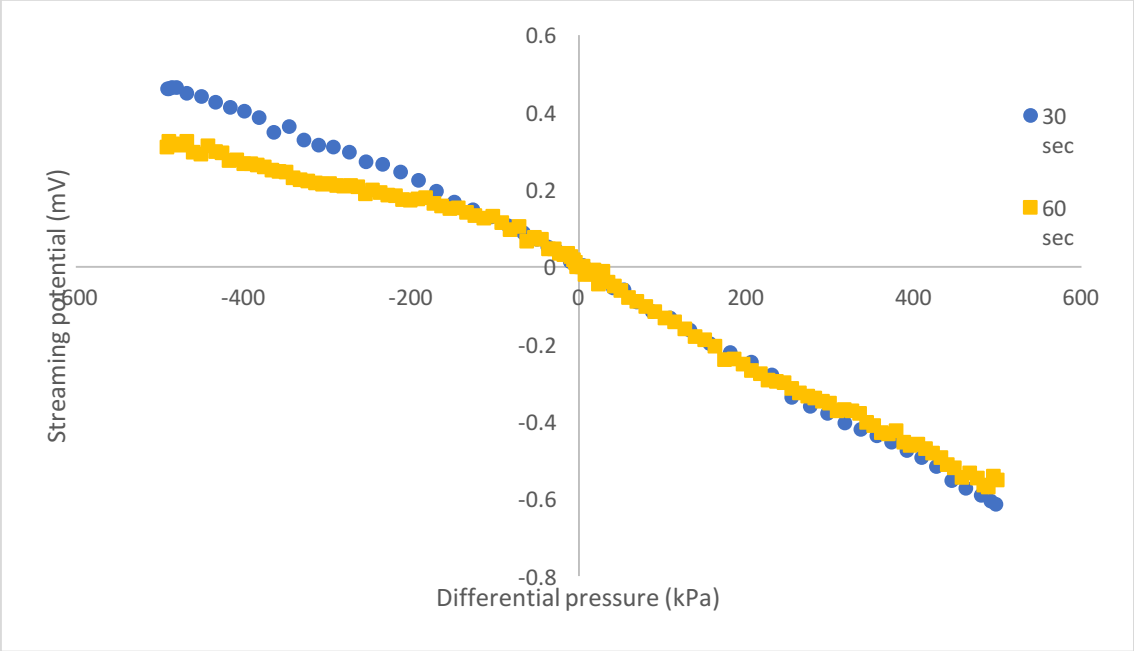

Graph 30: Pressure ramping of 0.1 M $CaCl_2$. The coupling coefficient by the slope of a linear regression yield 0.94 mV/MPa with R^2=0.9702 for the 60 second ramping time and 1.11 mV/MPa with R^2=0.9922 for the 30 second ramping time. Similar observation like for the previous experiment; the streaming potential does not manage to keep linear within the entire negative pressure region.

Table 17: Pressure ramping 0.1 M CaCl2.

Pressure ramping 0.1 M CaCl2		
Time range	C (mV/MPa)	Regression
240 sec		
120 sec		
60 sec	0.94	0.9702
30 sec	1.11	0.9922

4.2.4 0.2 M $CaCl_2$ experiment

The two next experiments presented contain the highest concentration of $CaCl_2$. The first one is previewed in Graph 31 below. Pressure ramping implemented with 120 second time range is even included here as they remained slightly stable during which the experiment was implemented. The coupling coefficients obtained from a linear regression was 0.41 mV/MPa with R^2=0.966 for the 120 second ramping time, 0.54 mV/MPa with R^2=0.994 for the 60 second ramping time and 0.38 mV/MPa with R^2=0.994 mV/MPa for the 30 second ramping time. This time, the linearity tended to deviate upward in the positive pressure region. The difference in magnitude of the coupling coefficient within the shortest and the longest ramping time was 0.035 mV/MPa which corresponds to 9.2 %.

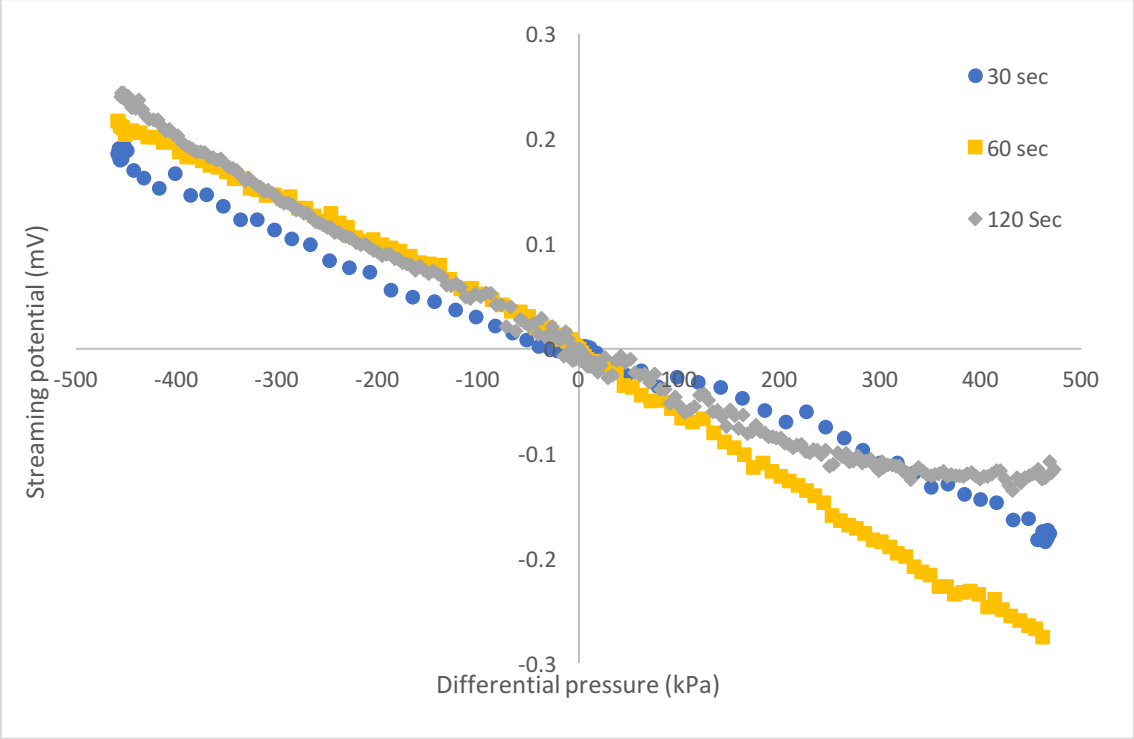

Graph 31: 0.2 M $CaCl_2$. The coupling coefficients obtained from a linear regression was 0.41 mV/MPa with R^2=0.966 for the 120 second ramping time, 0.54 mV/MPa with R^2=0.994 for the 60 second ramping time and 0.38 mV/MPa with R^2=0.994 mV/MPa for the 30 second ramping time.

Table 18: Pressure ramping 0.2 M CaCl2.

Pressure ramping 0.2 CaCl2		
Time range	C (mV/MPa)	Regression
240 sec		
120 sec	0.41	0.9664
60 sec	0.54	0.9943
30 sec	0.38	0.9936

Graph 32 presents an identical experiment of 0.2 M $CaCl_2$ with the same outcome as for the previous one. Coupling coefficients: 0.35 mV/MPa with R^2=0.966 for the 120 second ramping time, 0.35 mV/MPa with R^2=0.991 for the 60 second ramping time and 0.39 mV/MPa with R^2=0.993 for the 30 second ramping time. The difference within the shortest and longest ramping time corresponds to 0.046 mV/MPa (13.2%).

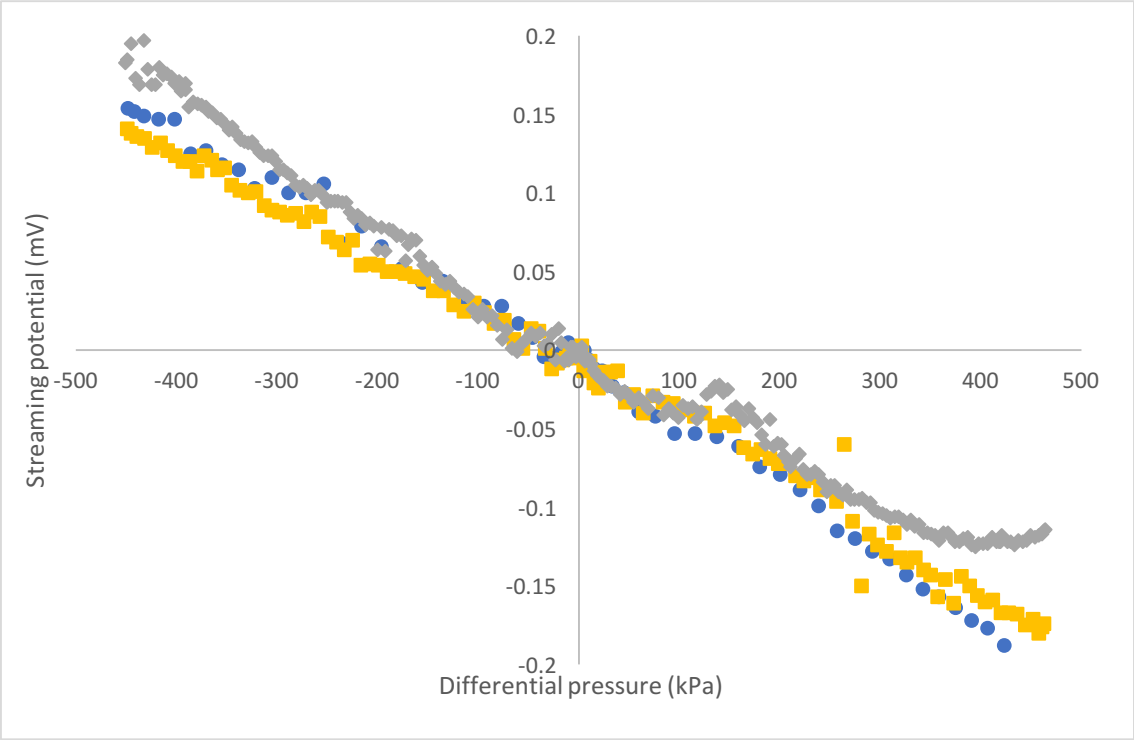

Graph 32: 0.2 M $CaCl_2$ pressure ramping, repeat. Coupling coefficients: 0.35 mV/MPa with R^2=0.966 for the 120 second ramping time, 0.35 mV/MPa with R^2=0.991 for the 60 second ramping time and 0.39 mV/MPa with R^2=0.993 for the 30 second ramping time.

Pressure ramping 0.2 M CaCl2		
Time range	C (mV/MPa)	Regression
240 sec		
120 sec	0.35	0.9664
60 sec	0.35	0.9906
30 sec	0.39	0.9933

Table 19: Pressure ramping 0.2 M CaCl2.

4.2.5 Overview coupling coefficient

All the experiments of $CaCl_2$ is plotted logarithmically in Graph 33 with the coupling coefficient vs. brine salinity. An empirical relation between the coupling coefficients and salinities within each different ramping time yield

Pressure ramping 120 sec $C = -0.062M^{-1.192}, R^2 = 0.976$ (3.19)

Pressure ramping 60 sec $C = -0.072M^{-1.156}, R^2 = 0.969$ (3.20)

Pressure ramping 30 sec $C = -0.068M^{-1.177}, R^2 = 0.969$ (3.21)

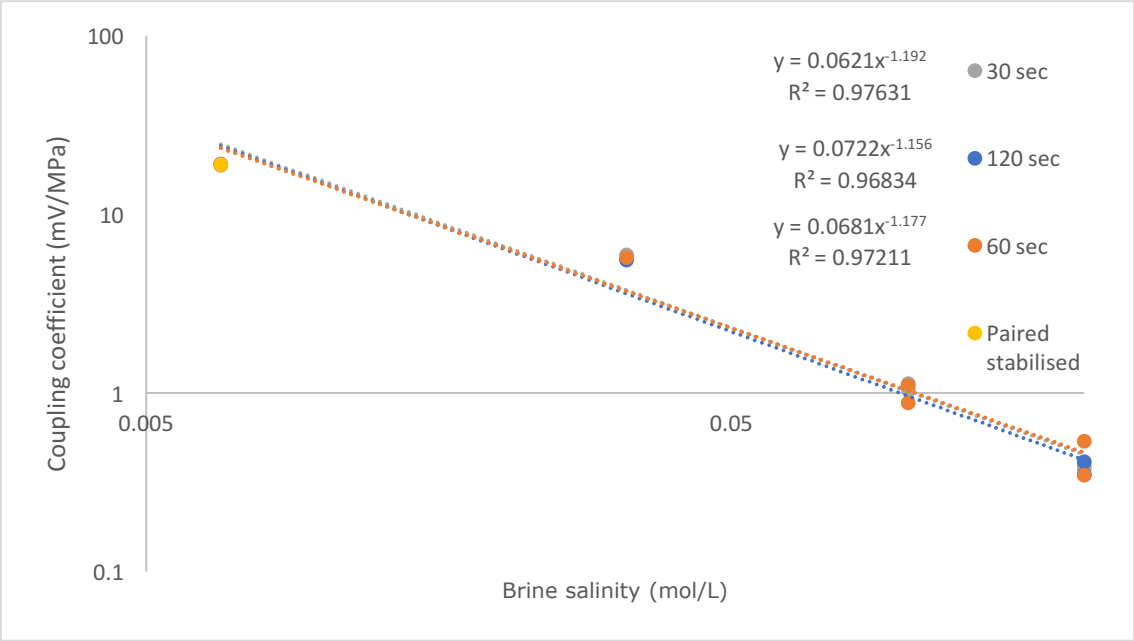

Graph 33: Coupling coefficient vs. brine salinity, CaCl2.

As seen visually from the plot, all the coupling coefficients are very similar for each distinct salinity regardless of what ramping time was implemented. The similarity of the empirical relationships ((3.19), (3.20) and (3.21)) acknowledge this.

4.2.6 Overview zeta-potential

Zeta-potentials are calculated using equation (3.10), presented in graph Graph 34 below. Underestimated values of Zeta-potential are corrected for as the formation factor and surface conductivity are accounted for. The overview demonstrates clearly that the higher salinity, the lower is the zeta-potential.

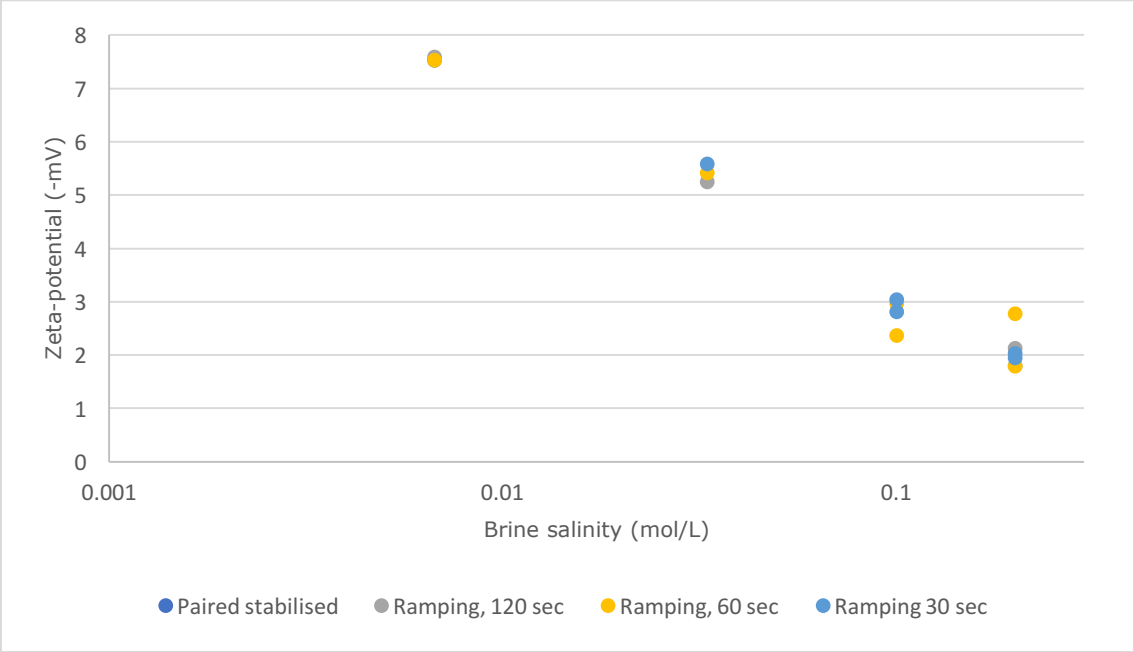

Graph 34: Zeta-potential $CaCl_2$. Underestimated values are corrected for.

Graph 35 below illustrates the impact of not take consideration of the formation conductance in the low-salinity region. Here, the zeta-potential are identical using 0.1 and 0.2 M $CaCl_2$, but differ for lower salinities. For 0.0067 M, the zeta-potential increased from -3 mV toward -7.5 mV when equation (2.22) was used, instead of (2.24).

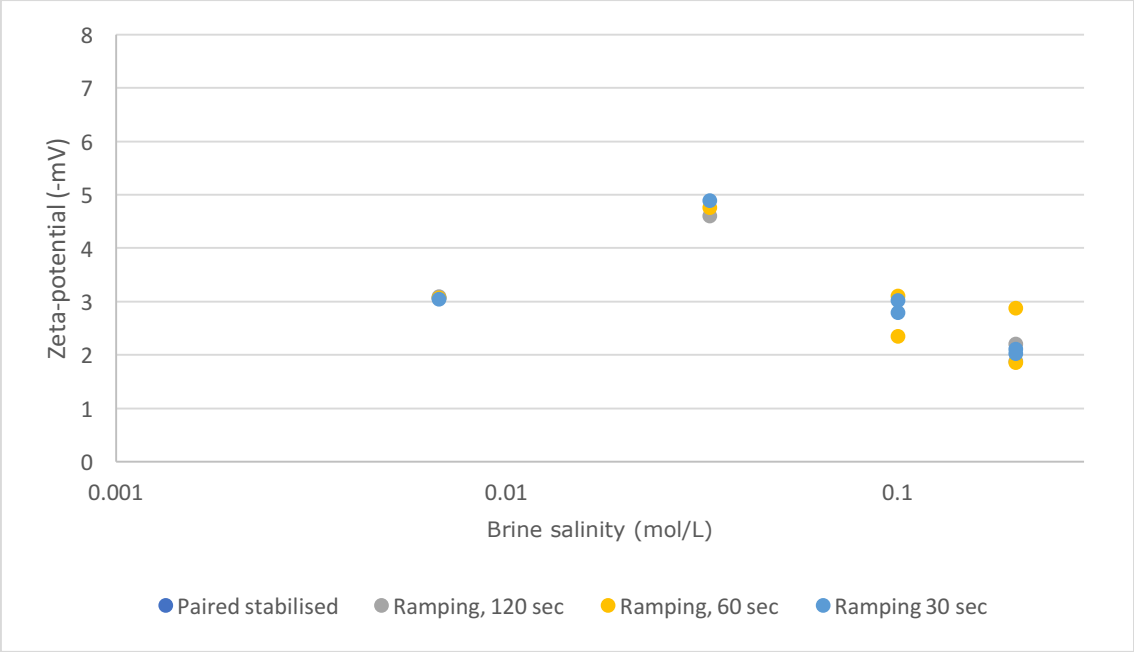

Graph 35: Zeta-potential vs. brine salinity using Smoluchowski's equation. Underestimated values are not corrected for. Clearly deviation for salinities less than 0.1 M.

4.3 NaCl + $CaCl_2$ experiment

4.3.1 0.02 M NaCl + $CaCl_2$ residuals

This experiment was originally meant to be a pure 0.02 M NaCl, and be presented along with the first experiments. However, the conductivity measurement of circulated sample was 0.23 S/m rather than 0.20 S/m (which was the case for the previous samples with 0.02 M NaCl). Because the last experiment conducted before this had a high concentration of Calcium Chloride and due to the fact that the conductivity is slightly increased, one should not exclude that small residuals of Calcium Chloride could accidently be retained in the core and mixed with the new brine. Because of this, the exact composition of this brine is not known. However, the intention for the experiments was to look for patterns or dissimilarities with different ramping times for low-salinity brines. This was poorly done for the first experiments of 0.02 M NaCl.

A summary of the results is shown in Table 20 below.

Table 20: Summary 0.02 M NaCl + CaCl2 residuals.

	pH		σ (S/m)		Coupling coefficient (mV/MPa)					Expt
Sal	Orig.	Equi.	Orig.	Equi.	Paired	240	120	60	30	
0.02		9.41	0.211	0.237	39.8	39.68	39.44	39.29	38.88	54,55
						39.73	39.61	39.48	38.99	51

The first experiment presented is the paired stabilised method (Graph 36). The stabilisation occurred relatively quickly for most of the pairs. The static voltage went back to its initial value after the experiment, -4.00 mV.

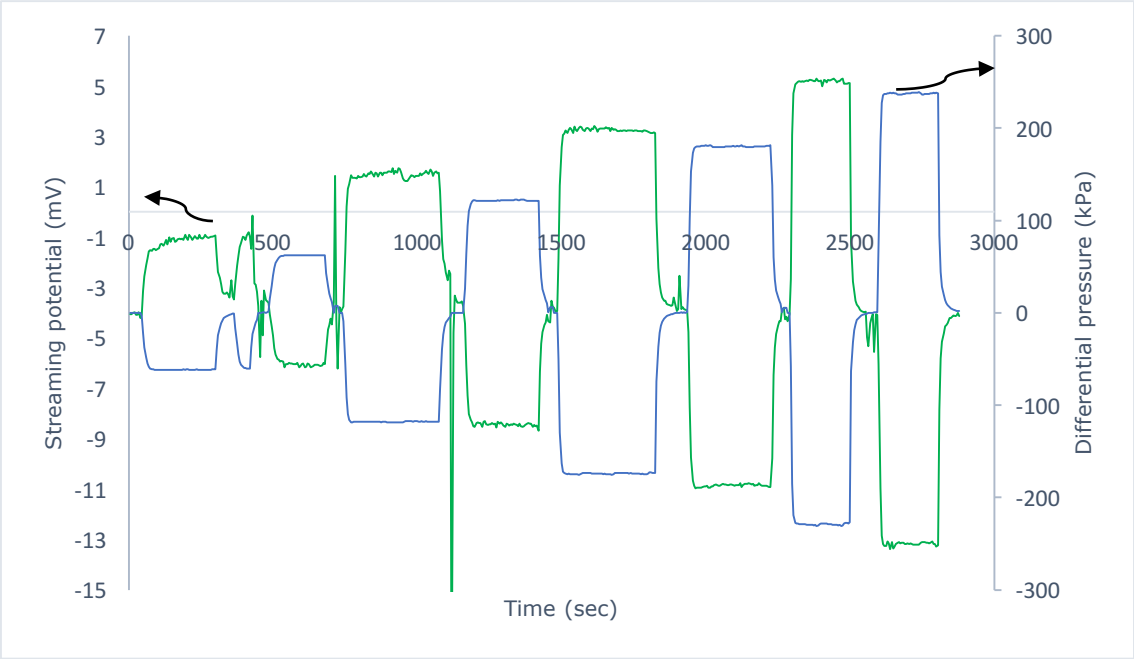

Graph 36: 0.02 M NaCl + CaCl2 residual.

The coupling coefficient yield 39.8 mV/MPa with a regression of 0.999. The linear regression is presented below Graph 37.

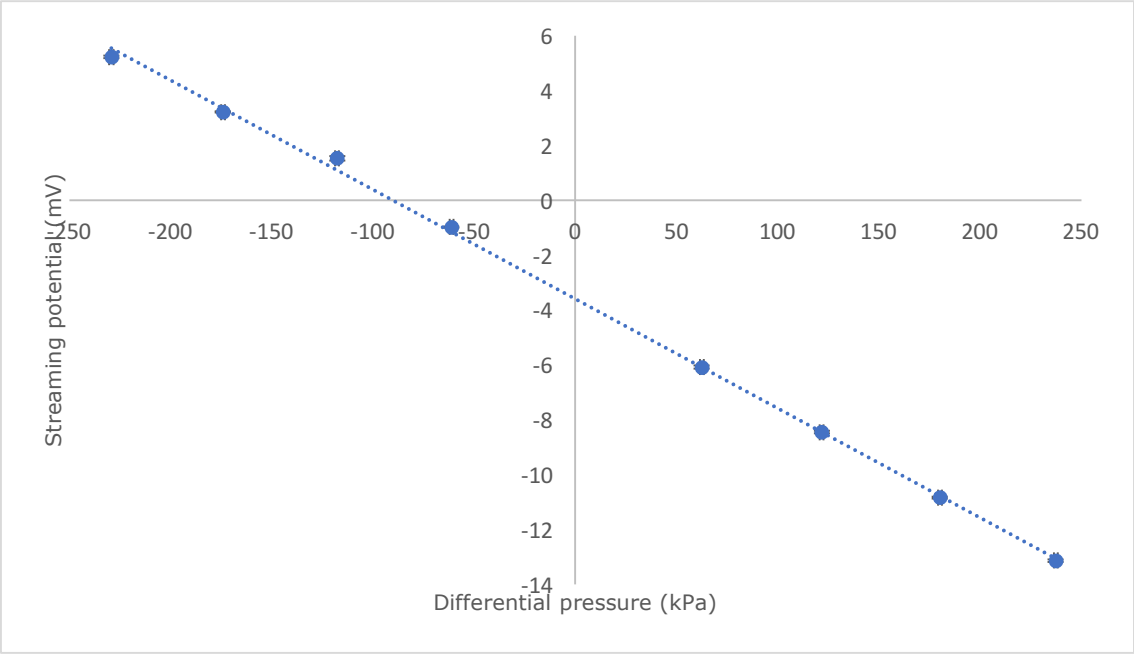

Graph 37: 0.02 M NaCl + $CaCl_2$ residual. The slope of a linear regression yield a streaming potential coupling coefficient of 39.8 mV/MPa with R^2=0.999.

Table 21: 0.02 M NaCl + $CaCl_2$ residual.

A-direction				B-direction				Paired stabilized	
Volt (mV)	dP (kPa)	STD. DEV	Vmax-Vmin	Volt (mV)	dP (kPa)	STD. DEV	Vmax-Vmin	(Vm1-Vm2)/2 (mV)	dP/2
-0.974	-61.2	0.024		-6.083	62.5	0.055		-2.555	61.8
1.534	-117.7	0.080		-8.452	121.7	0.056		-4.993	119.7
3.214	-174.2	0.025		-10.840	180.1	0.038		-7.027	177.2
5.229	-229.3	0.053		-13.138	237.5	0.043		-9.184	233.4

The two upcoming experiments is the pressure ramping method. Both are ramped with four different ramping time and the conditions are the same. It is of the interest to see if they will produce the same result.

The first result is presented below (Graph 38). The slope of a linear regression yield a coupling coefficient of 39.68 mV/MPa with R^2=0.9998 for the 240 second ramping time, 39.44 mV/MPa with R^2=0.9999 for the 120 second ramping time, 39.29 mV/MPa with R^2=0.998 for the 60 second ramping time and 38.88 mV/MPa with R^2=0.9993 for the 30 second ramping time. All the different ramping times could be conducted with no problem and the difference within them are small (2.1 % between the largest and the smallest coupling coefficient).

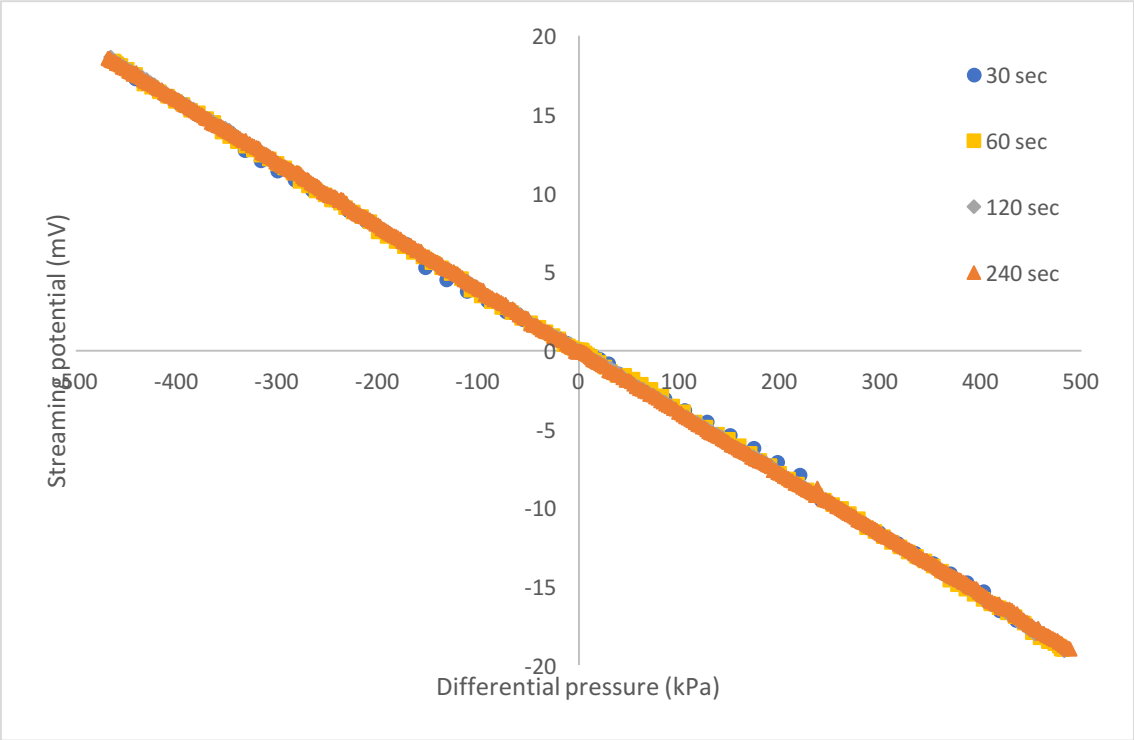

Graph 38: 0.02 M NaCl + $CaCl_2$ residual.

Table 22: 0.02 M NaCl + $CaCl_2$ residual.

0.02 M NaCl + <0.02 M CaCl2 Pressure ramping		
Time range	C (mV/MPa)	Regression
240 sec	39.68	0.9998
120 sec	39.44	0.9999
60 sec	39.29	0.9998
30 sec	38.88	0.9993

The same experiment was executed again. The coupling coefficient yield 39.73 mV/MPa with R^2=0.9998 for the 240 second ramping time, 39.61 mV/MPa for the 120 second ramping time with R^2=0.9999 and 39.48 mV/MPa for the 60 second ramping time with R^2=0.9998 and 38.99 mV/MPa with R^2=0.992 for the 30 second ramping time. The numbers are comparable with those of the previous experiment. The coupling coefficient of the longest ramping time was 1.9 % greater than one of the shortest ramping time.

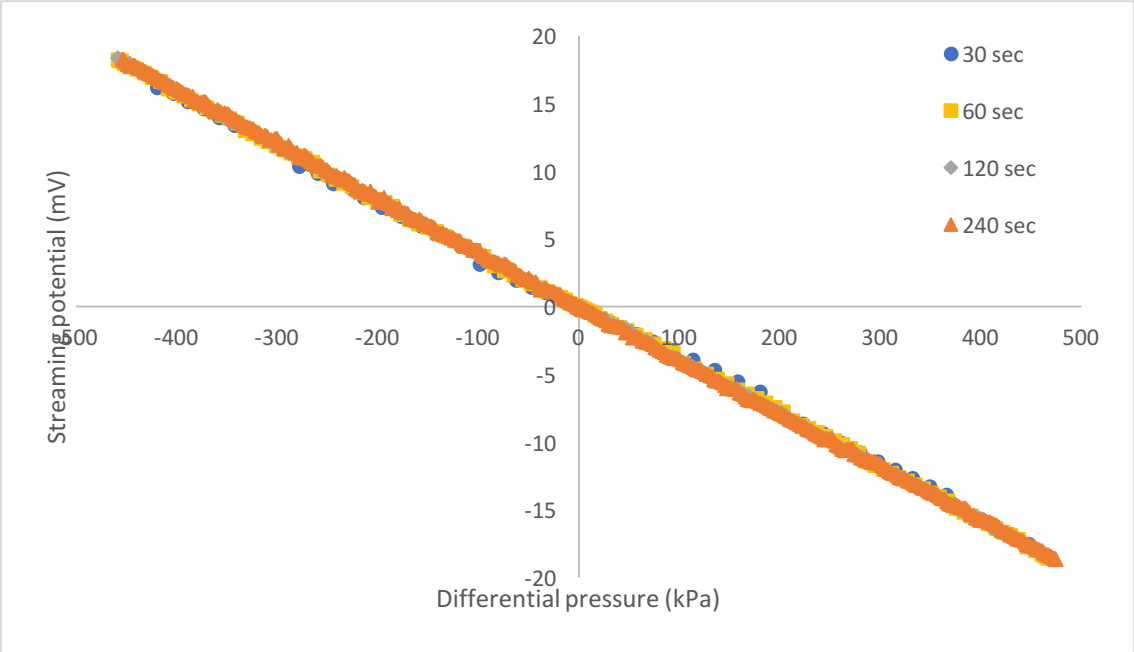

Figur 34: 0.02 M NaCl + $CaCl_2$ residual, repeated.

Table 23: 0.02 M NaCl + $CaCl_2$ residual pressure ramping.

0.02 M NaCl + <0.02 M CaCl2 Pressure ramping		
Time range	C (mV/MPa)	Regression
240 sec	39.73	0.9998
120 sec	39.61	0.9999
60 sec	39.48	0.9998
30 sec	38.99	0.9992

5 Discussion

The majority the streaming potential coupling coefficient calculated shows a clear correlation with salinity. The streaming potential decreased for higher concentrations of salt and increased linearly with respect to applied rate from the pump (and hence differential pressure), which supports the concept of the streaming current described in the theory section and in the Helmholtz-Smoluchowski equation.

To confirm the reliability of the results, they are compared with other similar experiments that was executed on sand and sandstones using mainly NaCl. Note that some variation is expected as the core plugs are different.

The researchers from Imperial College sampled experimental data from 12 published papers and made an empirical formula based on them. The regression matched the data with R^2=0.9182. The empirical formula is plotted as a function of the NaCl salinity that was used in this thesis along with the rest of the results, and it is encouraging that our results match with the Imperial College correlation.

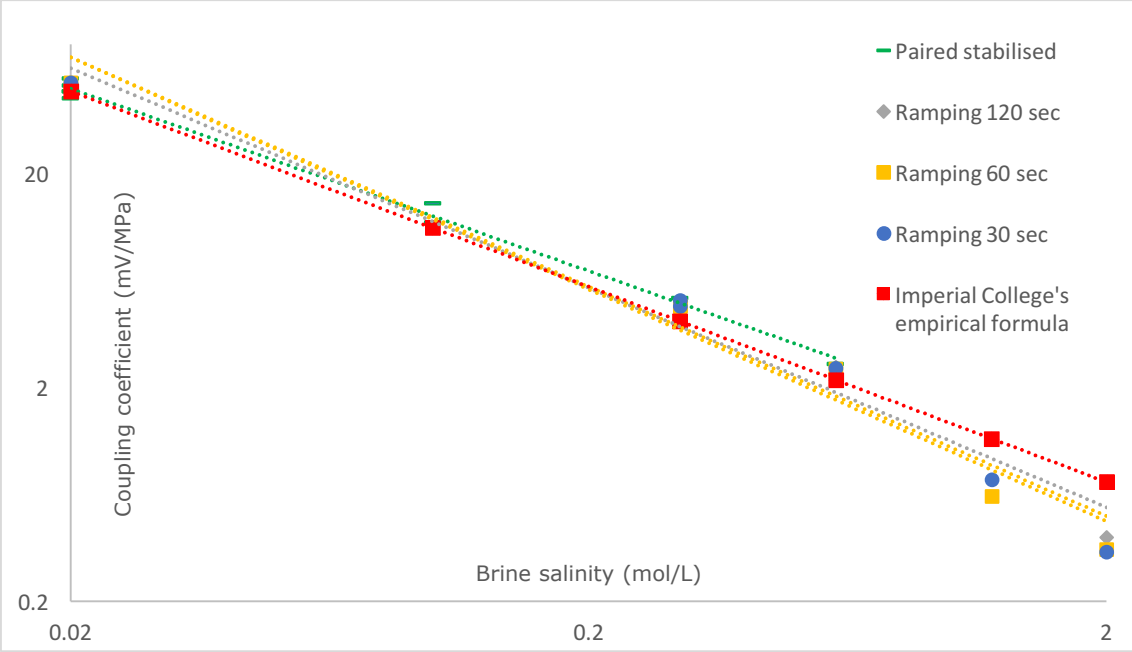

Graph 39: Empirical formulas based on different measurement methods + Imperial College's empirical formula based on 12 published data. The results are comparable.

5.1 The impact of salt type

The samples of CaCl2 brines was prepared with the same ionic strength as the ones flooded with NaCl. 0.0067 M CaCl2 is equivalent to 0.02 M NaCl, 0.033 M CaCl2 is

equivalent to 0.1 M NaCl etc. (with respect to their ionic strength). However, the streaming potential does not have the same values for the $CaCl_2$ as it has for NaCl for equal ionic strength. The coupling coefficient is almost three times larger for NaCl than for the $CaCl_2$ in the low salinity range. The difference increases as the coupling coefficient is about 5 times larger for NaCl than for $CaCl_2$ in the high salinity range.

This can probably be attributed to the fact that Ca^{2+} has a stronger interaction with the quartz surface, due to the valence. From the theory section, we saw that the solid surface generated a charge from the reactive silanol group in the mineral lattice, equation, eq. (2.1). In the process of protonation from the surface, an adsorption process occurs, eq. (2.2). Since the positively adsorbed cations are divalent instead of monovalent, this surface site (that was neutral for NaCl-brine) is now positively charged. Thus, the surface net charge is less negative than it is if monovalent ions are adsorbed to the Stern layer. The result is, as clearly proven by the streaming potential, less mobile counter ions in the diffuse layer.

5.2 Coupling coefficient vs. experimental methodology

Several experiments have been conducted, most of them with different methods. The magnitude of the coupling coefficient vs. the experimental methodology is divided into three sections as there are observed characteristic different pattern within each section. The low salinity sections are for <0.1 M NaCl and <0.033 M $CaCl_2$, medium salinities are for 0.1<M<0.6 for NaCl and 0.033<M<0.1 $CaCl_2$. The concentrations above belong to the high salinity section.

5.2.1 Low salinity

Regardless of the experimental methodology used, the coupling coefficients yield quite the same value. However, an observation is that the coupling coefficient from the longer pressure ramping period usually have a slightly greater magnitude than for the short pressure ramping period, but only by 2 %. The magnitude of the coupling coefficient from the paired stabilised methods does not have a specific pattern compared to the pressure ramping method based on the data from this thesis. For the CaCl2 experiment the value of the paired stabilised method (19.03 mV/MPa) matches the pressure ramping period of 60 seconds best (19.0 mV/MPa) while for the NaCl+$CaCl_2$ residual experiment the value of the paired stabilised method (39.8 mV/MPa) matches the pressure ramping of 240 seconds best (39.68 mV/MPa).

Which method that corresponds to the most accurate result is hard to conclude. It is believed that the disadvantage using pressure ramping is that steady state may not be achieved if the pressure is ramped too quickly. Since there was no problem executing a pressure ramping of a long-time range, this method might be the preffered.

5.2.2 Medium salinity

In this salinity range, problems often occurred regarding the paired stabilised experiments. Due to much instability, it was difficulties choosing the right value for the fundamental of the coupling coefficient. However, the pressure ramping method proved to work properly for the time ranges up to 120 seconds. Above this range, problem usually occurred as the static voltage could change during which the experiment was implemented and thus drift the streaming potential away from its logic path under the pressure build-up.

A common pattern when comparing the different pressure ramping methods is that the coupling coefficient increases for faster pressure ramping. This is exactly the opposite than for the low salinity brines. This effect can be significant. For example, for 0.3 M NaCl, the coupling coefficient of the 120 second time range yield 4.70 mV/MPa while for the 30 second, it increased to 5.10 mV/MPa, which is 8.5% more. The same result can be seen from one of the $CaCl_2$ experiments, with a difference of 6%. Note that this did not happen for all the experiments. For example, for 0.6 M NaCl, the coupling coefficient of the most rapid pressure build-up was 1.2 % lower than for the longest one.

One idea that this pattern is common may be related to the streaming current and the conduction current (equation (2.32) and (2.33) from the theory section). When the pressure is ramped too quickly, the magnitude of the streaming current (which relocate the excess of the counter ions from the diffuse layer) is higher than the conduction current (which counteracts the streaming current) as steady state is not achieved. If this was the case, one may question why this did not happened any time for the low salinity brines. As the diffuse layer is more compact for higher salinities, the streaming current and the conduction current may be more sensitive as more ions are present.

If the explanation is that equilibrium was not achieved for the more rapid ramping times, experiments should not be implemented in a short-range ramping time.

5.2.3 High salinity

For higher salinities of brine, no specific pattern was observed within the different types of experiments. Only pressure ramping techniques yielded good results. Short-range ramping times, like 60 second and 30 second worked fine, and in some cases 120 second time experiments worked.

However, the validity of these experiments might be questionable. Some of the results show that the slope of a linear regression differs between the negative pressure area and the positive pressure area (i.e. opposite flow direction). Experiment 2.0 M NaCl (Graph 19) clearly shows an example of this. The slope from the 120 second ramping time is a lot steeper than for the shorter ramping times.

It is reasonable that the static potential had time to fluctuate during which the pressure ramping was implemented, and hence, the fluctuations and other transient physical behaviour overrides the value of the coupling coefficient in itself. If the change in static voltage happens linearly during which the pressure ramping is implemented, the regression can be very good even the result is inaccurate.

In such situations, it is important to look for differences in the linearity between the negative and positive pressure ranges. If the slopes are different for the different flow directions, there is uncertainty and potential inaccuracy in the results. They are supposed to be similar.

Based on the results from the high salinity experiments, it is obvious that static voltage generation can be a problem also for the pressure ramping methods. The magnitude of the coupling coefficients for these experiments is so low that even small changes in static voltage may be significant compared to the signal itself and thus may impair the result. Hence, it seem as the more rapid the pressure ramping is done the less changes in static voltage will disturb the results.

5.3 Instability

Time is also a factor when conducting the paired stabilised experiments. According to Vinogradov's experimental methodology description, flow was terminated stable once stable voltage and pressure across the sample had been recorded with a variation of <10 μV and <2 kPa over 1200 seconds (20 min).

In our case, the voltage stabilized within a few seconds, but a variation in the signal less than 10 μV was very unlikely to obtain. A variation under 100 μV was more common. For the low salinity experiments, such a small variation does not have any affection the results. However, for the high salinity brines the impact was significant, as we have seen and discussed before. That is why the pressure ramping method was favoured.

It is difficult to understand the root of this problem as there are many factors that could be the cause. One theory could be that there is something that could be improved in the experimental set up, to avoid outside disturbances. Filling the pressure gauge with isopar oil was a fundamental discovery that enhanced the stability significantly. Clearly, it is of great importance to void any kind of short circuiting in the equipment. We have used an electrometer to measure the voltage, but maybe it is possible to replace this system with easier, special purpose build, measuring devices.

One should of course not fully exclude that the cause of the instability is related to physical processes within the core itself and that the measured values of the streaming

potential is correct. It could be an important observation that the fluctuation would occur only in one direction, which was the case for many of the paired experiments. Another common observation from several experiments is that stability seems easier to obtain for small rates, while for the higher rates (5-10 ml/min) the voltage fluctuated and drifted more. A possible reason could be that small fragments or particles inside the core could affect the results.

5.4 Zeta-potential

The zeta-potentials that was calculated had a clear difference in the low-salinity region with respect to the simplified Smoluchowski equation (2.24) and equation (2.22). Based on the results, noticeable differences occur for brine salinities <0.1 M NaCl. This number is supported among other researchers (Jaafar, Vinogradov et al. 2009);(Leroy, Devau et al. 2013).

The negatively charged zeta-potential decreases in magnitude when the brine salinity increases. This observation supports the theory for which the compaction of the diffuse layer decreases the net charge in the shear plane.

As also observed, the charge in the shear plane (zeta-potential) is smaller for CaCl2 brine than for NaCl brine (-10 mV for 0.1 M NaCl and -3 mV for 0.1 M CaCl2). The reason can be explained as the same as discussed in section 5.2.

6 Conclusion

In this thesis, we have for the first time (at IRIS) performed successful streaming potential measurements. Several improvements have been made during this thesis that has greatly improved the measurements, such as replacing the steel end pieces with plastic end pieces, filling the pressure gauge with oil, and making sure that there were no air bubbles in the electrodes. This thesis clearly shows that the small experimental details are of importance, one tine detail could ruin the whole experiments. We have come a long way in this thesis and have successfully measured the streaming potential at low salinity, but further work with this set up will potential resolve some of the issues we had with the fluctuating potentials at constant flooding rate and high salinity.

In addition, it was of interest to see if different measurement methods had any significant impact on the results. Among all observations and interpretation of the results, a conclusion can be set:

- The results of low salinity brines differ in small magnitude regardless of what method is implemented. The uncertainty and repeatability is low (within 2 %) compared to the magnitude of the streaming potential.
- In the medium salinity range, steady state does not seem to be achieved for the rapid pressure ramping experiments. A probable explanation is that the streaming current overrides the conduction current. Experiments with ramping time over 120 seconds would be favoured (or paired stabilised experiments – if possible).
- Changes in static voltage is a major problem for the experiments at high salinities. Rapid pressure ramping is the only way this problem can be minimized.
- To verify if pressure ramping results are trustworthy, the slope of a linear regression should be similar in both flooding directions. If not, it is an indication that static voltage has been fluctuating during time at which the pressure ramping was implemented.

7 Further work

Some of the conclusions from the observed results was based on a too low number of experiments in order to provide significant statistical evidence to draw firm conclusions. Even though the observations (and conclusions based on them) seem legit, more repeatable tests within each distinct brine sample would strengthen its trustworthiness. The groundwork is now verified and a lot of experiments for a distinct brine can easily be implemented during 1-2 days.

It could be an idea to have a shorter interval between the different salinities of the brines. The samples in this thesis had 3-5 times higher concentration (0.02 M, 0.1, 0.3 etc.) It could be worth looking at pattern regarding measurement techniques in between these salinities (like for example run experiments with 0.02 M, 0.05 M, 0.1 M, 0.2 M etc).

One can never be too perfectionist when it comes to the impact of fluctuating static voltage. Further hunting on the fluctuation source is always possible. It could be an idea to assemble a core holder made entirely of plastic to see if this will improve the stability of the measurements. The core used in this thesis should theoretically be fully isolated from the core holder (plastic end pieces, rubber sleeve). However, it was observed that fluctuations were trigged only by touching the core holder, indicating that there might be some current leakage.

It would be an idea to establish residual oil saturation of a core, assemble it in the core holder and run experiments similarly to Jackson and Vinogradov who did this with a chalk core (Jackson and Vinogrado 2012). However, the core had to be water-wet in order not to disrupt the continuity the double layers at the mineral-brine interface as if the core was oil-wet the double layer would not be continuous and a streaming potential would not necessary develop.

Another interesting study would be to investigate how the streaming potential coupling coefficient is affected by adjusting the viscosity of the brine by adding polymers. It could be of interest to see if the relationship between the viscosity and the coupling coefficient was linear, or if non-linear effects would occur from any electrostatic properties of the polymer chains. If it was not linear, the polymers themselves would affect the electrokinetic phenomena, which would be of interest. If on the other hand the relationship between the coupling coefficient and the viscosity was linear, streaming potential with polymers could be a powerful tool to investigate polymer degradation.

8 References

Aberdeen, U., International Drilling Fluid Limited (1982). "International Drilling Fluids (IDF)." Clay chemistry. Technical manual.

Anderson, W. G. (1986). "Wettability Literature Survey- Part 1: Rock/Oil/Brine Interactions and the Effects of Core Handling on Wettability."

Austad, T. (2013). Water-Based EOR in Carbonates and Sandstones-Chapter 13:New Chemical Understanding of the EOR Potential Using "Smart Water", Elsevier Inc.

Boleve, A., et al. (2007). "Streaming potentials of granular media: Influence of the Dukhin and Reynolds numbers." Journal of Geophysical Research: Solid Earth **112**(B8).

Chesick, J. P. (1972). "Physical chemistry, second edition (Castellan, Gilbert W.)." Journal of Chemical Education **49**(8): A433.

Craig, F. F. (1971). "The reservoir engineering aspects of waterflooding." Henry L. Doherty Memorial Fund of AIME.

Donaldson, E. and W. Alam (2008). Wettability, Gulf Publishing Company, Hourston, Texas.

Geoscience, A. (2017). "Non-Polarizable Electrode." from https://www.agiusa.com/non-polarizable-electrode.

Glover, P. W. and M. D. Jackson (2010). "Borehole electrokinetics." The Leading Edge **29**(6): 724-728.

Gottlieb, M. A. and R. Pfeiffer (1963). "The Kinetic Theory of Gases." from http://www.feynmanlectures.caltech.edu/I_39.html.

Hunter, R. J. (1981). "Zeta Potential in Colloid Science." Academpic press.

Jackson, M. D. and J. Vinogrado (2012). "Impact of wettability on laboratory measurements of streaming potential in carbonates." Colloids and Surfaces A: Physicochemical and Engineering Aspects **393**: 10.

Jouniaux, L. and J. P. Pozzi (2000). "Streaming potential in volcanic rocks from Mount." Journal of Geophysical Research **105**(B4): 8391-8401.

Jaafar, M. Z., et al. (2009). "Measurement of streaming potential coupling coefficient in sandstones saturated with high salinity NaCl brine." Geophysical Research Letters **36**(21): n/a-n/a.

Karplus, K. (2014). "Polarizing and Non-polarizing Electrodes." Applied Circuits.

Leroy, P., et al. (2013). "Influence of surface conductivity on the apparent zeta potential of amorphous silica nanoparticles." Journal of Colloid and Interface Science **410**: 81-93.

Manhardt, P. D. (1999). "Streaming potential in porous media 2. Theory and application to geothermal systems." Journal of Geophysical Research **Vol 104**: 20033-20048.

Revil, A. and P. A. Pezard (1999). "Streaming potential in porous media: 1. Theory of the zeta potential." Journal of Geophysical reseach **104**: 20021-20031.

Shaw, D. J. (1992). Introduction to Colloid and Surface Chemistry, Butterworth-Heinemann.

Whelan, P. M. and M. J. Hodgeson (1978). "Essential Principles of Physics (2nd edition)." John Murray.

Appendix A Core data estimation

Appendix A.1 Porosity

The porosity of a reservoir core is defined as the fraction of pore volume relative to the bulk volume

$$\phi = \frac{V_p\ [m^3]}{V_b\ [m^3]} \tag{A-1}$$

The pore volume is defined as

$$V_p = \frac{W_w - W_d\ [kg]}{\rho_w\ \left[\frac{kg}{m^3}\right]} \tag{A-2}$$

where W_w is the weight of the rock fully saturated with brine and W_d is the weight of the dry rock.

The bulk volume is simply the volume of the core measured using a slide capiler

$$V_b = \pi \left(\frac{d\ [m]}{2}\right)^2 L\ [m] \tag{A-3}$$

Substitute (A-2) and (A-3) in (A-1), we get

$$\phi = \frac{W_w - W_d\ [kg]}{\rho_w\ \left[\frac{kg}{m^3}\right] \pi \left(\frac{d\ [m]}{2}\right)^2 L\ [m]} \tag{A-4}$$

Appendix A.2 Permeability

The permeability of the cores was calculated by applying several injection rates in both directions and measure the differential pressure across the core. The average permeability could then be measured. The corresponding deviation was also calculated.

The permeability was calculated using Darcy's law

$$q\ \left[\frac{m^3}{s}\right] = \frac{k\ [m^2]}{\mu\ [Pas]} A\ [m^2] \frac{dP\ [Pa]}{L\ [m]} \tag{A-5}$$

where k is the unknown permeability, μ is the viscosity of the fluid, A is the area, L is the length of the core and dP is the differential pressure across the core.

Substituting (A-5):

$$k = \frac{q}{A}\mu\frac{L}{dP} \tag{A-6}$$

Because not all input values are given in SI-units, the following unit calculation was made:

$$k\ [mD] = \frac{[ml/min]\frac{10^{-3}}{1}\frac{l}{ml}\frac{10^{-3}}{1}\frac{m^3}{l}\frac{1}{60}\frac{min}{s}\ [Pas]}{m^2\ \frac{1000\ Pa}{1\ kPa}}\frac{1}{0.987\cdot 10^{-15}}\frac{mD}{m^2} \tag{A-7}$$

The data based on the permeability calculation is presented below:

Permeability estimation Core 1		
Rate [ml/min]	dP [kPa]	k [mD]
-10	-270.5	39.90
-9	-246.9	39.34
-8	-220.0	39.24
-7	-194.5	38.84
-6	-169.4	38.22
-5	-141.2	38.22
-4	-113.3	38.10
-3	-86.2	37.56
-2	-59.9	36.03
-1	-31.0	34.81
1	29.8	36.21
2	56.4	38.27
3	81.7	39.63
4	106.9	40.38
5	133.2	40.51
6	159.3	40.65
7	183.3	41.21
8	208.6	41.39
9	232.5	41.78
10	258.0	41.83
Average permeability		**39.11**
Standard deviation		**1.96**

Permeability estimation Core 2		
Rate [ml/min]	dP [kPa]	k [mD]
-8	-211.7	40.79
-6	-160.7	40.29
-4	-109.4	39.45
-2	-57.5	37.55
2	53.8	40.12
4	104.9	41.17
6	159.3	40.66
8	214.0	40.34
Average permeability		**40.05**
Standard deviation		**1.13**

Appendix A.3 Surface conductance

Data form resistivity measurement with different frequencies are listed below. The green highlighted boxes represent the value of resistance (R) that corresponded to least reactance (X). All values of R, X and Z are given in ohm (Ω) (equivalent to S^{-1}). Saturated rock conductivity (σ_f) is calculated using equation (3.9).

			0.1 kHz				1 kHz			
M NaCl	M CaCl2	Conductivity brine (S/m)	Z	Deg	R	X	Z	Deg	R	X
0.02		0.24	4812.0	-1	4811.3	84.0	4747.0	-6	4721.0	496.2
0.1		1.22	1076.9	-1.5	1076.5	28.2	1065.7	-0.4	1065.7	7.4
0.3		2.68	510.2	-2.4	509.8	21.4	503.8	-0.5	503.8	4.4
0.6		5.09	284.7	-4	284.0	19.9	279.2	-0.7	279.2	3.4
1.2		9.51	159.5	-6.1	158.6	16.9	154.3	-1	154.2	2.7
2		12.77	107.7	-8.8	106.4	16.5	102.2	-1.3	102.2	2.3
	0.0067	0.1946	5079.0	-0.9	5078.4	79.8	5039.0	-2.2	5035.3	193.4
	0.033	0.58	2193.0	-1	2192.7	38.3	2179.0	-0.3	2179.0	11.4
	0.1	1.75	796.5	-2.1	796.0	29.2	788.6	-0.4	788.6	5.5
	0.2	3.2	437.3	-3.3	436.6	25.2	430.7	-1.1	430.6	8.3

			10 kHz				100 kHz			
M NaCl	M CaCl2	Conductivity brine (S/m)	Z	Deg	R	X	Z	Deg	R	X
0.02		0.24	4684.0	-0.6	4683.7	49.0	4093	-4.7	4079.2	335.4
0.1		1.22	1060.2	-0.3	1060.2	5.6	1023	-1.4	1022.7	25.0
0.3		2.68	502.0	-0.2	502.0	1.8	492.9	-0.8	492.9	6.9
0.6		5.09	278.3	-0.2	278.3	1.0	275.2	-0.5	275.2	2.4
1.2		9.51	153.6	-0.2	153.6	0.5	152.56	-0.3	152.6	0.8
2		12.77	101.7	-0.3	101.7	0.5	101.3	-0.2	101.2	0.4
	0.0067	0.1946	4717.0	-15.6	4543.2	1268.5	2425.0	-30.4	2091.6	1227.1
	0.033	0.58	2170.0	-0.3	2170.0	11.4	2034.0	-2.6	2031.9	92.3
	0.1	1.75	786.6	-0.2	786.6	2.7	766.7	-1.5	766.4	20.1
	0.2	3.2	426.8	-5.5	424.8	40.9	322.7	-27.8	285.5	150.5

M NaCl	M CaCl2	Conductivity brine (S/m)	Best resistance	**Saturated rock conductivity σ_f**
0.02		0.24	4683.7	**0.0136**
0.1		1.22	1060.2	**0.0603**
0.3		2.68	502.0	**0.1272**
0.6		5.09	278.3	**0.2295**
1.2		9.51	153.6	**0.4158**
2		12.77	101.7	**0.6283**
	0.0067	0.19	5078.4	**0.0126**
	0.033	0.58	2170.0	**0.0294**
	0.1	1.75	786.6	**0.0812**
	0.2	3.20	430.6	**0.1483**

Appendix B Empirical formulas

Appendix B.1 Relative permittivity

The relative permittivity of the fluid was estimated using the following empirical relation, presented in (Manhardt 1999).

The permittivity as a function of temperature is given as

$$\epsilon_r(T) = a_0 + a_1 T + a_2 T^2 + a_3 T^3 \qquad \text{(A-8)}$$

where a0 = 295.68, a1 = -1.2283 K^-1, a2 = 2.094*19^-3 K^-2 and a3 = -1.41*10^-6 K^-3. T is given in Kelvin, and the range for which this empirical formula is valid is [273 K, 373 K].

Further, the permittivity as function of temperature and concentration of NaCl is given by

$$\epsilon_r(C;T) = \epsilon_r(T) + c_1 C + c_2 C^2 + c_3 C^3 \qquad \text{(A-9)}$$

where C is the salt concentration in mol/L, c1 = -13 L/mol, c2 = 1.065 (L/mol)^2 and c3 = -0.03006 (L/mol)^3.

Appendix B.2 Electrical conductivity

The electrical conductivity of a given Sodium Chloride brine (NaCl) as a function of temperature and salinity can be estimated by this empirical formula (derived by Send and Goode (1991) and presented by (Manhardt 1999):

$$\sigma_f(C_f;T) = (d_1 + d_2 T + d_3 T^2) C_f - \frac{d_4 + d_5 T}{1 + d_6 C_f} (c_f)^{\frac{3}{2}} \qquad \text{(A-10)}$$

where d1=5.6, d2=0.26, 3d = 1.510*10^-4, d4=2.36, d5=0.099, d6=0.214, σ_f is in S/m, T is in celcius and salinity in molarity.

Note that this equation was only used to verify the measured sample conductivity.

Appendix C Poiseuille's law

When deriving a mathematical expression for the streaming potential, one must start with expressing the Poiseuille's law. This expression is valid when assuming a constant rate of a Newtonian fluid trough a cylindrical pipe with a constant circular cross section. The flow must be laminar.

We consider a cylindrical tube of fluid with radius R and distance from the centre toward a given point in the cylinder, r.

The driving force of the liquid due to pressure difference is given as;

$$F_p = \Delta PA = \Delta P(\pi r^2) \tag{A-11}$$

The viscous drag force is dependent on the surface area of the tube. The sign is negative as the drag is working against the pressure drop;

$$F_\mu = -\mu 2\pi rl \left(\frac{dv}{dr}\right) \tag{A-12}$$

When the system is in equilibrium with constant velocity, the net force goes to zero;

$$F_P + F_\mu = 0 \rightarrow F_P = -F_\mu \tag{A-13}$$

$$\Delta P(\pi r^2) = \mu 2\pi rl \left(\frac{dv}{dr}\right) \tag{A-14}$$

Solve with respect to dv/dr;

$$\frac{dv}{dr} = \frac{\Delta P(\pi r^2)}{\mu 2\pi rl} = \frac{r}{2}\frac{\Delta P}{\mu l} \tag{A-15}$$

This is the velocity gradient. Due to frictional drag applied on the fluid the velocity profile is parabolic with a maximum velocity in the middle of the tube and zero velocity on the cylinder wall. Hence, the boundary conditions are as follows;

$$v(r) = \begin{cases} max, & r = 0 \\ 0, & r = R \end{cases} \tag{A-16}$$

To get an expression for the velocity on a specific given radius from the centre of the tube, we integrate the velocity gradient with respect to radius;

$$\int_{v}^{0} dv = \frac{1}{2}\frac{\Delta P}{\mu l}\int_{r}^{R} r\, dr \tag{A-17}$$

$$v(r) = \frac{1}{4}\frac{\Delta P}{\mu l}(R^2 - r^2) \tag{A-18}$$

This equation is the fundamental for deriving the streaming potential.